GEOTHERMAL SYSTEMS PERFORMANCE AND ENVIRONMENTAL IMPACTS

NEGAR DAEMI

A THESIS SUBMITTED TO THE FACULTY OF GRADUATE STUDIES
IN PARTIAL FULFILLMENT OF THE REQUIREMENTS FOR THE DEGREE OF
MASTER OF APPLIED SCIENCE

GRADUATE PROGRAMME IN CIVIL ENGINEERING
YORK UNIVERSITY
TORONTO, ONTARIO

SEPTEMBER 2017

ABSTRACT

The use of fossil fuels for heating and cooling purposes is plagued by problems including environmental impacts, unsustainable production, and increased greenhouse gas production. This had led to a worldwide interest in developing sustainable sources of energy. One such energy is ground source heat which is the ubiquitous low-enthalpy heat found in the shallow subsurface.

Vertical ground source heat pumps (GSHPs) can be used to extract or inject subsurface heat by installing borehole that circulate an antifreeze-based carrier fluid which is cooled or heated through the subsurface. Although GSHPs have many advantages, they might develop thermal subsurface plumes, which can affect the efficiency of the system and other subsurface infrastructures.

In the present research, the effect of a multi-borehole vertical GSHP system located in various locations in Canada was examined. To do so, a three-dimensional model was developed in FEFLOW that simulated a hypothetical GSHP system in different Canadian climates. Consequently, the resulting thermal plumes were studied and a sensitivity analysis was conducted to determine the effect of different groundwater and soil parameters on the development and movement of thermal plumes.

ACKNOWLEDGEMENTS

This thesis would not have been possible without the contribution of several people. Firstly, I would like to thank my supervisor, Dr. Magdalena Krol for giving me the opportunity of carrying out this research, her support and understanding and all the things that I have learned from her.

Secondly, I wish to express my deep gratitude to my lovely parents for believing in me and for making this degree possible.

I also wish to thank FEFLOW support team for answering all my questions with patience and kindness.

Last, but not least, I thank my sister, my research group and my friends, namely Amir Mirarab, Parin Izadi and Parnian Izadi.

TABLE OF CONTENTS

LIST OF TABLES

LIST OF FIGURES

NOMENCLATURE

Symbols

A	Cross-sectional Area (m^2 or ft^2)
b	Pipe Wall Thickness (mm)
c or C_p	Specific Heat Capacity (J kg^{-1} K^{-1})
C	Total Cooling Effect (W)
COP_C	Coefficient of Performance in Cooling Mode (-)
COP_H	Coefficient of Performance in Heating Mode (-)
d	Diameter (m)
D	Depth (m)
E	Electrical Energy (W)
E_t	Thermal Energy (J)
f_μ	Viscosity Relation Function (-)
F	Groundwater Flow (m^3 s^{-1})
F_{SA}	Lighting Special Allowance Factor (-)
F_{UL}	Lighting Use Factor (-)
G_c	Heat injected to the ground (kW)
G_H	Heat extracted from the ground (kW)
h	Hydraulic Head (m)
H	Total Heating Effect (W)
H_s	Thermal Sink/Source Term (W m^{-3})
HR	Humidity Ratio (-)
i	Hydraulic Gradient (-)
I	Identity Matrix (-)
I_z^e	Second Moment of Energy about the z-axis (J m^2)
K	Hydraulic Conductivity (m s^{-1})
m	Layer Thickness (m)
n	Porosity (-)
N	Number of Boreholes (-)
q	Volumetric Darcy Flux of Fluid (m s^{-1})

q_b	Heat Extraction Rate per Meter of Borehole (W m^{-1})
q_i	Infiltration Rate (cfm)
q_v	Ventilation Rate (cfm)
Q	Thermal Energy or Heat (J)
$\dot{Q}$	Heat Flow Rate (J s^{-1} or W or Btu hr^{-1})
Q_{env}	Heat flux extracted from or injected to an environmental reservoir (W)
$\dot{Q}_{gr}$	Total Ground Load (kW)
Q_l	Latent Heat Gain (Btu hr^{-1})
Q_r	Total Flow Rate of Refrigerant (m^3 s^{-1})
Q_s	Sensible Heat Gain (Btu hr^{-1})
Q_T	Total Heat Input Rate (J d^{-1})
r_b	Borehole Radius (m)
r_{spread}	Thermal Plume Radial Spread (m)
R_b	Borehole Thermal Resistance (J m^{-2} s^{-1} k^{-1})
Re	Reynolds Number (-)
S	Saturation of Fluid in the Void Space (-)
S_s	Storage Coefficient (m^{-1})
t	Time (s)
t_{end}	Simulation Time (d)
T	Temperature (°C)
T_0	Initial Subsurface Temperature (°C)
T_1	Heat Pump Delivered Temperature (°C)
T_2	Heat Pump Source Temperature (°C)
T_i	Inside Design Temperature (°C or °F)
T_m	Mean Outdoor Temperature (°C or °F)
T_o	Outside Design Temperature (°C or °F)
u	Velocity (m s^{-1})
U	Coefficient of Heat Transfer (Btu h^{-1} ft^{-2} $°F^{-1}$)
V	Volume (m^3)
w	Pipe Distance (cm)
W	Flow Supply (s^{-1}); Lighting Watts Input (W)
α_L	Longitudinal Thermodispersivity of Aquifer (m)
α_T	Transverse Thermodispersivity of Aquifer (m)
β	Thermal Expansion Coefficient ($°C^{-1}$)
Δ_{BHE}	Optimal Mesh Size around the BHE (m)
Δt_0	Initial Time Step Size (d)

ΔT	Temperature Difference (°C)
ϵ	RMS Error Tolerance (-)
λ	Thermal Conductivity (W m^{-1} K^{-1})
Λ	Thermal Hydrodynamic Dispersion (W m^{-1} K^{-1})
μ	Dynamic Viscosity (Kg m^{-1} s^{-1})
Ξ	Maximum Growth Factor between Subsequent Time Steps (-)
Ξ_{aniso}	Anisotropy (-)
ρ	Density (Kg m^{-3})
ρc	Volumetric Heat Capacity (J m^{-3} K^{-1})

Subscripts

0	Reference Value
b	Borehole
C	Cooling
ce	Center of Energy
H	Heating
i	Inlet Pipe
o	Outlet Pipe
r	Refrigerant
s	Steady State
w	Water or Groundwater

Superscripts

f	Fluid
g	Grout
r	Refrigerant
s	Solid

Abbreviations

1U	Single U-shape Pipe
1D	One Dimensional

2D	Two Dimensional
2U	Double U-shape Pipe
3D	Three Dimensional
ASHP	Air-Sourced Heat Pump
ASHRAE	American Society of Heating, Refrigerating and Air-conditioning Engineers
BC	Boundary Condition
BGS	Below Ground Surface
BHE	Borehole Heat Exchanger
BLAST	Building Loads And System Thermodynamics
BTES	Borehole Thermal Energy Storage
CFM	Cubic Foot per Minute
CLF	Cooling Load Factor
CLTD	Cooling Load Temperature Difference
CMA	Census Metropolitan Area
COP	Coefficient of Performance
CXA	Coaxial Pipe with Annular Inlet
CXC	Coaxial Pipe with Centered Inlet
DTH	Down-The-Hole hammer/drill
FDM	Finite Difference Method
FD3DM	Fully Discretized 3D Model
FEM	Finite Element Method
FVM	Finite Volume Method
GCHP	Ground Coupled Heat Pump
GFEM	Galerkin-based Finite Element Method
GSHP	Ground Source Heat Pump
GWHP	GroundWater Heat Pump
HDPE	High-Density PolyEthene
HGSHP	Hybrid Ground Source Heat Pump
HVAC	Heating, Ventilation and Air Conditioning
MDPE	Medium-Density PolyEthene
OP	Observation Point
PDE	Partial Differential Equation
SAT	Surface Air Temperature

SC	Shading Coefficient
SCL	Solar Cooling Load
TAZ	Thermal Affected Zone
TRCM	Thermal Resistance and Capacity Model
TRT	Thermal Response Test
USCS	United States Customary System

Chapter 1 Introduction

Ground source heat pumps have been widely used around the world to extract or inject heat into the ground. A ground source heat pump is a combination of a heat pump and groundwater wells, borehole heat exchanger (s), or horizontal heat exchanger pipes where a carrier fluid is heated or cooled. These systems are more efficient than other conventional heating and cooling systems, however their effect on the subsurface environment has not been examined and many questions remain on their environmental impacts.

In this chapter, geothermal heating, heat pumps and ground source heat pumps are described thoroughly. Different types of ground source heat pumps are introduced and usage of these systems around the world, as well as, their environmental impacts are explained.

1.1 Introduction to Geothermal Heating

The two terms “geothermal energy” and “ground source heat” should not be misused. Geothermal energy is the high-enthalpy heat derived from very deep subsurface. Ground source heat, on the other hand, is the ubiquitous low-enthalpy heat found in rather shallow subsurface at lower temperatures (Banks, 2008). The use of ground source heat

for space heating and cooling is referred to as “geothermal heating and cooling” or more frequently as “geothermal heating”.

There are different classifications of geothermal systems. Dickson et al. (2004) classified geothermal systems based on their temperature into four groups of ground source heat, low enthalpy, intermediate enthalpy and high enthalpy systems (Figure 1.1) Geothermal energy has different usage based on its temperature (Banks, 2008).

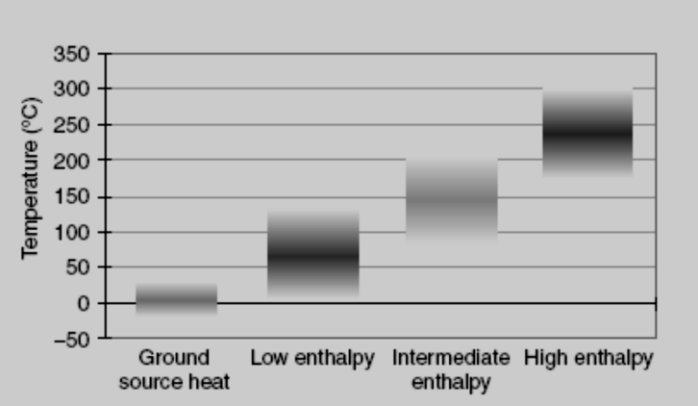

Figure 1.1 Temperature-based Classification of Geothermal Systems (Dickson et al., 2004)

American society of heating, refrigerating and air-conditioning engineers (ASHRAE) categorized geothermal systems into three groups of (1) high temperature (greater than 150°C) used by steam turbines to generate electricity, (2) intermediate and low temperature (less than 150°C) for direct use applications such as industrial and agricultural uses and swimming pools, and (3) ground source heat pump (GSHP) applications (less than 32°C) (ASHRAE, 1995).

Ground source heat is mainly a result of solar energy that is absorbed on the ground surface and stored in the subsurface. The heat flux from the earth crust may also contribute to the ground source heat, but solar energy is the main source (Banks, 2008).

The temperature at the ground surface increases due to solar radiation and higher air temperature in summer. This temperature change affects only the upper few meters of the subsurface named “zone of seasonal fluctuations”. This is because of the rather modest thermal conductivity of soils and rocks (Banks, 2008). Majorowicz et al. (2009) referred to this zone as “neutral zone” and reported it to be approximately 20 m below ground surface (BGS) in Canada.

Temperature of the ground beneath the zone of seasonal fluctuations is constant throughout the year and has a magnitude nearly equal to the annual average surface temperature. This temperature is higher than the ambient temperature in winter and lower than the ambient temperature in summer making the earth a convenient thermal source and sink in geothermal heating and cooling. This is due to high thermal storage and modest thermal conductivity of the ground. So when the subsurface is warmed during summer the heat is stored in the subsurface and can be extracted and used during winter. (Banks, 2008).

A factor that affects the ground temperature below the zone of seasonal fluctuations is the geothermal gradient from the earth’s interior. This gradient is measured to be approximately 1-3°C per 100 m which represents a geothermal flux of

0.04-0.09 W m^{-2} (Banks, 2008). Majorowicz et al. (2009) measured the geothermal gradient at southern Canada between the depths of 50-100 m, 100-150 m, 150-200 m and 200-250 m to be 0.01, 0.012, 0.014 and 0.01°C m^{-1} which is within the range reported by Banks (2008). Therefore the assumption that the ground temperature is equal to the annual average surface temperature can be modified to a more accurate estimation by considering the geothermal heat flux (Banks, 2008).

Heat is transferred within the subsurface via three methods of conduction, convection and radiation. In the shallow subsurface heat transfer mainly occurs due to conduction (Fourier's law) and convection by groundwater flow (Banks, 2008).

There are two properties that describe a material quality, in this case soils and rocks, in terms of heat transfer and heat storage. The former is presented by thermal conductivity (λ) which is defined as the ability of a material to conduct heat. Heat is conducted from hot objects to cold objects. The second property is the specific (c) or volumetric heat capacity (ρc) that quantifies the thermal storage of a material. Specific heat capacity is defined as the amount of heat stored in a medium for one-degree Kelvin of temperature. Specific heat capacity is typically measured in (J kg^{-1} K^{-1}) and volumetric heat capacity is measured in (J m^{-3} K^{-1}) (Banks, 2008).

These two parameters are obtained from generic tables, laboratory tests or in situ thermal response tests. A thermal response test (TRT), which is also known as borehole thermal conductivity test, is more accurate than the other two options because it includes

soil heterogeneity and effect of groundwater flow on ground thermal properties. In a TRT, heat is injected to the ground via a borehole and ground effective thermal conductivity (λ), borehole thermal resistance (R_b) and undisturbed ground temperature are measured based on the temperature change of the carrier fluid. These test are beneficial in the design and optimization of GSHP systems (Banks, 2008; J. Raymond, Therrien, Gosselin, & Lefebvre, 2011).

1.2 Overview of Heat Pumps

A heat pump is a system that uses mechanical work to transfer thermal energy from a low-temperature environment to a high-temperature environment. A fridge is a good example of a heat pump. It uses energy to extract heat from inside the fridge and rejects this unwanted heat into the kitchen (Banks, 2008).

The low-temperature source can be any environmental reservoir. For example, an air-sourced heat pump (ASHP) extracts heat from the atmosphere, while in the case of a GSHP, heat is extracted from the ground (Banks, 2008). Other environmental reservoirs that can be efficiently coupled with a heat pump are sea, fjords and sewage (Matte, 2002).

Heat pumps can be used for space heating and cooling. For example, in central and northern Europe GSHPs are commonly used for space heating while in central and southern USA they are used for both heating and air-conditioning.

In space heating, the environmental reservoir is treated as a source. Therefore, if a heat flux of Q_{env} is extracted form the reservoir and an electricity of E is used to run the system, the total heating effect (H) is measured as (Banks, 2008):

$$H = Q_{env} + E \tag{1-1}$$

In space cooling, the environmental reservoir is treated as a sink. Therefore, if a heat flux of Q_{env} is injected into the reservoir and an electricity of E is used to run the system, the total cooling effect (C) is measured as (Banks, 2008):

$$C = Q_{env} - E \tag{1-2}$$

The efficiency of a heat pump is presented by its coefficient of performance (COP) and is defined as heat delivered over electricity consumed in heating mode, and heat injected over electricity used in cooling mode.

$$COP_H = \frac{H}{E}$$
$$COP_C = \frac{C}{E} \tag{1-3}$$

Under operational conditions, COP_H is usually less than the ideal and is expected to be between 3 and 4 (Banks, 2008). In Canada, all GSHP systems with a power capacity of less than 35 kW must have a heating coefficient of performance greater than 3 (Bouma, 2002).

1.3 Overview of Ground Source Heat Pumps

GSHPs are also known as geothermal heat pumps, earth energy, or GeoExchange systems (Chiasson, 1999). A ground source heat pump system uses ground as a thermal source/sink. In heating mode, heat is extracted from the ground and eq. (1-1) can be written as:

$$G_H = H - E = H - \frac{H}{COP_H} = H\left(1 - \frac{1}{COP_H}\right) \quad \textbf{(1-4)}$$

Where G_H is the heat extracted from the ground. In cooling mode, a GSHP is switched into reverse, so it extracts heat from a building and injects it into the ground. Eq. (1-2) can be written as:

$$G_C = C + E = C + \frac{C}{COP_C} = C\left(1 + \frac{1}{COP_C}\right) \quad \textbf{(1-5)}$$

Where G_C is the total heat injected into the ground (Banks, 2008). To compare performance of a GSHP system in heating and cooling modes, a system with a constant *COP* of 4 is assumed to deliver 1 kW of heat in heating mode and reject 1 kW of heat in cooling mode, therefore:

$$G_H = 1 \times \left(1 - \frac{1}{4}\right) = 0.75\ kW$$
$$G_C = 1 \times \left(1 + \frac{1}{4}\right) = 1.25\ kW \quad \textbf{(1-6)}$$

This example shows that in cooling mode nearly 1.67 times more heat is injected into the ground than the heat absorbed in heating mode. The reason is, in heating mode the

electrical energy that powers the compressor is converted to more usable heat for space heating while in cooling mode it is treated as waste heat that is discharged into the ground. Banks (2008), therefore, concluded that using GSHPs for cooling is not as environmentally friendly as passive cooling systems, but still more efficient than ASHPs.

The maximum coefficient of performance of an ideal heat pump in heating mode can be measured as:

$$COP_H = \frac{H}{E} = \frac{T_1}{T_1 - T_2} \quad \textbf{(1-7)}$$

Where T_1 and T_2 are delivered and source temperatures (K), respectively. From eq. (1-7), it can be concluded that the lower temperature difference (T_1 - T_2) the higher the COP. In other words, a heat pump with lower difference between delivered temperature and source temperature has a higher efficiency. Delivered temperature can have different values depending on the domestic heating system (Table 1.1) (Banks, 2008).

Table 1.1 Value of Delivered Temperature for Different Domestic Heating Systems (Banks, 2008)

Delivered Temperature (T_1)	**Building Heating System**
Over 60°C	Old conventional hot water central heating
45-55°C	Modern low-temperature central heating
30-45°C	Underfloor Waterborne central heating
25-30°C	Warm air circulation

Therefore, for a more efficient system it is better to use a heating system that requires lower delivered temperature such as warm air circulation and an environmental reservoir with higher source temperature. Consequently, a GSHP system that uses ground at a

constant temperature of nearly 10°C as a reservoir has a higher efficiency than an ASHP system that uses fluctuating ambient air which can typically get as low as -5°C during winter (Banks, 2008). Moreover, the circulation fluid of GSHPs is water-based which has a high heat capacity as opposed to air in the case of ASHPs, leading to higher efficiency of these systems (Chiasson, 1999).

Furthermore, GSHPs have lower maintenance costs, longer lifetimes, lower visual impact on the building and most importantly lower CO_2 emissions compared to other conventional heating, ventilation and air conditioning (HVAC) systems. Although the initial cost of GSHPs are relatively high due to borehole drilling, it is still economically feasible due to its low maintenance cost and 20-25-year lifetime. Also, larger GSHP systems used for larger commercial and industrial buildings have lower initial cost per installed kW (Banks, 2008).

Ground source heat pumps also compete with other sources of green energy like wind turbines and solar systems. But it should be noted that GSHPs are electricity-powered and should be classified as a complementary technology instead of a green energy source. They use electricity more efficiently since they just use it to transfer energy from the ground to the building interior rather than produce and transfer energy. One advantage of GSHPs over its competing green energy sources is the fact that it does not depend on climatic and sidereal conditions (Banks, 2008).

1.3.1 Overview of Open-loop Systems

GSHPs are categorized into two main groups of open-loop and closed-loop systems. In open-loop systems, heat is extracted from the ground by taking groundwater from sources like springs, wells, boreholes or flooded mines. These systems are also known as groundwater heat pumps (GWHP) or groundwater-based systems. The amount of heat that can be extracted from a groundwater flow is expressed as:

$$G_H = (\rho c)_w F_w \Delta T \quad \textbf{(1-8)}$$

Where $(\rho c)_w$ is volumetric heat capacity of groundwater, F_w is groundwater flow and ΔT is temperature drop of the groundwater in heating mode or temperature rise in cooling mode (Banks, 2008).

One of the main disadvantages of open-loop systems is that they are geology-dependant. These systems can only be installed in aquifers with suitable transmissivity and heat storage properties. However, they also have some advantages over closed-loop systems. These systems extract heat via forced groundwater convection as opposed to closed-loop systems that use heat conduction to extract heat from the subsurface. Therefore, these systems extract more heat per borehole/well than closed-loop systems and consequently require fewer number of wells to provide the same heating/cooling effect (Banks, 2008). Other advantages of GWHPs is their low cost and simplicity compared to other GSHPs (Chiasson, 1999).

An example of installation of a groundwater heat pump system for space heating is a heat pump with a capacity of 88 kW installed at the Eco-Centre in Tyneside, northern England. The system pumps groundwater at a rate of 3 L s^{-1} from a well at depth of 60 m BGS at a temperature of 10°C. The schematic of this system is shown in Figure 1.2. The heat enters a central heating system at a temperature of 45°C (Banks, 2008).

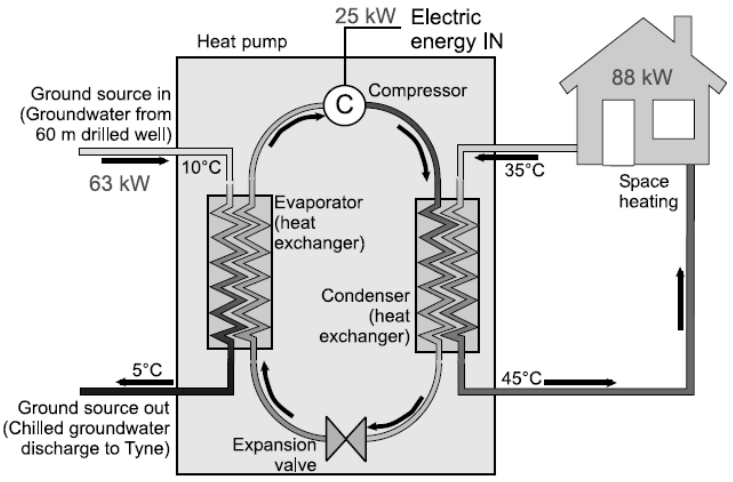

Figure 1.2 A Schematic Diagram of the Tyneside Eco-Centre GWHP (Banks, 2008)

In this example, the heat extracted from the ground (G_H) and electrical energy (E) are 63 and 25 kW respectively. A total heating effect (H) of 88 kW is provided (eq. (1-4)). From eq. (1-3), the system has a COP of 88/25=3.52 (Banks, 2008).

1.3.2 Overview of Closed-loop Systems

Closed-loop systems are also referred to as ground-coupled heat pump (GCHP) systems. Unlike open-loop systems, closed-loop systems can practically be installed in any

geology, from clays to permafrost. In a closed-loop system a fluid is circulated through one or multiple tubes to extract heat in winter and inject heat during summer to the subsurface. These tubes are installed in boreholes or horizontal trenches leading to vertical and horizontal categorization of closed-loop systems (Banks, 2008).

In another categorization, closed-loop systems can be either direct circulation or indirect circulation systems. In a direct circulation system, the heat pump's refrigerant is circulated through copper tubes installed in the subsurface (Figure 1.3). The advantage of direct circulation systems is the efficient heat transfer between the ground and the refrigerant. But, circulating a refrigerant in a copper tube may cause mechanical damage to the heat pump and even produce a risk of corrosion. This made direct circulation closed-loop systems less popular in many countries like England (Banks, 2008).

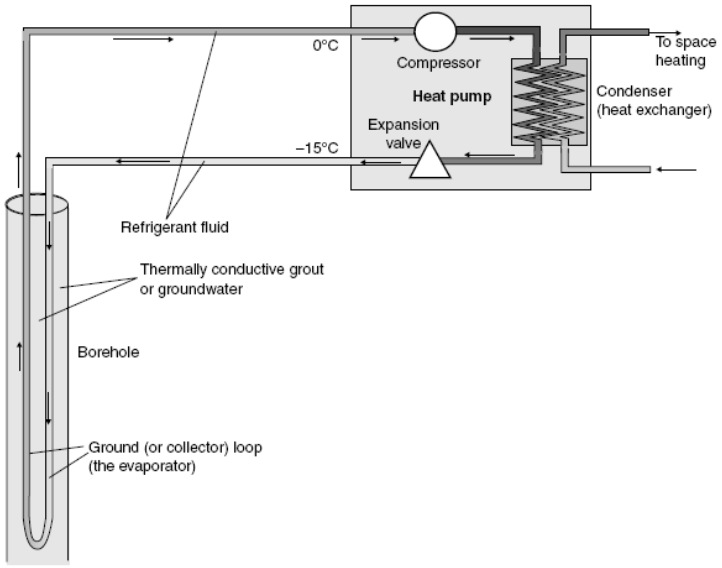

Figure 1.3 A Schematic Diagram of a Direct Circulation Closed-loop Scheme Installed in a Borehole

(Banks, 2008)

Indirect circulation systems, on the other hand, circulate a carrier fluid in the tubes buried in boreholes or a trench of horizontal pipes in the ground. Figure 1.4 illustrates such a system with a vertical borehole. The carrier fluid is usually a solution of water and antifreeze typically ethylene glycol, ethanol or salt which allows for freezing points as low as -20°C. In cooling systems, water is a suitable carrier fluid, but for heating schemes a solution of antifreeze is recommended since heat is absorbed from the fluid by the heat pump and its temperature might drop below zero (Banks, 2008).

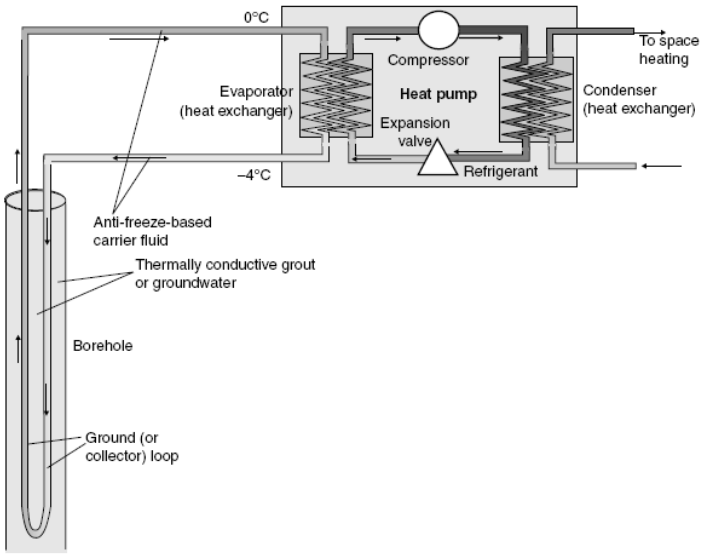

Figure 1.4 A Schematic Diagram of an Indirect Circulation Closed-loop Scheme Installed in a Borehole (Banks, 2008)

Closed-loop systems can be vertical or horizontal. In horizontal systems, pipes are installed in a trench at a depth of 1.2-2 m. The pipes are typically arranged in overlapping coils of pipe called slinky for better heat transfer (Figure 1.5). Horizontal systems require more area to be installed than vertical systems (Banks, 2008) and have lower efficiencies due to the fact that are more affected by air temperature changes (Chiasson, 1999).

Figure 1.5 The Installation of a Slinky-based Horizontal Closed-loop System in a Trench (Banks, 2008)

The primary focus of this thesis is on vertical closed-loop systems which are also called borehole-based closed-loop systems. In these systems, tubes are buried into vertical drilled boreholes known as borehole heat exchangers (BHE) which typically have depths between 30 and 200 m (Li & Lai, 2015). Depending on the soil and rock type, different drilling techniques can be used to drill these boreholes. For example, down-the-hole hammer (DTH) method is suitable for many different rocks. Other common drilling techniques are rotary drilling and percussion drilling methods (Banks, 2008).

Each borehole contains one or two u-shaped pipes. U-tubes are commonly made of high-density polyethene (HDPE) with diameters of 32-40 mm. HDPE has a high

thermal conductivity and is very resilient. Other common pipe materials are Polyethene, medium-density polyethene (MDPE), steel and copper. Although copper has a very high thermal conductivity, HDPE and MDPE are cheaper and do not impose the risk of corrosion (Banks, 2008).

The space between the U-tubes and borehole walls is typically filled with grout. Grout is usually a bentonite-cement mix which increases the thermal conductivity of the borehole while minimizing the potential water/anti-freeze leakage due to its low hydraulic conductivity. Boreholes are sometimes filled with groundwater or a porous backfill instead of grout. But grout is the typically the preferred option due to the advantages listed above (Banks, 2008).

Boreholes have different configurations. The simplest type is a single U-shape pipe with one inlet and one outlet shank. Another common configuration is a double U-shape pipe with two inlet and two outlet shanks. A 2U-shape borehole provides a better heat transfer between the fluid and the ground and consequently lower borehole thermal resistance, but it's more difficult to install. Other types of borehole configurations are coaxial pipes with centered or annular inlet, and vertical slinky boreholes (Banks, 2008). The top view of these configurations is shown in Figure 1.6.

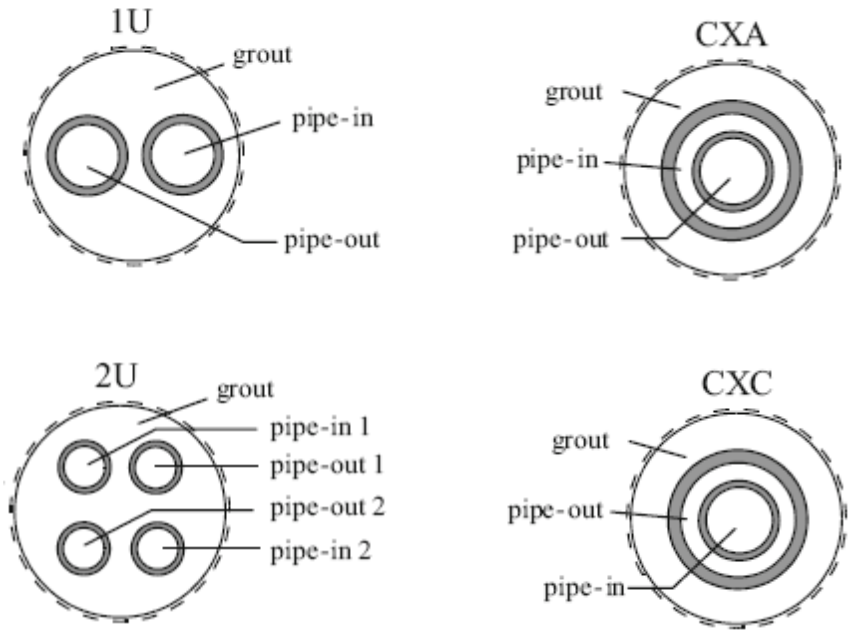

Figure 1.6 Top Cross Section of Different Configurations of Boreholes; Single U-shape Pipe (1U), Double U-shape Pipe (2U), Coaxial Pipe with Annular Inlet (CXA) and Coaxial Pipe with Centered Inlet (CXC) (H.-J. G. Diersch, 2014)

Another type of closed loop systems are surface water systems where heat exchanger pipes known as pond mats are submerged in a surface body like a pond or a lake (Figure 1.7). High thermal conductivity of water facilitates heat transfer in these systems. However, surface body systems are more vulnerable to damage and leakage than conventional systems installed in the ground (Banks, 2008).

Figure 1.7 Seven Pond Mats in an Artificial Lake in Northern England (Banks, 2008)

Another option is to place boreholes inside building foundations. This type of installation is called energy pile or geo-pile. Most large buildings need foundations as deep as 40 m with 1 m diameter that can be efficiently used for borehole installation. Energy piles have less capital cost but they have lower efficiency than conventional closed-loop systems since foundations are typically filled with concrete which has lower thermal conductivity than grout (Banks, 2008).

Vertical closed-loop systems are also used for dual applications which reject and store the unwanted heat into the subsurface during the summer and use this heat during winter to provide heating effect. These systems take advantage of thermal storage of the ground and can be balanced or imbalanced depending on the building heating and cooling load (Banks, 2008). For example, a system is installed at Richard Stockton College, New

Jersey with 400 boreholes of 135 m depth. The building is cooling dominated with cooling demand of around 5000 kW (Stiles, 1998).

1.4 Usage of GSHPs around the World

GSHP was patented in Switzerland in 1912 for the first time. In the late 1920s groundwater heat pumps were already being used for space cooling in Brooklyn and Long Island. Although Sweden, Switzerland, Austria and Germany were the pioneers of GSHPs, the oil crisis and the realization of the consequences of our fossil fuel dependence has brought worldwide attention to this technology (Banks, 2008). Lund et al. (2003) listed the countries with high GSHP installations as follows.

Table 1.2 Majority of GSHP Installations (Lund et al., 2003)

Country	Number of Installations	Power (MWt)
USA	500,000	3730
Sweden	200,000	2000
Germany	40,000	560
Canada	36,000	435
Switzerland	25,000	440
Austria	23,000	275

In the USA by year 2004, 80,000 GSHPs were being installed annually, 85% of which were closed loop systems (including 46% vertical and nearly 38% horizontal) and 15% of them were open loop systems (Banks, 2008).

Several studies show that there is a potential for high-temperature geothermal systems in northern and western Canada and potential for low-temperature systems almost anywhere Canada (Blackwell, Negraru, & Richards, 2006; Jessop, Ghomshei~, & Drury, 1991; Jones, Lam, & Majorowicz, 1985; J. A. Majorowicz, Jones, Lam, Linville, & Nguyen, 1985). A report by Ghomeshi et al. (2005) reported nearly 30,000 residential systems operating in Canada. Also, Canadian centre for energy net information (2007) reported 5000 systems used for non-residential space hating and cooling. Replacement of fossil fuel driven heating and cooling systems with ground source heat pumps in Canada would save 37 Mt CO_2 emission annually (J. Majorowicz, Grasby, & Skinner, 2009).

Majorowicz et al. (2009) calculated the potential thermal energy than can be extracted from or injected into a block of rock sizing 1 km by 1 km with a depth of 50 m located in southern Canada where permafrost is not developed (Figure 1.8). The potential thermal energy (Q) is calculated by:

$$Q = \rho C_p V \Delta T \qquad \textbf{(1-9)}$$

Where ρ is rock density, C_p is rock specific heat capacity at constant pressure, V is total volume of rock and ΔT is the temperature difference measured as the difference between ground temperature at 50 m BGS and the surface air temperature (SAT). Average values of 2550 kg m^{-3} and 1000 J kg^{-1} $°C^{-1}$ were used for rock's density and specific heat capacity respectively. Maps were compiled for both heating and cooling seasons. Majorowicz et al. (2009) defined the heating and cooling seasons based on the subsurface

temperature. Therefore, the 6 months of October until April with SATs lower than subsurface temperature were considered heating season (Figure 1.8 and Figure 1.9). These maps show that Canada has a very high thermal energy potential up to 2.6×10^{15} J and -1.4×10^{15} J in heating and cooling seasons respectively (J. Majorowicz et al., 2009).

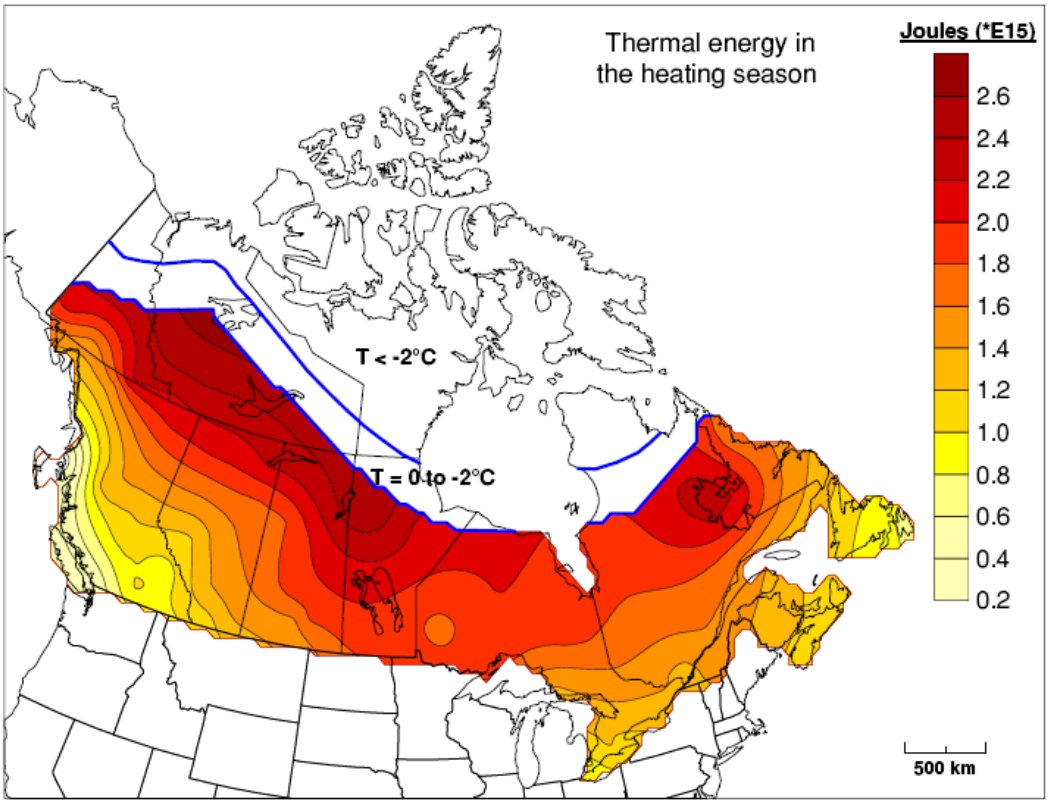

Figure 1.8 The Quantity of Thermal Energy, which Could Potentially Be Released from 1 km^2 Area Block of Rock Down to -50 m in Canada for the Heating Season (J. Majorowicz et al., 2009)

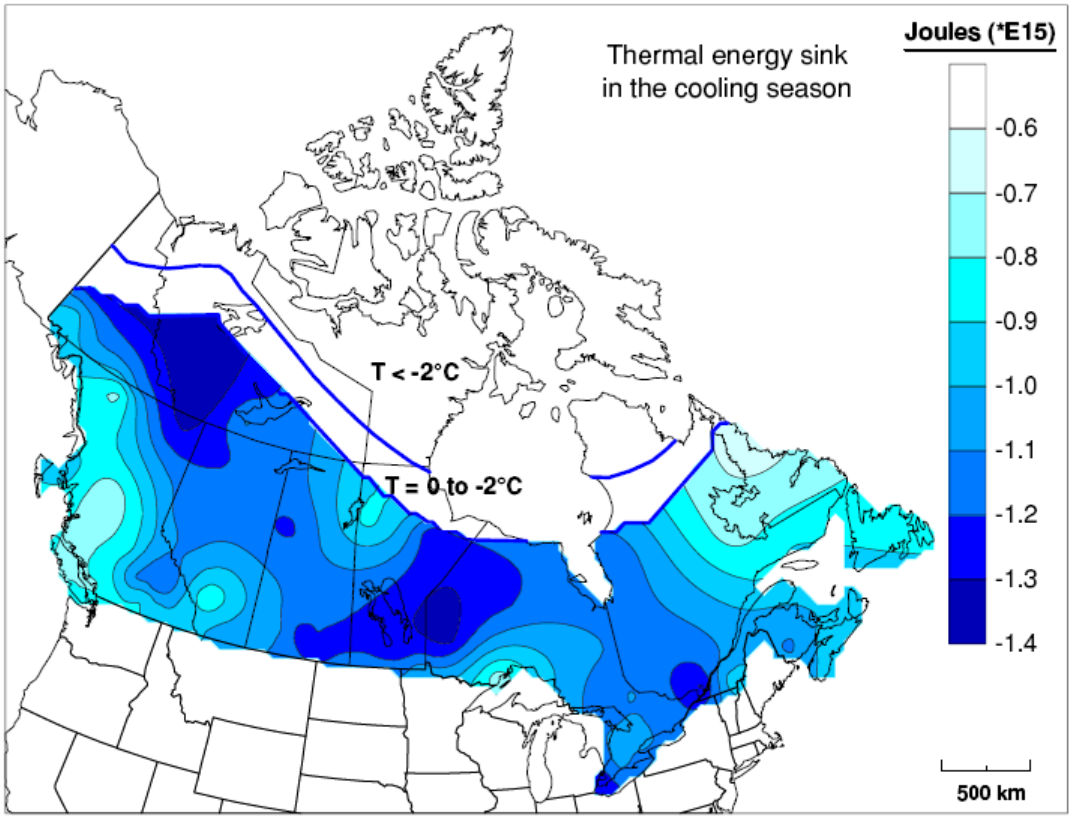

Figure 1.9 The Quantity of Energy Available from the Upper 50 m of the Rock for Cooling in the Summer Months (J. Majorowicz et al., 2009)

1.5 Sustainability and Environmental Impacts

The sustainability of a geothermal system can be diminished when the ground temperature changes to an unusable level because of system overuse. If the heat extracted from the ground (G_H) during a year of operation is greater than the total heat injected into the ground (G_C) the system is called a net heating ground source scheme or heating-dominated and long-term operation of such systems result in cooling down of the ground.

If G_C is greater than G_H the system is called a net cooling ground source scheme or cooling-dominated and the ground tends to heat up. In the course of long-term system operation, both of these schemes lead to change of ground temperature, system inefficiency and unsustainability and high initial costs due to longer boreholes. Although there are still some techniques to force such systems to become balanced. For example, in the case of a cooling-dominated scheme, the excessive heat in the summer can be discharged to the air using cooling towers or shallow ponds. These systems are called hybrid ground source heat pumps (HGSHP) (Banks, 2008; Lee, Song, Ahn, & Kim, 2015; Yang, Cui, & Fang, 2010).

Environmental regulators are often concerned about performance of heat pump systems, i.e., pump COP as well as effect of GSHP systems on hydrogeology of the aquifer and subsurface temperature termed as hydrogeological and thermogeological impacts respectively. Hydrogeological impact is more associated with open-loop systems. These systems impose higher environmental risks since they extract and discharge groundwater. Regulations usually control groundwater extraction rate and temperature of reinjected groundwater (Banks, 2008).

In the case of closed-loop systems, one of the concerns is that poor and unsupervised installation of these systems in contaminated sites might result in migration of contaminants from surface to the aquifer. The other concern is the potential leakage of

refrigerants or antifreeze-based carrier fluids in the subsurface (Banks, 2008; Slenders, Dols, Verburg, & de Vries, 2010).

Thermogeological impacts deal with ground freezing due to excessive heat extraction which can have damaging effects on plant roots, building structures and other subsurface installations. Thermogeological impacts also include ground warming and development of thermal plumes due to excessive heat recharge which can decrease system efficiency. The thermally affected zone typically has a radius of 20 m (Banks, 2008). However, this is not based on any general studies and more research is required on the extent of thermally affected zone.

Even though there are numerous aforementioned environmental impacts, in many countries there is no supervision on GSHP installations. For example, in the UK by the year 2008 closed-loop systems could be installed without any permission or license required. In the US by the year 1998, nearly half of the states had no or minimal environmental regulation for closed-loop system installation (Banks, 2008). The only GSHP regulation that was found in Canada was the one mentioned in section 1.2 about heating COP.

1.6 Thesis Objectives

The literature review shows that there are limited studies done on GSHP performance in Canada. In addition, little is known about the effect of subsurface parameters on the environmental impacts of GSHP. As such, this study examines a closed-loop GSHP

system with multiple boreholes designed to provide heating and cooling for a building located in different climatic regions around Canada.

There are four main objectives to this study:

1. Develop a 3D model in FEFLOW 7 to simulate a GSHP nest in different Canadian climates.
2. Identify the thermally affected zone and study the developed thermal plumes under different building thermal loads.
3. Examine the effect of groundwater flow on development and transport of thermal plumes.
4. Study the sensitivity of the model to soil type, and various subsurface parameters.

First and second objectives are addressed in Chapter 3. An office building was assumed in three cities in different climatic zones around Canada. The annual thermal load of the building was calculated and a GSHP system with multiple boreholes that was capable of providing the loads was considered. The ten-year operation of the GSHP system in different cities was simulated. Consequently, the resulting thermal plumes and the effect of building load were examined.

Chapter 4 deals with the third and fourth objectives. A sensitivity analysis was conducted studying the effect of groundwater flow and soil types on thermal plume formation. Three cases with low, medium and high groundwater flow velocity were

considered and, two cases with coarse sand and clay were examined. Lastly, as a more realistic representation of a geologic formation, a layered subsurface consisting of soil and rock was studied.

Chapter 2 Literature Review on Numerical Modelling of GSHP Systems

In this chapter, an introduction to numerical methods and their application in modelling GSHP systems is presented, followed by a literature review on GSHP modelling and overview of groundwater flow and heat transport equations. The chapter is completed by presenting thesis objectives.

2.1 Numerical Methods

The basis of any numerical method is in the approximate solution of the governing partial differential equations (PDE) via spatial and temporal discretizations. In this approximation, the PDE is replaced by often a very large number of linear algebraic equations which are then solved by computers. Numerical methods are classified as follows (H.-J. G. Diersch, 2014):

- Finite difference method (FDM)
- Finite element method (FEM)
- Finite volume method (FVM)

2.1.1 Finite Difference Method

The finite difference method is a very simple numerical approach which has been widely used. The main drawback of this method is that it is incapable of solving problems with

complex geometries and/or complex boundary conditions (BC). FDM requires the mesh to be set up in a structured way. The advantage of FDM is the use of regular grids which allow for efficient approximations (H.-J. G. Diersch, 2014).

2.1.2 Finite Element Method

Finite element method is widely used for numerical analysis in many engineering fields such as structural mechanics, fluid dynamics, heat transfer and numerical mathematics. This method is based on the weak formulation of the governing equations as opposed to FDM which means that FEM uses the integral form of the equations, while FDM uses the differential form of the governing equations. This formulation is a natural and adequate approach to approximate the governing equations and provides a smoother solution compared to FDM (H.-J. G. Diersch, 2014).

FEM naturally leads to unstructured meshes. Therefore, it can be applied to arbitrary geometries with a wide range of BC's. This feature makes FEM a powerful and flexible numerical method that is superior to other methods.

2.1.3 Finite Volume Method

FVM is sometimes termed as control volume method (CVM). Today, FVM is the most widely applied method in computational fluid dynamics because of its generality, simplicity and easy implementation on arbitrary structured and unstructured grids (Hirsch, 1988).

Similar to FEM, finite volume method is also based on weak formulations of the basic problem (H.-J. G. Diersch, 2014). The main advantage of the FVM is its direct connection to the physical properties of the flow (Hirsch, 1988).

2.2 Numerical Groundwater Flow and Heat Transport Models

There are several free or commercially-available and numerical software codes that are suitable for groundwater flow and heat transport simulations. Hecht-Méndez et al. (2003) provided a list of these codes with their characteristics in terms of numerical method, processes that they can simulate, their availability and coupling (Hecht-Méndez, Molina-Giraldo, Blum, & Bayer, 2010). The list was updated and is presented in Table 2.1.

In this table, H, T and C denote hydraulic, temperature, and contaminant processes, respectively, and H→T shows that groundwater flow is independent of temperature while H↔T denotes that groundwater flow depends on temperature changes. M and CH represent dependency of the groundwater flow on mechanical deformation and chemical reaction, respectively.

Table 2.1 Available Numerical Groundwater Flow and Heat Transport Models

Code Name	Numerical Method	Processes	Coupling	Availability
AQUA3D	FEM	H, T, C	H→T	Commercial
AST/TWOW	FDM	H, T	H→T	Commercial
BASIN2	FDM	H, T, C	H↔T, M, CH	Free
COMSOL	FEM	H, T, C	H↔T	Commercial
FEFLOW	FEM	H, T, C	H↔T, M, C	Commercial
FRACHEM	FEM	H, T, C	H↔T, M, C	Scientific
FRACture	FEM	H, T	H↔T, M	Scientific
ROCKFLOW/GeoSys	FEM	H, T, C	H↔T, C	Scientific
HEATFLOW	FEM	H, T	H↔T	Free
HST2D/3D	FDM	H, T, C	H↔T, M, CH	Free
HydroTherm	FDM	H, T	H↔T	Free
HYDRUS-2D	FEM	H, T, C	H→T	Commercial
MT3DMS	FDM	H, C	H→T	Free
SEAWAT	FDM	H, T, C	H↔T, C	Free
SHEMAT	FDM	H, T, C	H↔T, C	Commercial
SUTRA	FEM/FDM	H, T, C	H↔T, C	Free
THETA	FDM	H, T, C	H↔T, CH	Scientific
TOUGH2	FDM	H, T, C	H↔T, C, CH	Commercial
TRADIKON 3D	FDM	H, T	H→T	Free
VS2DH	FDM	H, T	H→T	Free

In the current thesis, FEFLOW version 7.0 was selected as a numerical model due to the coupled nature of the model, as well as, FEFLOW's ability to simulate GSHP systems in

many studies (Emad Dehkordi, Schincariol, & Olofsson, 2015; Hecht-Méndez, de Paly, Beck, & Bayer, 2013; Lo Russo, Taddia, & Verda, 2012). Also, it has high computational performance and is capable of flexible meshing.

2.3 Literature Review on GSHP Modelling

Although GSHPs have been widely used worldwide, many of these developments have occurred without sufficient hydrogeological evaluations which may result in environmental impacts (Ferguson & Woodbury, 2005). Therefore, effects of a GSHP system on the subsurface should be studied to optimize the performance of these systems and limit their environmental impacts. In this section, a literature review on GSHP modelling is presented.

GSHP modelling is a concept that has been known for several decades, therefore there is a rich literature available on this concept. Yang et al. (2010) conducted a comprehensive literature review on existing simulation models of borehole-based GSHP systems. The first method ever used was the "rule of thumb" approximation which was reviewed by Ball et al. in 1983 (Ball, Fischer, & Hodgett, 1983). Due to its inapplicability in places where soil and weather experience some nonuniformity, several alternative methods for design and performance assessment of GSHPs have been developed (Yang et al., 2010).

These methods can be categorized into two main approaches of analytical solutions, and numerical modelling. Analytical or numerical models can be further

categorized into two groups that simulate either heat conduction outside the borehole or heat transfer inside the borehole. A number of analytical simulation models for the heat transfer outside the borehole exist in the literature; Kelvin's line source, Cylindrical source model, Eskilson's model, finite line-source solution and short time-step model to name a few. Furthermore, several one-dimensional (1D), two-dimensional (2D), and quasi-three-dimensional (3D) models exist that determine the temperature of the heat carrier fluid inside the borehole (Yang et al., 2010). Analytical methods have simple physical meanings and are easy to understand and apply (Li & Lai, 2015), but they're incapable to model complicated geometries and boundary conditions. Numerical models, on the other hand, are used for many applications in the field of GSHP systems. They are also used to optimize their design, assess their performance or examine their effect on neighboring systems.

2.3.1 Analytical methods

In most analytical models, the heat conduction outside the borehole is simulated by treating the borehole as a heat source in a homogeneous soil and heat transfer inside the borehole is assumed to be a steady-state process. The steady-state assumption is not suitable for short-term simulations (Lei, Hu, Zhu, & Wu, 2015).

The performance of a GSHP system depends on many factors like building heating and cooling load, geological properties, subsurface temperature distribution, borehole properties and groundwater movement (Diao, Li, & Fang, 2004). Therefore,

studying the performance and environmental impacts of a BHE field requires a comprehensive approach and this can often be done with numerical models.

2.3.2 Numerical methods

Numerical modelling of the GSHP systems is capable of simulating problems with complicated boundary conditions and geometries, as well as accounting for time-variant sources and sinks, and soil heterogeneities (Ferguson & Woodbury, 2005). However, numerical approaches can be time-consuming and are sensitive to the initial conditions (Garcia-Gil, Vazquez-Sune, Schneider, Sanchez-Navarro, & Mateo-Lazaro, 2014).

Many studies have been conducted to develop numerical models that simulate the performance of a GSHP system. Ozudogru et al. (2014) developed a 3D numerical model in COMSOL Multiphysics that calculated the transient heat and mass transfer in the borehole or energy pile accurately with relatively short computation time. In this model, 1D linear elements were utilized to simulate flow and heat transfer inside the borehole pipes which was then coupled with the 3D geometry representing the soil. The proposed method was validated simulating two problems of a single U-tube borehole and a double U-tube energy pile (Ozudogru, Olgun, & Senol, 2014).

In 2015, Rees proposed an extended 2D numerical model that combined a horizontal finite volume representation of the borehole and surrounding medium with a pipe model to simulate very short to medium-timescale problems. He then compared the performance of this model with existing experimental data, a 3D model, TRNSYS and

EnergyPlus simulation tools. The comparisons showed good agreement. The model was capable of capturing short timescale effects as accurate as a detailed 3D model (Rees, 2015).

Numerous PC-programs are developed based on analytical models as design tools for vertical GSHPs. For example, the Lund programs, the Earth Energy Designer (EED) program and the GLHEPRO program are design tools based on the Eskilson's approach which is described in section 2.4.2.1 (Yang et al., 2010).

Raymond et al. (2011) studied the effect of using a new HDPE pipe with higher thermal conductivity in comparison with the regular pipe on performance of a vertical BHE using steady-state 2D and transient 3D numerical models developed in COMSOL Multiphysics. This study showed that these new thermally enhanced pipes reduced the borehole thermal resistance by up to 24%. Furthermore, the 3D modelling showed a decrease of 1ºC and an increase of 0.6 ºC in the carrier fluid temperature in cooling and heating modes, respectively (Jasmin Raymond, Frenette, Leger, Magni, & Therrien, 2011).

2.3.3 Simulation of Environmental Impacts

One of the environmental impacts of GSHP systems is the development of thermal plumes that can affect groundwater flow and subsurface temperature. For example, a survey conducted in 2013 in the city of London, UK showed that nearly 3% of central London was affected by thermal plumes due to GSHP installations (Herbert et al. 2013).

Another study reported a groundwater temperature change of 10°C induced by geothermal energy use in the city of Zaragoza, Spain (Garcia-Gil et al., 2014). Thermal plumes can impact the efficiency of GSHPs and other underground infrastructures.

The zone that is affected by thermal plumes is known as Thermal Affected Zone (TAZ). The precise estimation of the TAZ is very important due to its effect on neighboring wells, GSHPs and other underground infrastructures. Lo Russo et al. (2014) studied the TAZ of an instrumented GWHP system located in northwest Italy using FEFLOW 6.0 program (Lo Russo, Gnavi, Roccia, Taddia, & Verda, 2014).

Ferguson and Woodbury (2005) analyzed factors affecting temperature increase at production wells in GWHP plants used in cooling mode with the means of both numerical modelling and observations. METRA which is a submodule of MULTIFLO was used in this study. Ferguson et al. (2005) studied temperature profiles under different well spacing and pumping rates within ten years of operation. They first conducted a generic study and then validated their results using existing data from an industrial site in the city of Winnipeg, Manitoba that used GWHP systems for cooling four separate buildings since 1965 (Ferguson & Woodbury, 2005, 2006).

Both numerical model and observations showed that the use of groundwater for cooling is not sustainable in Winnipeg due to temperature increase at the production wells during the first few years of operation. An increase in groundwater temperature reduced its efficiency as a carrier fluid. The numerical modelling also indicated thermal

interference between three of the four systems led to greater increases in temperature. Therefore, the distance between these systems had to be smaller than the ideal spacing (Ferguson & Woodbury, 2005, 2006).

Liuzzo-Scorpo et al. (2015) studied conflicts between boreholes that are installed too close to each other and how they can be avoided. They studied the groundwater flow influence on the minimum required spacing between boreholes in the direction perpendicular to groundwater flow using a 2D numerical model developed in COMSOL Multiphysics along with a TRT. Their study showed that groundwater flow increased the value of the effective thermal conductivity measured by TRT and consequently enhanced the heat transfer (Liuzzo-Scorpo, Nordell, & Gehlin, 2015).

Chiasson (1999) studied the effect of groundwater flow on a closed-loop GSHPs for two cases of a single borehole which simulated a TRT and a multi-borehole field with 16 boreholes in a 4×4 arrangement. Chiasson (1999) first used building load analysis and system thermodynamics (BLAST) software to calculate the hourly heating and cooling load of a building located in north-central Oklahoma and then used GLHEPRO program to estimate the optimum number of boreholes, their length, and bore spacing to satisfy the calculated load. He ultimately simulated groundwater flow and heat transfer using finite element AQUA3D computer code. This study showed that groundwater flow is favourable to thermal performance of ground heat exchangers (Chiasson, 1999).

Dehkordi et al. (2015) also examined the effect of groundwater flow on multiple BHE systems, as well as, conducting a through sensitivity analysis on parameters like number of boreholes, layout, bore spacing and load. They developed a 3D model in FEFLOW and used the BHE solution based on an analytical method by Eskilson and Claesson (1988) available in FEFLOW (Emad Dehkordi et al., 2015). They concluded that in a long-term operation, multi-borehole systems with balanced loads show less sensitivity to array properties and groundwater flow than systems with imbalanced loads, where the effect intensified with time. They also showed that increasing the number of boreholes and changing their arrangement from line (4×1) to square (2×2), in the no groundwater flow case with imbalanced load, deteriorates system performance. Lastly, they illustrated that a groundwater flow of 10^{-7} m/s improved systems performance and decreased the required time for the system to become near-steady state compared to a no-groundwater flow case. Also, groundwater flow was found to be more effective in moderating loop temperature compared to array properties such as increasing bore spacing (Emad Dehkordi et al., 2015).

Hecht-Méndez et al. (2013) optimized the operation of a 25-BHE field by simulating groundwater flow and heat transfer using FEFLOW. Simulation scenarios were different in terms of groundwater seepage velocity and boreholes operation. The borehole field was used to provide nine months of heating consistent with annual demand in Central Europe. The optimization was aimed to enhance heat pump performance by

minimizing the thermal impact of the BHE field on the ground (Hecht-Méndez et al., 2013).

Camdali et al. (2015) modeled a horizontal GSHP used for heating a room located in Turkey using MATLAB software. The influence of several factors such as type of refrigerant, working mode, heating load, brine and mass ratio on the COP of the system was studied (Camdali, Bulut, & Sozbir, 2015).

Given the fact that ground source heat pumps are mostly used in urban aquifers and many cities are in the vicinity of large rivers, García-Gil et al. (2014) studied the thermal interaction of GWHPs and rivers, in Zaragoza, Spain. The use of heat pumps is widespread in Zaragoza, where approximately 50% of Spain's total power coming from heat pumps is generated in this city (GEOPLAT, 2010). 75% of the installed GWHPs are designed for cooling during summer and the rest are designed for heating in the winter (Garcia-Gil et al., 2014). García-Gil et al. (2014) used TRANSIN IV to model groundwater heat transfer in an urban aquifer of Zaragoza with 27 GWHPs and also determined the critical distance at which river thermal impact on the aquifer becomes considerable. In the case of Zaragoza, this distance was measured to reach up to 200 m (Garcia-Gil et al., 2014).

2.3.4 Canadian Studies

Unlike American and European countries, studies on geothermal systems located in Canada are very limited and mostly focused on open-loop systems. Some of these studied are mentioned below.

According to Huttrer (1997), former mine conduits are very permeable systems that are suitable for geothermal energy extraction (Huttrer, 1997). Using a flooded underground mine as a ground heat exchanger can reduce the installation costs of the system. In Canada, more than 2,262 former flooded mines with a total energy potential of 18,642 TJ were detected (J. Raymond & Therrien, 2014). For example, a factory located in Springhill, Nova Scotia has been extracting groundwater at 18°C from the Springhill coal mine to heat and cool industrial buildings since 1989 (Jasmin Raymond & Therrien, 2008).

Raymond and Therrien (2008) estimated the potential geothermal energy of the flooded Gaspé Mines using a long-term TRT and a numerical model developed in HydroGeoSphere to be 765 kW. Their method can be used to assess the geothermal energy of any mine site as a preliminary study (Jasmin Raymond & Therrien, 2008).

In a further study, Raymond et al. (2014) applied a calibrated HydroGeoSphere model to optimize a groundwater heat pump system located in the town of Murdochville, Canada. The model was used to predict the best flow rate for 50-year of operation

accounting for realistic heating and cooling loads, subsurface heterogeneities and coefficient performance of the heat pump (J. Raymond & Therrien, 2014).

In 2015, Dehkordi et al. used FEFLOW and TRT to propose a tight borehole heat exchanger design. Numerical results were validated using a fully discretized 3D model (FD3DM). FD3DM is accepted as an accurate model because of finite elemental discretization of all borehole elements including fluid and grout. Therefore, it is usually used for sensitivity analysis and model verification. The test was conducted in a site in Burlington, Ontario, Canada. This study showed that the new design with tight boreholes provides better placement of the pipes inside the borehole compared to typical boreholes with or without spacers. Furthermore, installation of the presented design is more time and cost efficient due to elimination of spacers and reduction of drilling and grouting volumes (Dehkordi, Schincariol, & Reitsma, 2015).

2.4 Groundwater Flow and Heat Transport Governing Equations

In this section, the process of solving a coupled groundwater flow and heat transport problem including borehole heat exchangers in FEFLOW is described and governing equations are presented. More detailed equations can be found in (H.-J. G. Diersch, 2014; H. J. G. Diersch, Bauer, Heidemann, Rühaak, & Schätzl, 2010). In FEFLOW, a BHE problem is divided into two parts: global and local problems. These represent subsurface

and borehole processes, respectively. Global and local problems are linked by thermal transfer relationships (H. J. G. Diersch et al., 2010).

2.4.1 Subsurface Equations

The global problem is solved by solving conservation equations of fluid mass, fluid momentum and thermal energy of soil and fluid. The current research simulates steady-state groundwater flow and transient heat transport which is a specific option in FEFLOW that assumes groundwater flow does not change with time (H.-J. G. Diersch, 2014). The equation for conservation of fluid mass is given by:

$$S_s \frac{\partial h}{\partial t} + \nabla . q = W \qquad \textbf{(2-1)}$$

where S_s is storage coefficient, h is hydraulic head, q is the Darcy flux that is expressed by Darcy law in eq. (2-2), W external sink/source term (H. J. G. Diersch et al., 2010).

$$q = -K f_\mu \left(\nabla h + \frac{\rho^f - \rho_0^f}{\rho_0^f} e \right), \quad e = -\frac{g}{|g|} \qquad \textbf{(2-2)}$$

$$\rho^f = \rho_0^f [1 - \beta (T - T_0)]$$
$$f_\mu = \frac{\mu_0^f}{\mu^f} \qquad \mu^f = \mu^f (T) \qquad \textbf{(2-3)}$$

Where K is hydraulic conductivity, f_μ is viscosity relation function, ρ^f and ρ_0^f are fluid density and reference fluid density respectively, and e is gravitational unit vector. β is thermal expansion coefficient, T is soil temperature and T_0 is reference temperature, and

μ^f and μ_0^f are fluid dynamic viscosity at temperature T and reference temperature, respectively (H. J. G. Diersch et al., 2010). Transient term of eq. (2-1), i.e., $\left(S_s \frac{\partial h}{\partial t}\right)$ is assumed to be zero due to steady-state groundwater flow simulation.

The conservation of thermal energy (first law of thermodynamics) in the soil is given by eq. (2-4), where the sum of energy stored in the subsurface, heat transfer through convection, and conduction equals the heat added through a sink/source and any external heat supply

$$\frac{\partial}{\partial t}[(n\rho^f c^f + (1-n)\rho^s c^s)T] + \nabla.(\rho^f c^f qT) - \nabla.(\Lambda.\nabla T) = H_s \quad \textbf{(2-4)}$$

Where n is porosity, $\rho^f c^f$ and $\rho^s c^s$ are volumetric heat capacity of fluid and solid, respectively. H_s is thermal sink/source term and Λ is the tensor of thermal hydrodynamic dispersion which is defined as (H. J. G. Diersch et al., 2010):

$$\Lambda = [n\lambda^f + (1-n)\lambda^s]I + \rho^f c^f \left[\alpha_T \|q\| I + (\alpha_L - \alpha_T)\frac{q \otimes q}{\|q\|}\right] \quad \textbf{(2-5)}$$

Where I is identity matrix, α_T and α_L are transverse and longitudinal thermodispersivity, respectively.

2.4.2 BHE Equations

Modelling borehole heat exchangers requires specific considerations due to their slender geometry. Boreholes typically have a diameter of 0.15 m and length of 100 m. However, some finite element and finite volume based tools are available that simulate fully

discretized BHEs and account for actual borehole geometry. Fully discretized models require huge computational time and effort. FEFLOW uses a geometry approximation method which is based on thermal resistance and capacity model (TRCM) presented by Bauer et al. (Bauer, Heidemann, Mü ller-Steinhagen, & Diersch, 2011). The TRCM has shown to be accurate and computationally efficient for both steady-state and transient simulations (H.-J. G. Diersch, 2014).

In the TRCM, each borehole is treated as an internal boundary condition and discretized by N_{BHE} nodes that are linked to 1D elements representing the pipe. Therefore, each BHE is a singular point condition of N_{BHE} nodes. Each borehole element contains 1D elements representing different components of the borehole, i.e., inlet and outlet shanks of the U-tube and grout capacities. The TRCM simulates the grout with one capacity per pipe, therefore, a 1U exchanger has 2 components for inlet and outlet shanks and 2 components of grout, and similarly a 2U exchanger has 4 components for inlet and outlet shanks and 4 components of grout. The schematic of this type of discretization is shown in Figure 2.1 for a 2U exchanger borehole (H.-J. G. Diersch, 2014).

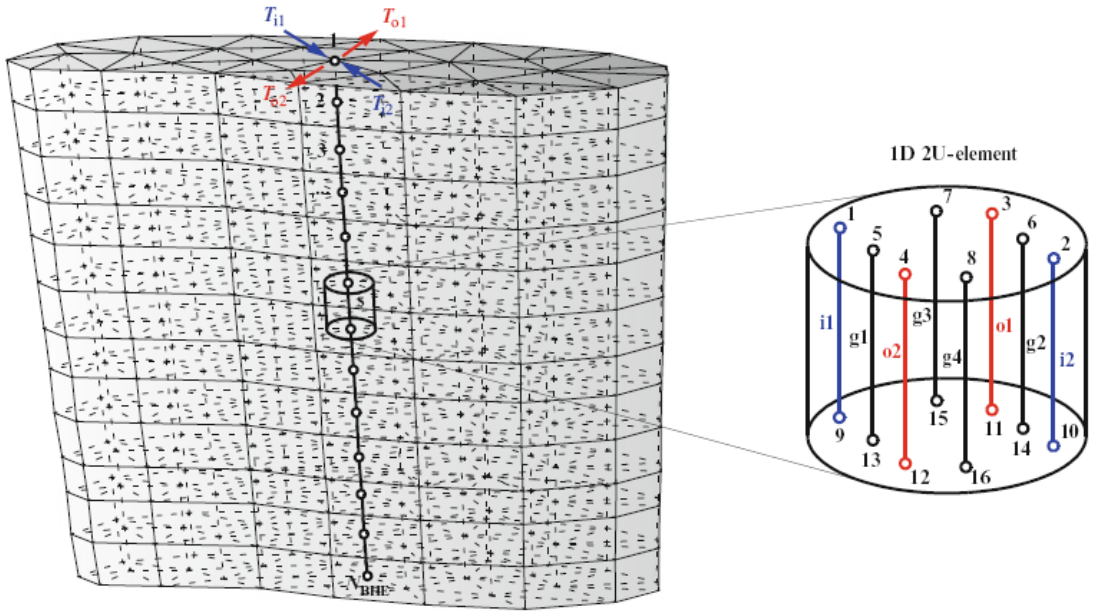

Figure 2.1 Discretized Single 2U Exchanger Borehole (H.-J. G. Diersch, 2014)

Conservation equation of thermal energy is solved for each BHE component. For example, for the case of 2U exchanger, the conservation of thermal energy is solved for all the 8 components of the BHE. The equation for inlet 1 of a 2U exchanger is written as follows:

$$\frac{\partial}{\partial t}(\rho^r c^r T_{i1}) + \nabla.(\rho^r c^r u T_{i1}) - \nabla.(\Lambda^r.\nabla T_{i1}) = H_{i1} \qquad \textbf{(2-6)}$$

Where $\rho^r c^r$ is volumetric heat capacity of refrigerant, T_{i1} is inlet pipe 1 temperature of refrigerant, u is refrigerant fluid velocity, Λ^r is refrigerant thermal hydrodynamic dispersion and H_{i1} is thermal sink/source term for inlet pipe 1 (H. J. G. Diersch et al., 2010).

In the next step, borehole thermal resistance (R_b) is computed from BHE engineering parameters (H. J. G. Diersch et al., 2010). As an alternative, FEFLOW allows for inputting the borehole thermal resistance that is obtained from a TRT. Borehole thermal resistance associates with the thermal resistance between the carrier fluid and the subsurface which depends on thermal conductivity of different components like grout, subsurface, borehole wall and the carrier fluid as well as thermal short-circuiting. Thermal short-circuiting is defined as heat leakage between the upflow and downflow (i.e., inlet and outlet) shanks of the pipe (Banks, 2008).

The equation of thermal energy conservation is then discretized by finite elements and then using the Galerkin-based finite element method (GFEM), the BHE equations can be written in the generalized matrix system (H. J. G. Diersch et al., 2010). Lastly, this equation is discretized temporally. FEFLOW has two borehole solutions to solve the resulting sets of equations, the analytical BHE method based on Eskilson and Claesson solution (Claesson and Eskilson, 1987a; Claesson and Eskilson, 1987b; Eskilson & Claesson, 1988), and the numerical BHE method based on Al-Khoury et al.'s solution (R. Al-Khoury & Bonnier, 2006; R. Al-Khoury, Bonnier, & Brinkgreve, 2005). These methods are described in the following sections.

2.4.2.1 *Eskilson and Claesson's Analytical BHE Method*

Eskilson and Claesson (1987) conducted a thorough study on the numerical and analytical simulation of heat extraction from a closed-loop borehole-based system

(Claesson and Eskilson, 1987a; Claesson and Eskilson, 1987b). They presented an analytical solution of the borehole problem named after them, "Eskilson and Claesson's solution" that was based on two main assumptions:

1. The geothermal gradient was negligible and the subsurface was assumed to have an initial temperature equal to the average temperature over the borehole depth (T_0).
2. The heat flux from the surface was negligible.

An early phase solution and a steady-state solution were proposed for heat transport equation that are applicable for both heat extraction and heat injection to the subsurface (Banks, 2008):

$$T_0 - T_b \approx q_b R_b + \frac{q_b}{4\pi\lambda}\left[\ln\left(\frac{4\lambda t}{r_b^2 \rho c}\right) - 0.5772\right] \quad for\ \frac{5r_b^2\rho c}{\lambda} < t < \frac{t_s}{10} \qquad \textbf{(2-7)}$$

$$t_s \approx \frac{D^2 \rho C}{9\lambda} \qquad \textbf{(2-8)}$$

$$T_0 - T_{s,b} \approx qR_b + \frac{q}{2\pi\lambda}\ln\left(\frac{D}{2r_b}\right) \quad if\ D \gg r_b \qquad \textbf{(2-9)}$$

Where T_0 is the initial temperature and T_b is the average temperature of the carrier fluid in the borehole at time t, q_b is the heat extraction rate per meter of borehole, R_b is the borehole thermal resistance, λ is soil thermal conductivity, r_b is borehole radius, ρc volumetric heat capacity of soil, D is borehole depth and t_s is the time that steady state

condition is achieved. It should be noted that subsurface consists of both solid (soil) and fluid (groundwater) and its properties can be expressed as:

$$\rho c = n\rho^f c^f + (1-n)\rho^s c^s \quad \textbf{(2-10)}$$

$$\lambda = n\lambda^f + (1-n)\lambda^s \quad \textbf{(2-11)}$$

Where n is porosity, $\rho^f c^f$ and λ^f are volumetric heat capacity and thermal conductivity of groundwater, and $\rho^s c^s$ and λ^s are volumetric heat capacity and thermal conductivity of soil, respectively (Banks, 2008).

The analytical BHE method is a robust and efficient method especially for long-term simulations. The main drawback of this method is its inapplicability for short-term simulations. As mentioned in eq. (2-7) the solution is invalid for a time scale less than $\frac{5r_b^2\rho c}{\lambda}$. Short-term simulations are typically used to simulate thermal response tests within a simulation time ranging from a few hours to few days (H.-J. G. Diersch, 2014).

2.4.2.2 *Al-Khoury et al.'s Numerical BHE Method*

The numerical BHE method was proposed by Al-Khoury et al. for both steady-state and transient simulations (R. Al-Khoury & Bonnier, 2006; R. Al-Khoury et al., 2005). Al-khoury et al. validated their method by simulating an experiment. They also compared numerical results and analytical solutions of a line heat source embedded in an infinite

medium. Both comparisons showed good agreement between the numerical results and analytical/experimental results (R. Al-Khoury & Bonnier, 2006).

Unlike Eskilson and Claesson's analytical BHE solution, numerical BHE method of Al-Khoury et al. has shown accuracy in both short-term and long-term simulations. Al-Khoury et al.'s method was extended and adopted to FEFLOW. Some alterations to the original numerical scheme were made such as increasing the number of grout components to improve the pipe-to-grout approximation method (H. J. G. Diersch et al., 2010). Many references compared the two methods and showed their agreement in different examples (H.-J. G. Diersch, 2014; H. J. G. Diersch et al., 2010).

Chapter 3 Assessment of Environmental Impacts of a Closed-loop GSHP System on the Subsurface in Canada: Model Development and Results

3.1 Introduction

In this section, environmental impacts of a closed-loop GSHP system on the subsurface in Canada is examined. Firstly, a single borehole GSHP system is verified against previous work and secondly, a case study of a multi-borehole GSHP system is developed. Lastly, the multi-borehole model is used to simulate three regions in Canada and assess their environmental impacts.

3.2 Case Study: A Multi-borehole GSHP System

As seen from the literature review (Chapter 2), there is a lack information on the performance of GSHP systems in Canada. Therefore, the first module of the current research studies the performance and environmental impacts of a closed-loop multi-borehole GSHP system on the subsurface in typical Canadian climates. The GSHP system is used to provide annual heating and cooling of a typical office building. The same building and geological properties are assumed in three different cities of Canada to study the effect of different climatic conditions on the environmental impacts of GSHPs.

In this section, the process of selecting different cities is described, building thermal load is calculated for each city and finally, this data is used to size the GSHP system.

3.2.1 Selecting Different Cities in Canada

The environmental impacts of a GSHP system are more critical in contaminated areas due to possible migration of contaminants from surface to the aquifer (Banks, 2008). Therefore, three main factors were considered while selecting the cities:

1. Cities that have low-contaminated sites (brownfields)
2. Cities where different ground loads are required to heat/cool the building.
3. Cities that are suitable for shallow geothermal system installation.

Three different cities that satisfy above criteria were selected, namely Toronto, Vancouver and Windsor. The process of selecting these cities are as follows:

Low-contaminated sites can be found in urbanized areas and all these three cities are listed as the top 20 largest metropolitan areas in Canada (by population) (Canada Census, 2016).

The daily average temperature of these metropolitan areas was gathered from 1981-2010 climate normals and averages published by Environment Canada (Table 3.1). Environment Canada updates the climatic normals every ten years and climate normals of three periods of 1961-1990, 1971-2000 and 1981-2010 are available on Environment Canada website (Environment Canada).

Table 3.1 Climate Normals of the CMAs of 1981-2010 (Environment Canada) in °C

Month	Jan	Feb	Mar	Apr	May	Jun	Jul	Aug	Sep	Oct	Nov	Dec
Station Name: Toronto Lester B. Pearson INT'L A												
Daily Average	-5.5	-4.5	0.1	7.1	13.1	18.6	21.5	20.6	16.2	9.5	3.7	-2.2
Station Name: Montreal/Pierre Elliot Trudeau INT'L A												
Daily Average	-9.7	-7.7	-2	6.4	13.4	18.6	21.2	20.1	15.5	8.5	2.1	-5.4
Station Name: Vancouver INT'L A												
Daily Average	4.1	4.9	6.9	9.4	12.8	15.7	18	18	14.9	10.3	6.3	3.6
Station Name: Calgary INT'L A												
Daily Average	-7.1	-5.4	-1.6	4.6	9.7	13.7	16.5	15.8	11	5.2	-2.4	-6.8
Station Name: Ottawa Macdonald-Cartier INT'L A												
Daily Average	-10.3	-8.1	-2.3	6.3	13.3	18.5	21	19.8	15	8	1.5	-6.2
Station Name: Edmonton INT'L A												
Daily Average	-12.1	-9.9	-4.4	4.2	10.2	14.1	16.2	15.2	10.2	3.8	-5.4	-11
Station Name: Quebec/Jean Lesage INT'L A												
Daily Average	-12.8	-10.6	-4.6	3.7	11.2	16.4	19.3	18.1	12.7	6.6	-0.7	-8.6
Station Name: Winnipeg Richardson INT'L A												
Daily Average	-16.4	-13.2	-5.8	4.4	11.6	17	19.7	18.8	12.7	5	-4.9	-13.2
Station Name: Hamilton A												
Daily Average	-5.5	-4.6	-0.1	6.7	12.8	18.3	20.9	20	15.8	9.3	3.7	-2.3
Station Name: Waterloo Wellington A												
Daily Average	-6.5	-5.5	-1	6.2	12.5	17.6	20	18.9	14.5	8.2	2.5	-3.3
Station Name: London INT'L A												
Daily Average	-5.6	-4.5	-0.1	6.8	13.1	18.3	20.8	19.7	15.5	9.2	3.4	-2.6
Station Name: St Catharines A												
Daily Average	-3.8	-2.9	1.1	7.4	13.7	19	21.9	20.8	16.6	10.4	4.6	-0.9
Station Name: Halifax Stanfield INT'L A												
Daily Average	-5.9	-5.2	-1.3	4.4	10	15.1	18.8	18.7	14.6	8.7	3.5	-2.4
Station Name: Oshawa WPCP												
Daily Average	-4.8	-3.6	0.4	6.6	12.3	17.6	20.6	20	15.9	9.5	4.2	-1.2
Station Name: Victoria INT'L A												
Daily Average	4.6	5.1	6.8	9	12.1	14.9	16.9	16.8	14.2	10	6.4	4
Station Name: Windsor A												

Daily Average	-3.8	-2.6	2.3	8.9	15	20.5	23	22	17.9	11.3	5.1	-1.2
Station Name: Saskatoon Diefenbaker INT'L A												
Daily Average	-15.5	-12.5	-5.4	4.7	11.2	15.8	18.5	17.6	11.4	4	-6	-13.2
Station Name: Regina INT'L A												
Daily Average	-14.7	-11.7	-4.8	4.8	11.3	16.2	18.9	18.1	11.8	4.3	-5.2	-12.4
Station Name: Stillwater Sherbrooke												
Daily Average	-6.2	-5.3	-1.2	4.1	9.5	14.5	18.5	18.6	14.6	9	4.1	-1.6
Station Name: St John's A												
Daily Average	-4.5	-4.9	-2.6	1.9	6.4	10.9	15.8	16.1	12.4	7.4	3	-1.5

Since ambient temperature and duration of hot and cold seasons affect the annual required thermal load of the building, Toronto, Vancouver and Windsor were selected because of their different climate normals and winter/summer durations. Vancouver with a daily average temperature of 15.7°C in June and 18°C in July and August has very moderate summer temperatures. Small residential buildings might not even need any type of air conditioning in summer. Windsor, on the other hand, with daily average temperature of 20.5, 23 and 22°C in June, July and August has the hottest summers. Toronto is the most populated metropolitan area and has colder winters (December, January and February) than Vancouver and Windsor (Figure 3.1). Therefore, a building located in these cities requires different thermal loads resulting in different ground loads which satisfies the purpose of current research.

The average Canadian temperature climatology maps of summer and winter months are shown in Figure 3.2.

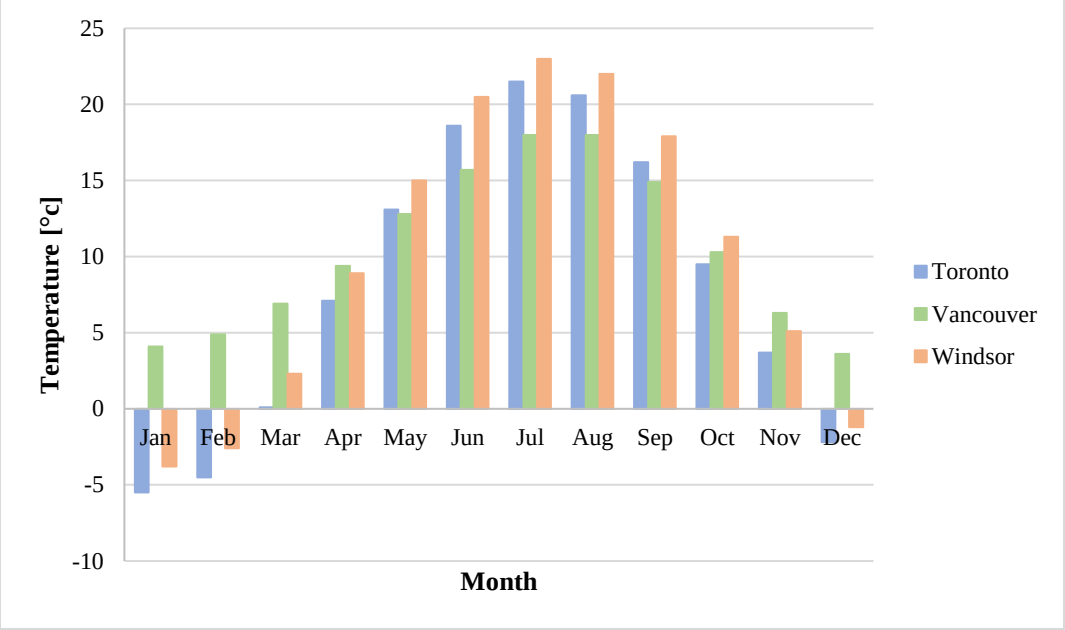

Figure 3.1 Daily Average of the Selected Cities

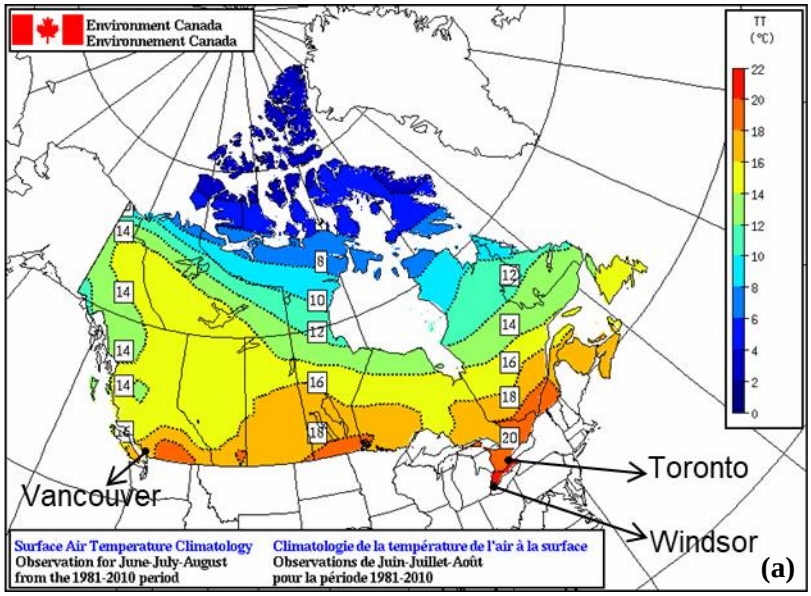

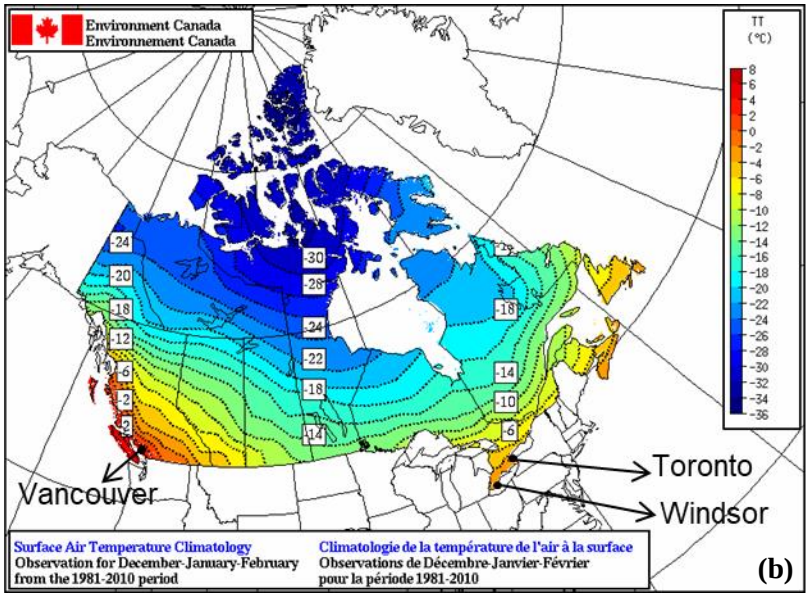

Figure 3.2 Canada temperature map during (a) summer and (b) winter (Environment Canada)

Lastly, to review the last criterion, the subsurface temperatures were examined to ensure the cities were suitable for geothermal applications. Majorowicz et al. (2009) compiled temperature maps across Canada based on well temperature-depth logs. Theses maps are illustrated for depths of 50, 100, 150, 200 and 250 m BGS (Figure 3.3). According to these maps, most of northern areas of Canada has a sub-zero temperature resulting in permafrost development which limits the usage of shallow geothermal systems in these areas. Majorowicz et al. (2009) used a 5°C temperature isoline to select zones that are suitable for shallow geothermal system installation. Based on this selection, southern Canada is the best area for shallow geothermal systems which justifies the selection of Toronto, Vancouver and Windsor as the three cities for this study.

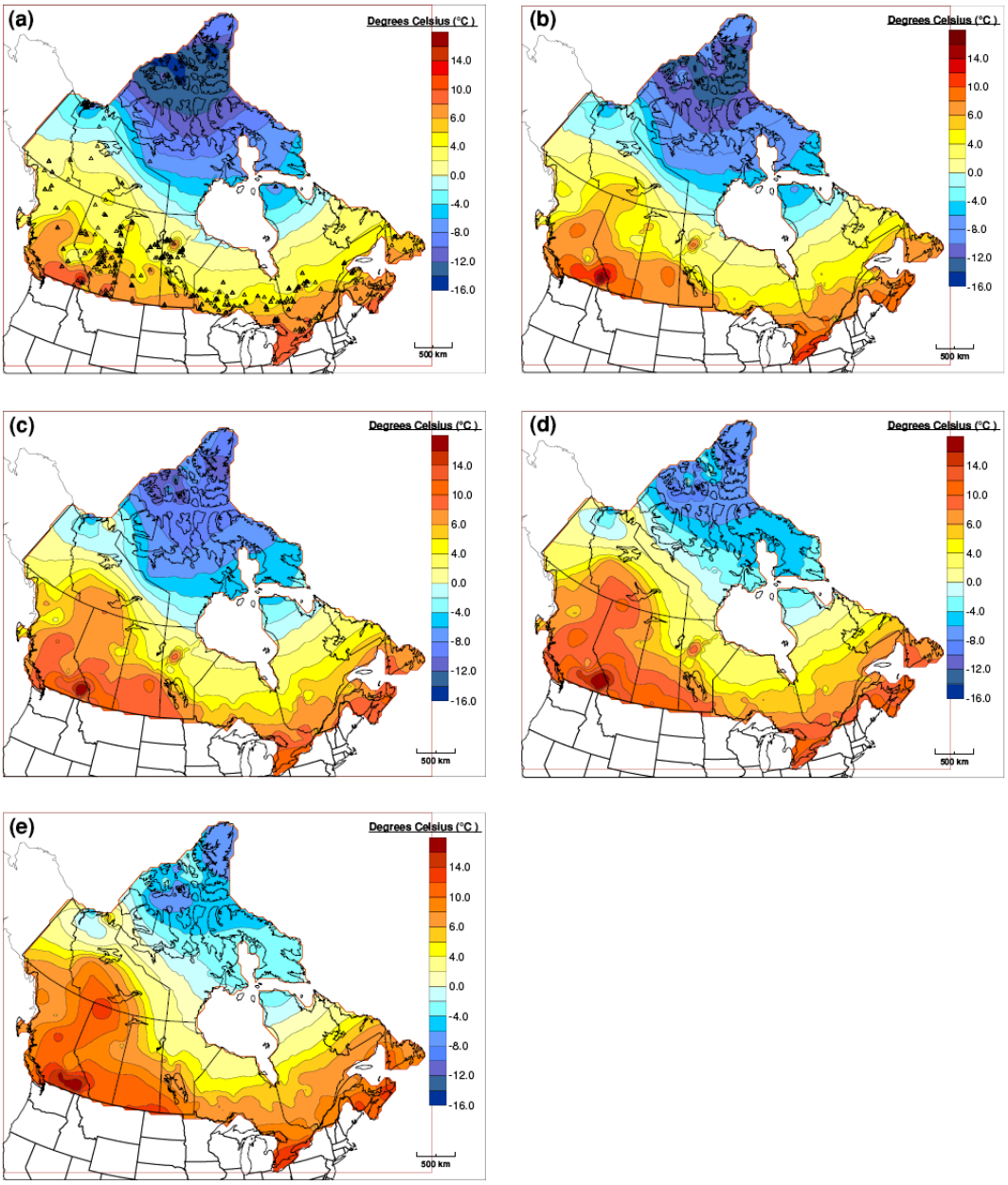

Figure 3.3 Temperature Distribution in Canada at (a) 50 m depth, (b) 100 m depth, (c) 150 m depth, (d) 200 m depth, and (e) 250 m depth (J. Majorowicz et al., 2009)

3.2.2 Building Thermal Load Calculation

There are several approaches and computer programs that are used to calculate the heating and cooling load of a building. (Chiasson, 1999) used BLAST to determine annual building loads. BLAST is a free building energy simulation software which was released in the late 1970s. It is mainly used for HVAC equipment sizing, cost analysis, and building energy consumption optimization. BLAST is now integrated into the EnergyPlus program (EnergyPlus version 8.6 documentation).

There are also rules of thumb to calculate the heating load of a building. Assuming indoor and outdoor temperatures of 20°C and 0°C, a well-insulated house requires 36 W m^{-3} heating (Sumner, 1976b). Assuming typical floor to floor height of 2.4 m, Sumner's rule can be converted to 87 Wm^{-2}. Today British engineers use a much lower estimation of 50 Wm^{-2}, which is justifiable considering the improvements in building insulation since 1976 (Banks, 2008).

Another way to evaluate building heating and cooling load is to calculate heat loss and heat gain of the building. ASHRAE (1997) presented this method to manually calculate the building heating and cooling load. This method was used in the current research because it is very user-friendly and easy to apply. The method is described in the following sections.

3.3.2.1 Reference Building Properties

An office building was assumed in the three cities of Toronto, Vancouver and Windsor. This building is called "reference building" henceforth. The reference building was selected from a report by Bhatia (n.d) and its specifications are tabulated in Table 3.2.

Table 3.2 Reference Building Specifications (Bhatia, n.d.)

Specification	**Value**
Type of building	Office
Number of floors	3
Floor area	64ft×80ft=5120 ft^2
Floor to floor height	12 ft.
Wall Construction	
Face brick	4 in
Styrofoam insulation	2 in
Concrete block	8 in
Air space	1.5 in
Plaster board	0.5 in
Wall U-value	0.09 Btu/hr ft^2 °F
North and South Facing Walls Area	2160 ft^2
East and West Facing Walls Area	1728 ft^2
Walls Area	7776 ft^2
Roof construction	
Tar and gravel (built-up)	0.375 in
Rigid insulation	2 in
Concrete	8 in
Air space	4 in
Acoustic tile	0.5 in
Roof U-value	0.04 Btu/hr ft^2 °F
Roof Area	5120 ft^2
Windows	
Type	Double glazed
Windows U-value	0.7 Btu/hr ft^2 °F
Windows Area (25% of wall)	2592 ft^2

It should be noted that both Bhatia's report and ASHRAE fundamentals handbook used United States customary system (USCS) units rather than SI units. Hence, for the sake of

simplicity and consistency, USCS units were used in the following sections and the calculated building loads were ultimately converted to SI units.

3.3.2.2 Building Heating Load Calculation

To calculate the required heating load, the heat loss during cold seasons must be calculated. Heat loss occurs due to conduction and convection processes:

- Conductive heat loss is the thermal energy lost through building surfaces such as walls, doors, windows, floor and ceiling due to temperature difference between inside and outside of the building. The dividing line between inside and outside of the building is referred to as the "Building Envelope".
- Convective heat loss is due to air movement such as heat losses through cracks and ventilation heat loss which is the heat required to warm up the air used for ventilation (Bhatia, n.d.).

Internal and solar heat gains are ignored in design heating load calculations since in this procedure heating load is estimated for the worst case corresponding to night timing when solar and internal heat gains are absent (ASHRAE, 1997). Therefore, the sum of conductive and convective heat losses is calculated to determine the total heating load of a building.

$$Heating\ Load = \dot{Q}_{conduction} + \dot{Q}_{convection} \quad \textbf{(3-1)}$$

Heat Loss Due to Conduction

Conductive heat loss is defined in terms of an overall heat transfer coefficient as follows:

$$\dot{Q} = AU(T_o - T_i) \quad \textbf{(3-2)}$$

Where $\dot{Q}$ is the total conductive heat loss, U is the overall coefficient of heat transfer of walls, roof, ceiling, windows and floor, T_o is the outside design temperature, and T_i is the inside design temperature. The coefficient of heat transfer or U-value determines how well a building surface like a window keeps heat inside the building during winter. The higher the U-value, the higher the heat loss. U-value is the inverse of R factor or thermal resistance. Total thermal resistance of a multi-layer component like a wall is the sum of the thermal resistances of each layer. Since a building has different components with different U-values, conductive heat loss for each component is calculated to estimate the total conductive heat loss of the building (Bhatia, n.d.).

In eq. (3-2) A is the net area of walls, roof, ceiling, windows and floor which is available in the drawings of the building, T_i and T_o are winter inside and outside design temperatures respectively (Bhatia, n.d.). The outside temperature for different cities is known from climate normals **(**Table 3.1**)**.

In order to get inside design temperature (T_i), a building is usually divided into thermal zones to separate areas with different temperature requirements. For example, occupied and unoccupied areas require different temperatures and hence independent

thermostats. In the current research though, for the simplicity the whole building is assumed to require the same temperature.

The inside design temperature is also termed as the baseline temperature. The baseline temperature depends on the building type and location. ASHRAE 55-2010 lists the standard for office temperatures as shown in Table 3.3. The winter inside design temperature (T_i) is usually assumed to be 18°C (Bhatia, n.d.). Internal heat generated from people, appliances and lighting as well as solar heat gain is enough to provide the ASHRAE standard temperature while setting thermostat to 18°C.

Table 3.3 Office Temperature Standard (ASHRAE 55-2010)

Conditions	Relative Humidity	Acceptable Operating Temperature [°C]
Summer (light clothing)	If 30%	24.5-28
	If 60%	23-25.5
Winter (warm clothing)	If 30%	20.5-25.5
	If 60%	20-24

The total conductive heat loss of the reference building is the sum of conductive heat loss through walls, windows and roof of the building:

$$\dot{Q}_{Conduction} = \dot{Q}_{walls} + \dot{Q}_{roof} + \dot{Q}_{windows} \quad \textbf{(3-3)}$$

Each of the right-hand side terms can be calculated from eq. (3-2):

$$\dot{Q}_{walls} = A_{wall} U_{wall} \Delta T$$
$$\dot{Q}_{roof} = A_{roof} U_{roof} \Delta T \quad \textbf{(3-4)}$$
$$\dot{Q}_{windows} = A_{window} U_{window} \Delta T$$

Substituting net area and U-values of walls, roof and windows from Table 3.2 and assuming temperature difference between winter inside design temperature of 18°C (64.4°F) and winter outside temperature (Table 3.1), conductive heat loss was calculated for the reference building located in the three cities of Toronto, Vancouver and Windsor. The results are shown in Table 3.4, Table 3.5 and Table 3.6 respectively.

Table 3.4 Toronto Conductive Heat Loss [Btu/hr]

Month	Jan	Feb	Mar	Apr	May	Sep	Oct	Nov	Dec
$\dot{Q}_{walls}$	-29603.2	-28343.5	-22548.8	-13730.9	-6172.6	-2267.5	-10707.6	-18013.9	-25446.2
$\dot{Q}_{windows}$	-76749.1	-73483.2	-58460	-35598.5	-16003	-5878.7	-27760.3	-46702.7	-65971.6
$\dot{Q}_{roof}$	-8663	-8294.4	-6598.7	-4018.2	-1806.3	-663.6	-3133.4	-5271.6	-7446.5
$\dot{Q}_{Cond.}$	-115015.4	-110121.1	-87607.5	-53347.6	-23981.9	-8809.8	-41601.3	-69988.2	-98864.3

Table 3.5 Vancouver Conductive Heat Loss [Btu/hr]

Month	Jan	Feb	Mar	Apr	May	Sep	Oct	Nov	Dec
$\dot{Q}_{walls}$	-17510	-16502.2	-13982.8	-10833.5	-6550.5	-3905.1	-9699.8	-14738.6	-18139.9
$\dot{Q}_{windows}$	-45396.3	-42783.6	-36251.7	-28086.9	-16982.8	-10124.4	-25147.6	-38211.3	-47029.2
$\dot{Q}_{roof}$	-5124.1	-4829.2	-4091.9	-3170.3	-1916.9	-1142.8	-2838.5	-4313.1	-5308.4
$\dot{Q}_{Cond.}$	-68030.4	-64115	-54326.4	-42090.7	-25450.2	-15172.3	-37685.9	-57263	-70477.5

Table 3.6 Windsor Conductive Heat Loss [Btu/hr]

Month	Jan	Feb	Mar	Apr	May	Sep	Oct	Nov	Dec
$\dot{Q}_{walls}$	-27461.7	-25950.1	-19777.5	-11463.4	-3779.1	-126	-8440.1	-16250.3	-24186.5
$\dot{Q}_{windows}$	-71197.1	-67278	-51274.9	-29719.9	-9797.8	-326.6	-21881.7	-42130.4	-62705.7
$\dot{Q}_{roof}$	-8036.4	-7594	-5787.6	-3354.6	-1105.9	-36.9	-2469.9	-4755.5	-7077.9
$\dot{Q}_{Cond.}$	-106695.2	-100822.1	-76840	-44537.9	-14682.8	-489.5	-32791.7	-63136.2	-93970.1

Heat Loss Due to Convection

Convection heat loss is the sum of heat loss due to ventilation and infiltration which are defined as (ASHRAE, 1997):

$$\dot{Q}_{ventilation} = 60(\rho c)_{air} q_v (T_o - T_i) = 1.1 q_v (T_o - T_i)$$
$$\dot{Q}_{inflitration} = 60(\rho c)_{air} q_i (T_o - T_i) = 1.1 q_i (T_o - T_i) \quad \textbf{(3-5)}$$

Where q_v and q_i are ventilation and infiltration rates and $(\rho c)_{air}$ for standard air is calculated to be 0.075×0.2445=0.01834 Btu ft^{-3} °F^{-1}. ASHRAE Standard 62 recommends minimum office ventilation rate of 20 cubic foot per minute (cfm) per person. Office occupancy is taken as 1 person per 100 ft^2 as recommended by (Ramamoorthy, Jin, & Chiasson, 2001):

$$N_{Occupants} = 0.01 A_{building} = 0.01 \times (3 \times 80 \times 64) \approx 154 \quad \textbf{(3-6)}$$

Which results in a ventilation rate of 20×154=3080 cfm.

$$\dot{Q}_{ventilation} = 1.1 \times 3080 \times \Delta T = 3388 \Delta T \quad \textbf{(3-7)}$$

Infiltration occurs through windows, doors, and walls. Windows are assumed to be properly sealed and wall infiltration is considered insignificant. An infiltration rate of 67 cfm is assumed (ASHRAE, 1997):

$$\dot{Q}_{infiltration} = 1.1 \times 67 \times \Delta T = 73.7 \Delta T \quad \textbf{(3-8)}$$

Convection heat loss for all the three cities was calculated and is listed in Table 3.7, Table 3.8 and Table 3.9.

Table 3.7 Toronto Convective Heat Loss [Btu/hr]

Month	Jan	Feb	Mar	Apr	May	Sep	Oct	Nov	Dec
$\dot{Q}_{ventilation}$	-143312.4	-137214	-109161.4	-66472.6	-29882.2	-10977.1	-51836.4	-87207.1	-123187.7
$\dot{Q}_{infiltration}$	-3117.5	-2984.9	-2374.6	-1446	-650	-238.8	-1127.6	-1897	-2679.7
$\dot{Q}_{convection}$	-146429.9	-140198.9	-111536	-67918.6	-30532.2	-11215.9	-52964	-89104.1	-125867.4

Table 3.8 Vancouver Convective Heat Loss [Btu/hr]

Month	Jan	Feb	Mar	Apr	May	Sep	Oct	Nov	Dec
$\dot{Q}_{ventilation}$	-84767.8	-79889	-67692.2	-52446.2	-31711.7	-18905	-46957.7	-71351.3	-87817
$\dot{Q}_{infiltration}$	-1844	-1737.8	-1472.5	-1140.9	-689.8	-411.2	-1021.5	-1552.1	-1910.3
$\dot{Q}_{convection}$	-86611.8	-81626.8	-69164.7	-53587.1	-32401.5	-19316.2	-47979.2	-72903.4	-89727.3

Table 3.9 Windsor Convective Heat Loss [Btu/hr]

Month	Jan	Feb	Mar	Apr	May	Sep	Oct	Nov	Dec
$\dot{Q}_{ventilation}$	-132945.1	-125627	-95744.9	-55495.4	-18295.2	-609.8	-40859.3	-78669.4	-117089.3
$\dot{Q}_{infiltration}$	-2892	-2732.8	-2082.8	-1207.2	-398	-13.3	-888.8	-1711.3	-2547.1
$\dot{Q}_{convection}$	-135837.1	-128359.8	-97827.7	-56702.6	-18693.2	-623.1	-41748.1	-80380.7	-119636.4

Total Heating Load

Total heating load is the sum of conductive and convective heat losses. A safety factor of 10% was added to the total heat loss as suggested by (Bhatia, n.d.). Results for the three cities are given in Table 3.10 in Btu hr^2 and then converted to kW.

Table 3.10 Total Heating Load [Btu/hr]

Month	Jan	Feb	Mar	Apr	May	Sep	Oct	Nov	Dec
$\dot{Q}_{Toronto}$	-287589.7	-275352	-219057.9	-133392.8	-59965.5	-22028.3	-104021.8	-175001.5	-247204.89
$\dot{Q}_{Vancouver}$	-170106.4	-160316	-135840.2	-105245.6	-63636.9	-37937.4	-94231.6	-143183	-176225.3
$\dot{Q}_{Windsor}$	-266785.5	-252100.1	-192134.5	-111364.6	-36713.6	-1223.9	-81993.8	-157868.6	-234967.2

Table 3.11 Total Heating Load [kW]

Month	Jan	Feb	Mar	Apr	May	Sep	Oct	Nov	Dec
$\dot{Q}_{Toronto}$	-84.28	-80.7	-64.2	-39.09	-17.57	-6.46	-30.49	-51.29	-72.45
$\dot{Q}_{Vancouver}$	-49.85	-46.98	-39.81	-30.84	-18.65	-11.12	-27.62	-41.96	-51.65
$\dot{Q}_{Windsor}$	-78.19	-73.88	-56.31	-32.64	-10.76	-0.36	-24.03	-46.27	-68.86

3.2.2.1 *Building Cooling Load Calculation*

To estimate building cooling load, the heat gain during hot seasons must be calculated. Cooling load calculations are more complicated than heating load calculations, because unlike cold seasons, in hot seasons outside temperature changes significantly during the day due to sunlight. Furthermore, in cooling load calculations, internal heat generation (respiration and electrical equipment) must be calculated accurately since it adds to the heat gain that must be counterbalanced to deliver a comfortable indoor temperature (Bhatia, 2001).

The space design cooling load is calculated by CLTD/SCL/CLF[1] method presented in ASHRAE fundamental handbook, 1997. According to this method, cooling load is divided into external and internal loads. External cooling load includes conduction through roof, walls and windows, solar radiation through glass and cooling load from partitions, ceilings and floors. Internal cooling load includes people, lights, appliances and ventilation and infiltration (ASHRAE, 1997):

[1] CLTD: Cooling Load Temperature Difference, SCL: Solar Cooling Load, CLF: Cooling Load Factor

$$Cooling\ Load = \dot{Q}_{roof} + \dot{Q}_{walls} + \dot{Q}_{windows} + \dot{Q}_{solar} + \dot{Q}_{people} + \dot{Q}_{lights} + \dot{Q}_{appliances} + \dot{Q}_{ventilation} + \dot{Q}_{infiltration} \quad \textbf{(3-9)}$$

The contribution of each term to the total cooling load of the reference office building is calculated in the following sections.

Heat Gain Due to Conduction

Conductive heat gain through roof, walls and windows is defined as:

$$\dot{Q} = AU(CLTD) \quad \textbf{(3-10)}$$

Where *CLTD* is cooling load temperature difference. The CLTD value obtained form (ASHRAE, 1997) and some sample calculations are given in Appendix A. The CLTD values were determined for a specific case corresponding to an inside temperature of 78°F, outdoor maximum and mean temperatures of 95°F and 85°F which are typical of 40°N latitude on July 21. Therefore, CLTDs obtained from these tables must be adjusted for the current case. The corrected CLTD is calculated as (ASHRAE, 1997):

$$CLTD_{Corr.} = CLTD + (78 - T_i) + (T_m - 85) \quad \textbf{(3-11)}$$

Where T_m is mean outdoor temperature of each city during summer and T_i is summer inside design temperature which is set to 68°F (20°C). Winter inside design temperature is usually lower than summer inside design temperature and is set to 18°C (ASHRAE, 1997).

Substituting roof properties from Table 3.2 into eq. (3-10), conductive heat gain through roof for the three cities was calculated (Table 3.12).

Table 3.12 Conductive Heat Gain Through Roof

City	Toronto			Vancouver			Windsor		
Month	**Jun**	**Jul**	**Aug**	**Jun**	**Jul**	**Aug**	**Jun**	**Jul**	**Aug**
$CLTD_{Corr.}$[°F]	18.5	23.7	22.1	13.3	17.4	17.4	21.9	26.4	24.6
$\dot{Q}_{roof}$	3784.7	4853.8	4522	2715.6	3563.5	3563.5	4485.1	5406.7	5038.1

The same procedure applies to walls. The CLTD value obtained form ASHRAE (1997) and some sample calculations are given in Appendix A. Corrected CLTD values and conductive heat gain through walls is tabulated in Table 3.13.

Table 3.13 Conductive Heat Gain Through Walls ($CLTD_{corr.}$ given in $°F$ and $\dot{Q}$ given in Btu/hr)

City	Toronto			Vancouver			Windsor		
Month	**Jun**	**Jul**	**Aug**	**Jun**	**Jul**	**Aug**	**Jun**	**Jul**	**Aug**
North walls $CLTD_{Corr.}$	-0.6	4.6	3	-5.8	-1.7	-1.7	2.8	7.3	5.5
$\dot{Q}_{North\ walls}$	-120.5	894.2	579.3	-1135.3	-330.5	-330.5	544.3	1419.1	1069.2
East walls $CLTD_{Corr.}$	11	16.2	14.6	5.8	9.9	9.9	14.4	18.9	17.1
$\dot{Q}_{East\ walls}$	1707.6	2519.4	2267.5	895.8	1539.6	1539.6	2239.5	2939.3	2659.4
South walls $CLTD_{Corr.}$	2	7.2	5.6	-3.2	0.9	0.9	5.4	9.9	8.1
$\dot{Q}_{South\ walls}$	384.9	1399.7	1084.8	-629.9	175	175	1049.8	1924.6	1574.6
West walls $CLTD_{Corr.}$	3. 8	9	7.4	-1.4	2.7	2.7	7.2	11.7	9.9
$\dot{Q}_{West\ walls}$	591	1399.7	1150.8	-217.7	419.9	419.9	1119.7	1819.6	1539.6
$\dot{Q}_{walls}$	2563	6213	5082.4	-1087.1	1804	1804	4953.3	8102.6	6842.8

The mean CLTD for conductive heat gain through windows is 8.8°F , from Table 34 of ASHRAE (1997). Substituting windows properties (Table 3.2) and the mean CLTD into eq. (3-10) gives the conductive heat gain through windows for three cities as tabulated in Table 3.14. sample calculation is given in Appendix A

Table 3.14 Conductive Heat Gain Through Windows ($CLTD_{corr.}$ given in $°F$ and $\dot{Q}$ given in Btu/hr)

City	Toronto			Vancouver			Windsor		
Month	**Jun**	**Jul**	**Aug**	**Jun**	**Jul**	**Aug**	**Jun**	**Jul**	**Aug**
$CLTD_{Corr.}$	-0.7	4.5	2.9	-5.9	-1.8	-1.8	2.7	7.2	5.4
$\dot{Q}_{windows}$	-1306.4	8164.8	5225.5	-10777.5	-3265.9	-3265.9	4898.9	13063.7	9797.8

Heat Gain Due to Solar Radiation

Heat gain due to radiation through glass is given by:

$$\dot{Q}_{solar} = A_{window} \times SC \times SCL \qquad \textbf{(3-12)}$$

Where *SC* is shading coefficient and *SCL* is solar cooling load factor. The values of *SC* and *SCL* obtained form ASHRAE (1997) and some sample calculations are given in Appendix A. The heat gain due to solar radiation is tabulated in Table 3.15.

Table 3.15 Heat Gain due to Solar Radiation (Btu/hr)

$\dot{Q}_{North\ windows}$	13028.4
$\dot{Q}_{East\ windows}$	28005.1
$\dot{Q}_{South\ windows}$	23047.2
$\dot{Q}_{West\ windows}$	25027.2
$\dot{Q}_{Solar}$	**89107.9**

Heat Gain Produced by People

People cooling load is classified into latent and sensible heat gain. Sensible heat gain is the heat that is added to the building by one of the common means of heat transfer, i.e., conduction, convection and/or radiation. Latent heat gain happens when moisture is

added to the building interior, and in the case of people heat gain, it is the vapor emitted by people. Sensible and latent heat gain produced by people is expressed as (ASHRAE, 1997):

$$\dot{Q}_{sensible} = N_{Occupants} \times Q_s \times CLF$$
$$\dot{Q}_{latent} = N_{Occupants} \times Q_l \quad \textbf{(3-13)}$$

Where N is the number of people in space (eq. (3-6)), CLF is cooling load factor and Q_s and Q_l are sensible and latent heat gains respectively. The values of Q_s, Q_l and CLF obtained form ASHRAE (1997) and a sample calculation are given in Appendix A. The total heat gain produced by people is calculated as follows:

$$\dot{Q}_{people} = \dot{Q}_{sensible} + \dot{Q}_{latent} = 55185.9\ Btu/hr \quad \textbf{(3-14)}$$

Heat Gain Produced by Lights

Lights contribution to cooling load is given by (ASHRAE, 1997):

$$\dot{Q}_{lights} = 3.41 \times W \times F_{ul} \times F_{sa} \times CLF \quad \textbf{(3-15)}$$

Where W is watts input, F_{ul} is lighting use factor and F_{sa} is special allowance factor. A use factor of 1 and a special allowance factor of 1.2 is assumed for fluorescent lamps with wattage of 17,500:

$$\dot{Q}_{lights} = 3.41 \times 17500 \times 1 \times 1.2 \times 0.83 = 59436.3\ Btu/hr \quad \textbf{(3-16)}$$

Heat Gain Produced by Appliances

The simple assumption of 1.1 W/ft^2 office equipment plug load, as suggested by (Komor, 1997) was used to determine appliances cooling load:

$$\dot{Q}_{appliances} = 1.1\frac{W}{ft^2} = 1.1 \times (3 \times 5120) = 16896\ W$$
$$= 57615.36\ Btu/hr \quad \textbf{(3-17)}$$

Heat Gain Due to Convection

Convection heat gain is the sum of heat gain due to ventilation and infiltration which for the case of ventilation is defined as (ASHRAE, 1997):

$$\dot{Q}_{sensible} = 1.1 \times q_v \times (T_o - T_i)$$
$$\dot{Q}_{latent} = 4840 \times q_v \times (HR_o - HR_i) \quad \textbf{(3-18)}$$

Where q_v is ventilation rate, T_o and T_i are outside and inside air temperatures, HR_o and HR_{in} are outside and inside air humidity ratio. In the case of infiltration, q_v is substituted by infiltration rate (q_i). The values of each parameter and a sample calculation are given in Appendix A. Outside air humidity, sensible, latent and total cooling load from ventilation is calculated in Table 3.16. Sensible, latent and total cooling load from infiltration is calculated in Table 3.17.

Table 3.16 Heat Gain Due to Ventilation [Btu/hr]

City	Toronto			Vancouver			Windsor		
Month	Jun	Jul	Aug	Jun	Jul	Aug	Jun	Jul	Aug
HR_o	0.0135	0.0162	0.0153	0.0112	0.013	0.013	0.0152	0.0178	0.0167
$\dot{Q}_{sensible}$	-8537.8	9147.6	3659	-26223.1	-12196.8	-12196.8	3049.2	18295.2	12196.8
$\dot{Q}_{latent}$	-18753.3	21883.8	8526.9	-53159.1	-26355.9	-26355.9	7080.9	45690.6	29605.7
$\dot{Q}_{ventilation}$	-27291	31031.4	12186	-79382.2	-38552.7	-38552.7	10130.1	63985.8	41802.5

Table 3.17 Heat Gain Due to Infiltration [Btu/hr]

City	Toronto			Vancouver			Windsor		
Month	Jun	Jul	Aug	Jun	Jul	Aug	Jun	Jul	Aug
$\dot{Q}_{sensible}$	-185.7	199	79.6	-570.4	-265.3	-265.3	66.3	398	265.3
$\dot{Q}_{latent}$	-407.9	476	185.5	-1156.4	-573.3	-573.3	154	993.9	644
$\dot{Q}_{infiltration}$	-593.7	675	265.1	-1726.8	-838.6	-838.6	220.4	1391.9	909.3

Total Cooling Load

Total cooling load for the reference building located in the three cities of Toronto, Vancouver and Windsor is calculated from eq. (3-9) and given in Table 3.18.

Table 3.18 Total Cooling Load

City	Toronto			Vancouver			Windsor		
Month	Jun	Jul	Aug	Jun	Jul	Aug	Jun	Jul	Aug
$\dot{Q}_{Cooling}$ [Btu/hr]	238499	312283.5	288623.3	171081.3	224055.7	224055.7	286033.3	353296.1	325736.04
$\dot{Q}_{Cooling}$ [kW]	69.9	91.5	84.6	50.14	65.7	65.7	83.8	103.5	95.46

3.3.2.3 Building Thermal Load

Combining Table 3.11 and Table 3.18, total monthly thermal load of the reference building in each city is listed in Table 3.19 and shown in Figure 3.4. Heating load is shown with negative sign and cooling load is shown with positive sign.

Table 3.19 Monthly Thermal Load of the Reference Building Located in Different Cities (kW)

Month	Jan	Feb	Mar	Apr	May	Jun	Jul	Aug	Sep	Oct	Nov	Dec
$\dot{Q}_{Toronto}$	-84.3	-81	-64	-39.1	-17.6	69.9	91.5	84.6	-6.5	-30.5	-51.3	-72.4
$\dot{Q}_{Vancouver}$	-49.8	-47	-39.8	-30.8	-18.6	50.1	65.7	65.7	-11.1	-27.6	-42	-51.6
$\dot{Q}_{Windsor}$	-78.2	-74	-56.3	-32.6	-10.8	83.8	103.5	95.5	-0.4	-24	-46.3	-68.9

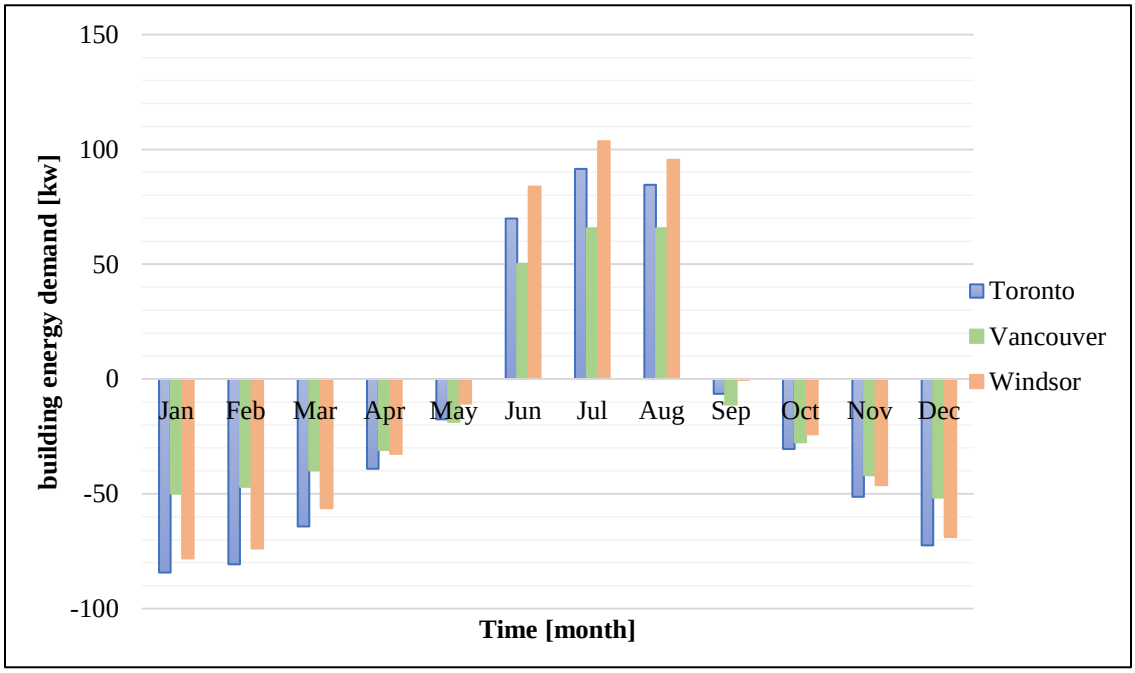

Figure 3.4 Monthly Thermal Load of the Reference Building Located in Toronto, Vancouver and Windsor

The difference between thermal load of the reference building located in three cities is clearly noticeable. Vancouver has temperate climate and requires significantly less cooling during summer and less heating during cold seasons compared to two other cities.

Windsor and Toronto, on the other hand, require the most heating and cooling loads, respectively.

3.2.3 Conversion of Building Load to Ground Load

Calculated building loads were converted to ground loads using eq. (1-4) and eq. (1-5) and assuming a constant COP of 4 for both heating and cooling modes as suggested by (Chiasson, 1999):

$$G_H = H - E = H - \frac{H}{COP_H} = \frac{3}{4}H \quad \textbf{(3-19)}$$

$$G_C = C + E = C + \frac{C}{COP_C} = \frac{5}{4}H \quad \textbf{(3-20)}$$

Where H and C are total heating and cooling effects required by the building, and G_H and G_C are heat extracted from the ground and heat injected into the ground, i.e., ground load to provide the building demand.

The ground load was calculated for the three cities and listed in Table 3.20. G_H and G_C were combined into a new symbol of Q_{gr} that represents the ground load.

Table 3.20 Monthly Ground Loads of the Reference Building Located in Different Cities (kW)

Month	Jan	Feb	Mar	Apr	May	Jun	Jul	Aug	Sep	Oct	Nov	Dec	Imbalance
$\dot{Q}_{gr,Toronto}$	-63.2	-60.5	-48.2	-29.3	-13.2	87.4	114.4	105.7	-4.8	-229	-38.5	-54.3	-27.38
$\dot{Q}_{gr,Vancouver}$	-37.4	-35.2	-29.9	-23.1	-14.0	62.7	82.1	82.1	-8.3	-20.7	-31.5	-38.7	-12.04
$\dot{Q}_{gr,Windsor}$	-58.6	-55.4	-42.2	-24.5	-8.1	104.8	129.4	119.3	-0.3	-18.0	-34.7	-51.7	60.06

Figure 3.5 illustrates calculated ground load for different cities. Heating load is negative representing heat extraction from the ground and cooling load is positive, representing heat injection to the ground.

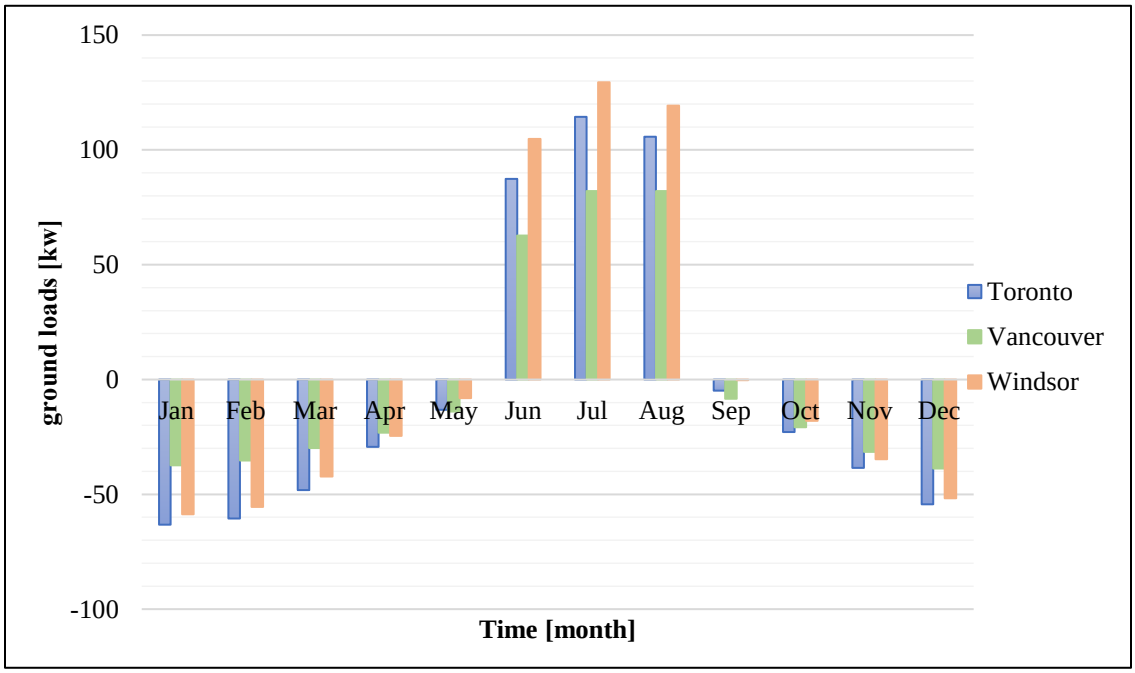

Figure 3.5 Monthly Ground Load of the Reference Building Located in Toronto, Vancouver and Windsor

3.2.4 Sizing the GSHP System

In the current section, the process of sizing the GSHP system is described. Sizing a GSHP system is a detailed process that determines number of boreholes, their depth, spacing and layout based on the ground loads. It can be conducted via commercially available design programs such as GLHEPRO (Spitler et al., 1996).

In the current research, a simpler calculation is used to size the GSHP system. The number of boreholes required to deliver calculated ground loads is given by (Hecht-Méndez et al., 2013):

$$N = \frac{Q_{gr}}{q_b \times D} \quad \textbf{(3-21)}$$

Where N is number of boreholes, q_b is heat extraction rate per meter of borehole[2] and D is borehole depth.

A heat extraction rate of 50 W m^{-1} was assumed (R. Al-Khoury & Bonnier, 2006; Hecht-Méndez et al., 2013). The typical capacity of a borehole with a depth of 40 to 180 m is between 2 kW and 17 kW resulting in an extraction rate of 50 to 94 W per drilled meter. Assuming a coefficient of performance of 3.4 in heating mode and using eq. (1-4), leads to an average heat extraction rate of 50 W m^{-1}. Since most thermal subsurface properties does not change significantly with rock and soil type, the rule of thumb of 50 W m^{-1} specific heat absorption rate was assumed (Banks, 2008).

It should be noted that a GSHP system satisfying the thermal load of the reference building can be designed specifically for each city, but since the objective of the current research was to determine the effect of climate on GSHP performance, one GSHP system were designed for all three cities. Therefore, the peak load which was 129.43 kW

[2] Also known as heat pipe capacity (R. Al-Khoury & Bonnier, 2006)

corresponding to July of Windsor was substituted for Q_{gr} in eq. (3-21). Assuming a typical borehole length of 150 m, N was calculated to be 18.

$$N = \frac{Q_{gr}}{q_b \times D} = \frac{129.43 \times 1000}{50 \times 150} \approx 18 \qquad \textbf{(3-22)}$$

In the following sections, a numerical model of an 18-borehole GSHP system is developed and verified in FEFLOW for the three cities of Toronto, Vancouver and Windsor.

3.2.5 Model Setup Verification

To verify model setup and enhance understanding of FEFLOW BHE solutions, two examples from Diersch (2014) were generated using FEFLOW. The first example was a single 2U exchanger with constant heat input rate, and the second one was a single coaxial BHE system with time-varying heat input rate and no groundwater flow. Although it was preferable to regenerate a multi-borehole system, no such example was found.

3.2.5.1 *2U Exchanger Example*

The first example simulated a 2U BHE system located in the center of a 20×20×55m domain. A steady-state groundwater flow with a constant hydraulic gradient (W-E) was assigned. Both analytical and numerical BHE solutions were applied. Parameters used in

this example are given in Table 3.21 while the boundary and initial conditions are given in Table 3.22.

Table 3.21 2U Example Parameters and Material Properties (H.-J. G. Diersch, 2014)

Quantity	***Symbol***	***Value***	***Unit***
Depth of borehole	D	55	m
Borehole Diameter	d	12	cm
Outer diameter of pipes-in/pipes-out	d_i^o & d_o^o	3.2	cm
Pipes-in/pipes-out wall thickness	b_i & b_o	2.9	mm
Pipe distance	w	4.2	cm
Reference temperature	T_0	10	°C
Thermal conductivities of pipe walls	λ_i & λ_o	0.38	J m^{-1} s^{-1} K^{-1}
Total flow rate of refrigerant	Q_r	38.284	m^3 d^{-1}
Total heat input rate[3]	$\lvert Q_T \rvert$	6.3242×10^9	J d^{-1}
Volumetric heat capacity of refrigerant	$\rho^r c^r$	4.13×10^6	J m^{-3} K^{-1}
Thermal conductivity of refrigerant	λ^r	0.65	J m^{-1} s^{-1} K^{-1}
Dynamic viscosity of refrigerant	μ^r	0.52×10^{-3}	kg m^{-1} s^{-1}
Mass density of refrigerant	ρ^r	0.938×10^3	kg m^{-3}
Volumetric heat capacity of grout	$\rho^g c^g$	2.19×10^6	J m^{-3} K^{-1}
Thermal conductivity of grout	λ^g	2.3	J m^{-1} s^{-1} K^{-1}
Porosity of soil	n	0.2	-
Volumetric heat capacity of groundwater	$\rho^f c^f$	4.2×10^6	J m^{-3} K^{-1}
Volumetric heat capacity of soil	$\rho^s c^s$	2.405×10^6	J m^{-3} K^{-1}
Thermal conductivity of groundwater	λ^f	0.65	J m^{-1} s^{-1} K^{-1}
Thermal conductivity of soil	λ^s	2.46	J m^{-1} s^{-1} K^{-1}
Anisotropy of soil	Ξ_{aniso}^{λ}	1	-
Longitudinal thermodispersivity of aquifer	α_L	0.5	m
Transverse thermodispersivity of aquifer	α_T	0.05	m
Initial time step size[4]	Δt_0	10^{-8}	d
Simulation time	t_{end}	365	d
RMS error tolerance	ϵ	10^{-3}	-
Maximum growth factor between subsequent time steps	Ξ	2	-

[3] The inlet temperature is calculated to be $T_i = Q_T/(\rho^r c^r Q_r) + T_0 = 6.3242 \times 10^9/(4.13 \times 10^6 \times 38.284) + 10 = 50°C$.

[4] The predictor-corrector scheme is set to first-order accurate (FE/BE).

Table 3.22 2U Example Initial and Boundary Conditions (H.-J. G. Diersch, 2014)

Condition	*Value*	*Unit*
Dirichlet type BC for h at left boundary	0	m
Dirichlet type BC for h at right boundary	-0.02	m
No-flow boundary at North and South	-	-
Initial condition of T	10	°C
Adiabatic boundary at North and South	-	-

Diersch (2014) used a mesh consisting of 55 layers and 130,185 pentahedral elements which were refined around the BHE (H.-J. G. Diersch, 2014). In the current attempt of regeneration 129,855 elements and 55 layers were used. The produced finite element mesh is shown in Figure 3.6.

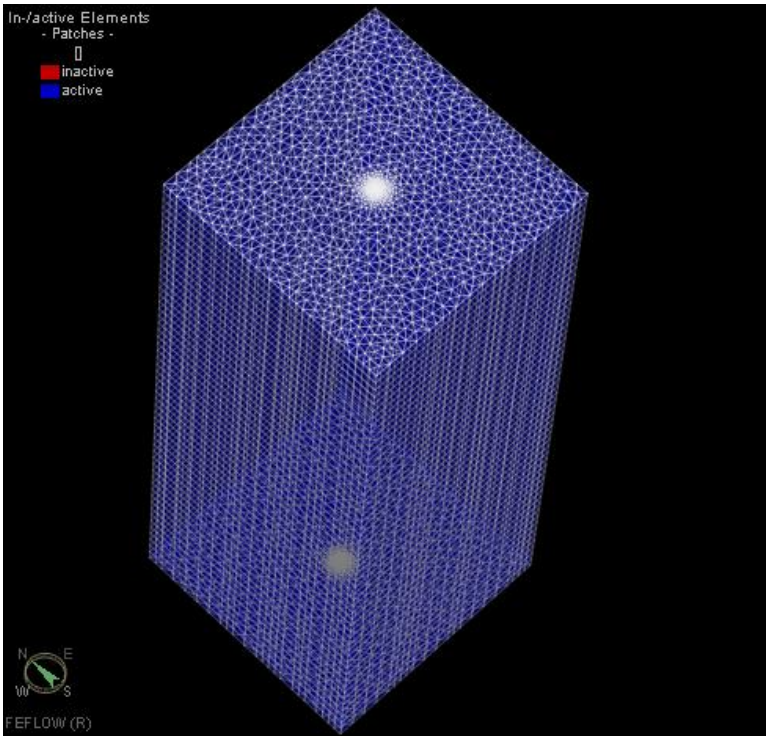

Figure 3.6 Finite Element Mesh Consisting of 129,855 Pentahedral Elements Produced for 2U Example

Two computational methods of fully transient (Al-Khoury et al.) and quasi-stationary (Eskilson and Claesson) were used. In FEFLOW, these methods are termed as BHE numerical and BHE analytical solutions, respectively. Thermal resistances and heat transfer of coefficients were calculated and the values were the same as those listed by Diersch (2014). The outlet temperature of the numerical and analytical BHE solutions after 90 minutes (short-term) were compared to Diersch (2014) and shown in Figure 3.7. The current model showed the same trend of short-term outlet temperature for both analytical and numerical BHE solutions as Diersch (2014) results, but overestimated the outlet temperature by approximately 2°C in both solutions.

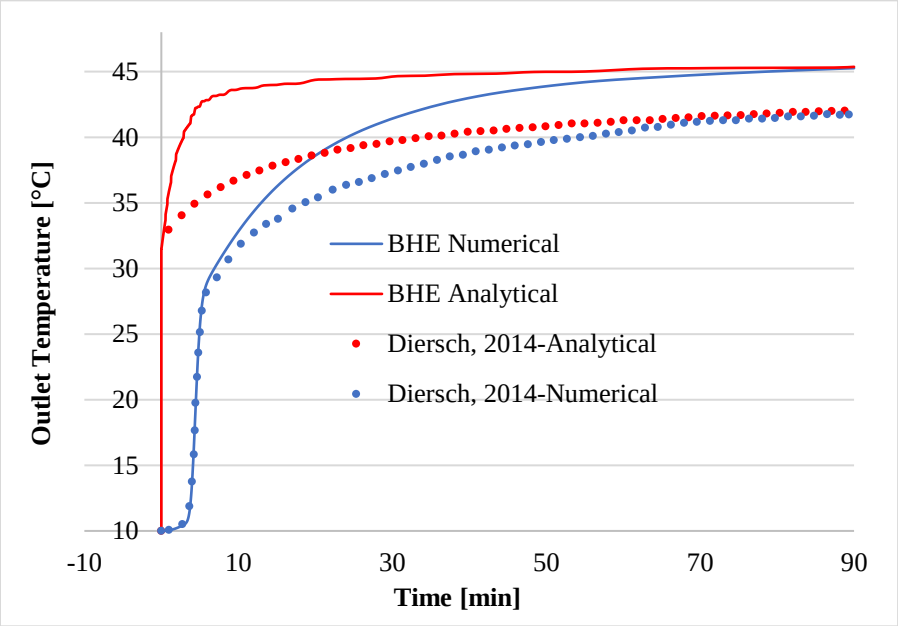

Figure 3.7 Short-term Outlet Temperature History of the Analytical and Numerical BHE Solutions, Comparison between Current Model and Diersch (2014) Results

The long-term (1 year) outlet temperature of the analytical BHE solution was also simulated and compared with Diersch (2014) and shown in Figure 3.8. The comparison also shows a small (<2°C) overestimate of the outlet temperatures by the model.

The difference can be due to the different meshing applied, or possibly some model settings that was not mentioned by Diersch (2014), and hence was assumed as FEFLOW default in the current model. Since the current research deals with long-term simulations, the observed difference between the FEFLOW model and Diersch (2014) long-term solutions were deemed acceptable.

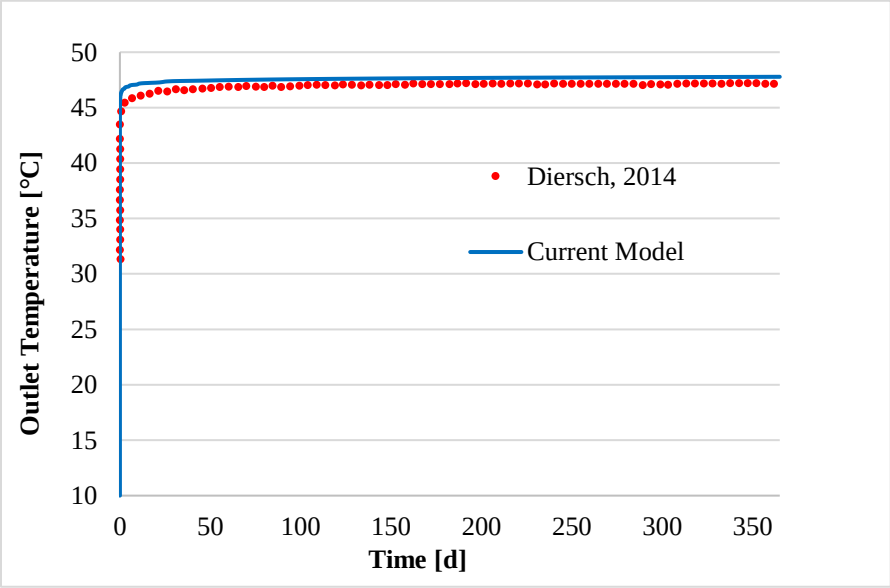

Figure 3.8 Long-term Outlet Temperature History of the Analytical BHE Solution, Comparison between Current Model and Diersch (2014) Results

3.2.5.2 *Coaxial Exchanger Example*

As another verification, a simple BHE example presented by Diersch (2014) was regenerated. The example is called “transient solution of coaxial BHE system” and simulates a BHE coaxial pipe system of CXA type located in the center of the domain. The domain measures 100×100×100 m and the soil is considered impervious with no groundwater flow. A time-varying heat injection is simulated where in the time range of ($0 < t \leq 90\ d$) the temperature of the injected water is set to 80°C and in the time range of ($90 < t \leq 180\ d$) the injection temperature is 10°C. Both analytical and numerical BHE solutions are applied. Parameters used in this example and the applied boundary and initial conditions are given in Table 3.23 and Table 3.24 (H.-J. G. Diersch, 2014).

Table 3.23 Coaxial Example Parameters and Material Properties (H.-J. G. Diersch, 2014)

Quantity	*Symbol*	*Value*	*Unit*
Depth of borehole	D	100	m
Borehole Diameter	d	10	cm
Outer diameter of pipes-in	d_i^o	5	cm
Outer diameter of pipes-out	d_o^o	2.4	cm
Pipe-in wall thickness	b_i	4	mm
Pipe-out wall thickness	b_o	3	mm
Reference temperature	T_0	10	°C
Thermal conductivities of pipe walls	λ_i & λ_o	0.38	J m^{-1} s^{-1} K^{-1}
Total flow rate of refrigerant	Q_r	1.0931	m^3 d^{-1}
Total heat input rate	$\lvert Q_T(t)\rvert$	3.1602×10^8 (0<t≤90 d) 0 (90<t≤180 d)	J d^{-1}
Volumetric heat capacity of refrigerant	$\rho^r c^r$	4.13×10^6	J m^{-3} K^{-1}
Thermal conductivity of refrigerant	λ^r	0.48	J m^{-1} s^{-1} K^{-1}
Dynamic viscosity of refrigerant	μ^r	0.52×10^{-3}	kg m^{-1} s^{-1}
Mass density of refrigerant	ρ^r	0.988×10^3	kg m^{-3}
Volumetric heat capacity of grout	$\rho^g c^g$	2.19×10^6	J m^{-3} K^{-1}
Thermal conductivity of grout	λ^g	2.3	J m^{-1} s^{-1} K^{-1}
Porosity of soil	n	0	-
Volumetric heat capacity of soil	$\rho^s c^s$	2.21×10^6	J m^{-3} K^{-1}
Thermal conductivity of soil	λ^s	2.2	J m^{-1} s^{-1} K^{-1}
Anisotropy of soil	Ξ^{λ}_{aniso}	1	-
Initial time step size[5]	Δt_0	10^{-6}	d
Simulation time	t_{end}	180	d
RMS error tolerance	ϵ	10^{-3}	-
Maximum growth factor between subsequent time steps	Ξ	2	-

Table 3.24 Coaxial Example Initial and Boundary Conditions (H.-J. G. Diersch, 2014)

Condition	*Value*	*Unit*
No-flow boundary at North and South	-	-
Initial condition of T	10	°C
Adiabatic boundary at North and South	-	-

In the current model, a hydraulic head of -1 m was assigned at western and eastern boundaries to apply a zero groundwater flow condition. Finite element mesh that was

[5] The predictor-corrector scheme is set to first-order accurate (FE/BE).

used by Diersch (2014) consisted of 239,100 pentahedral elements, here 232,200 elements were used.

Short-term and long-term outlet temperature histories computed by current model and Diersch (2014) are compared in Figure 3.9 and Figure 3.10 for numerical BHE solution. There is a good agreement between the two models, but current model overestimates outlet temperature by approximately 1°C in the short-term case. The reason for that could be different meshing.

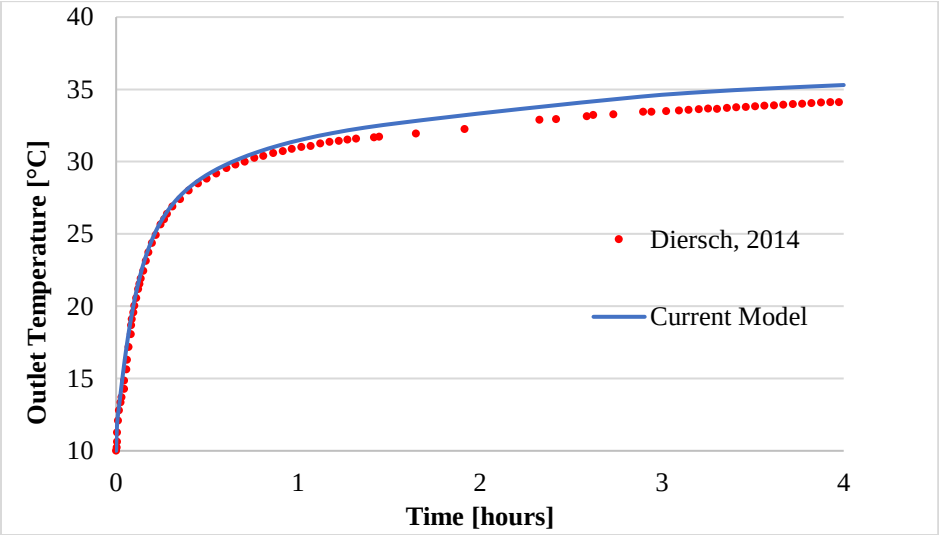

Figure 3.9 Short-term Outlet Temperature History of the Numerical BHE Solution, Comparison between Current Model and Diersch (2014) Results

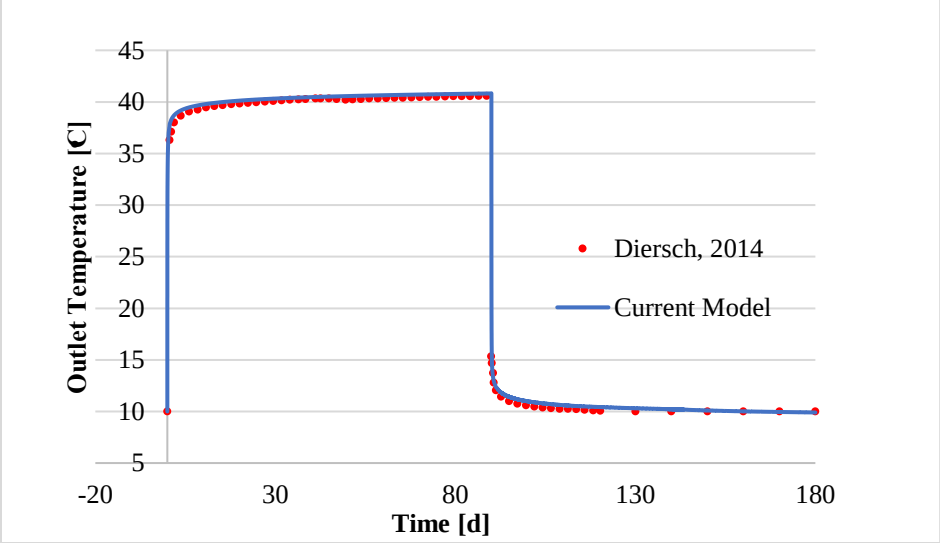

Figure 3.10 Long-term Outlet Temperature History of the Numerical BHE Solution, Comparison between Current Model and Diersch (2014) Results

In both examples, developed model showed good agreement with Diersch (2014) results showing that model setup in FEFLOW is verified.

3.2.6 Model Development

In this section, a 3D model simulating an 18-BHE ground source heat pump system is developed in FEFLOW and the model setup is described. To develop the model, properties like domain size, meshing, initial and boundary conditions, as well as, material properties must be specified. In the following sections, each one of these settings are discussed.

3.2.6.1 *Parameters and Material Properties*

The model as sized in section 3.2.4 is a BHE field with heat pump capacity of 130 kW containing 18 boreholes. The borehole parameters and material properties of the current model are listed in Table 3.25.

Boreholes were arranged in a 6×3 layout. Various borehole array configurations are available, such as lines of boreholes, rectangular blocks of boreholes, open rectangles (boreholes are placed on the perimeter of a rectangle) and L-shaped arrays. For single-mode systems a more open layout such as line of boreholes and open rectangles are preferred since these layouts facilitate migration of the thermal plume. In dual mode systems, on the other hand, closed layouts like rectangular blocks are favorable since they trap the heat inside the Borefield during summer and extract it in winter (Banks, 2008). Consequently, a 6×3 layout was a reasonable choice for the current model.

A horizontal and vertical bore spacing of 10 m was assigned per suggested by (Hecht-Méndez et al., 2013). Banks (2008) also suggested a bore spacing of 10 m for heating or cooling dominated systems and less spacing for balanced-load schemes.

A 2U exchanger was selected and FEFLOW default parameters were used for the properties of the borehole heat exchanger such as borehole diameter, pipes diameter, pipes wall thickness, pipe distance and pipes thermal conductivity. In addition, the refrigerant was assumed to be a solution of water and antifreeze. FEFLOW default properties were used for both refrigerant and grout properties.

The subsurface was assumed to be homogeneous and isotropic and coarse sand was assumed for the whole domain. Soil properties were taken from Chiasson (1999).

Simulation time was taken to be 10 years in order to examine the effect of a long GSHP operation. Most GSHPs have a lifetime of 20 to 25 years.

Table 3.25 Borehole Parameters and Material Properties

Quantity	***Symbol***	***Value***	***Unit***
Domain Size	Length×Width×Depth	300×150×200	m^3
Borehole Array Configuration	Columns×Rows	6×3	-
Horizontal and Vertical Bore Spacing	$\Delta x \; or \; \Delta y$	10	m
Depth of borehole	D	150	m
Borehole Diameter	d	15	cm
Outer diameter of pipes-in/pipes-out	d_i^o & d_o^o	3.2	cm
Pipes-in/pipes-out wall thickness	b_i & b_o	2.9	mm
Pipe distance	w	4	cm
Reference temperature	T_0	10	°C
Thermal conductivities of pipe walls	λ_i & λ_o	0.42	J m^{-1} s^{-1} K^{-1}
Total flow rate of refrigerant	Q_r	0.0072	m^3 s^{-1}
Volumetric heat capacity of refrigerant	$\rho^r c^r$	4 ×10^6	J m^{-3} K^{-1}
Thermal conductivity of refrigerant	λ^r	0.48	J m^{-1} s^{-1} K^{-1}
Dynamic viscosity of refrigerant	μ^r	3×10^{-3}	kg m^{-1} s^{-1}
Mass density of refrigerant	ρ^r	1.052×10^3	kg m^{-3}
Volumetric heat capacity of grout	$\rho^g c^g$	2.5×10^6	J m^{-3} K^{-1}
Thermal conductivity of grout	λ^g	1	J m^{-1} s^{-1} K^{-1}
Porosity of soil	n	0.385	-
Hydraulic Conductivity of Soil	K	7.3×10^{-5}	m s^{-1}
Volumetric heat capacity of groundwater	$\rho^f c^f$	4.2×10^6	J m^{-3} K^{-1}
Volumetric heat capacity of soil	$\rho^s c^s$	1.4×10^6	J m^{-3} K^{-1}
Thermal conductivity of groundwater	λ^f	0.65	J m^{-1} s^{-1} K^{-1}
Thermal conductivity of soil	λ^s	0.8	J m^{-1} s^{-1} K^{-1}
Anisotropy of soil	Ξ_{aniso}^{λ}	1	-
Longitudinal thermodispersivity of aquifer	α_L	0.5	m
Transverse thermodispersivity of aquifer	α_T	0.05	m
Initial time step size	Δt_0	10^{-3}	d
Simulation time	t_{end}	3650	d
RMS error tolerance	ϵ	10^{-3}	-
Maximum growth factor between subsequent time steps	Ξ	2	-

3.2.6.2 *Model Domain*

The borefield contains 18 boreholes of 150 m depth. Therefore, the model domain should be big enough to show the possible thermal plumes of the borefield, but not too big to induce unnecessary computational time and effort. As an example, Hecht-Méndez et al. (2013) used a domain of 200 m×200 m×100 m (L×W×D) to simulate a 25 BHE system with borehole depth of 100 m. Therefore, initially a domain measuring 200 m×200 m×150 m with the borefield located at the centre of the domain was selected (Appendix B) similar to others (H.-J. G. Diersch, 2014; Hecht-Méndez et al., 2013; Nam, Ooka, & Hwang, 2008). Chiasson (1999), on the other hand, modelled a BHE field located at one side of the domain and the model was extended in the direction of the groundwater flow (Chiasson, 1999).

Since the city of Windsor has the highest input temperatures, it was chosen to check the possibility of resizing the model. According to the results, temperature isolines formed an elliptical pattern around the BHE field and did not extend to the whole domain. Therefore, the model was resized to decrease computational time and effort. Further information about model resizing can be found in Appendix B.

The final model domain measures 300 m×150 m×200 m and the BHE field is situated at on the left of the domain (Figure 3.11).

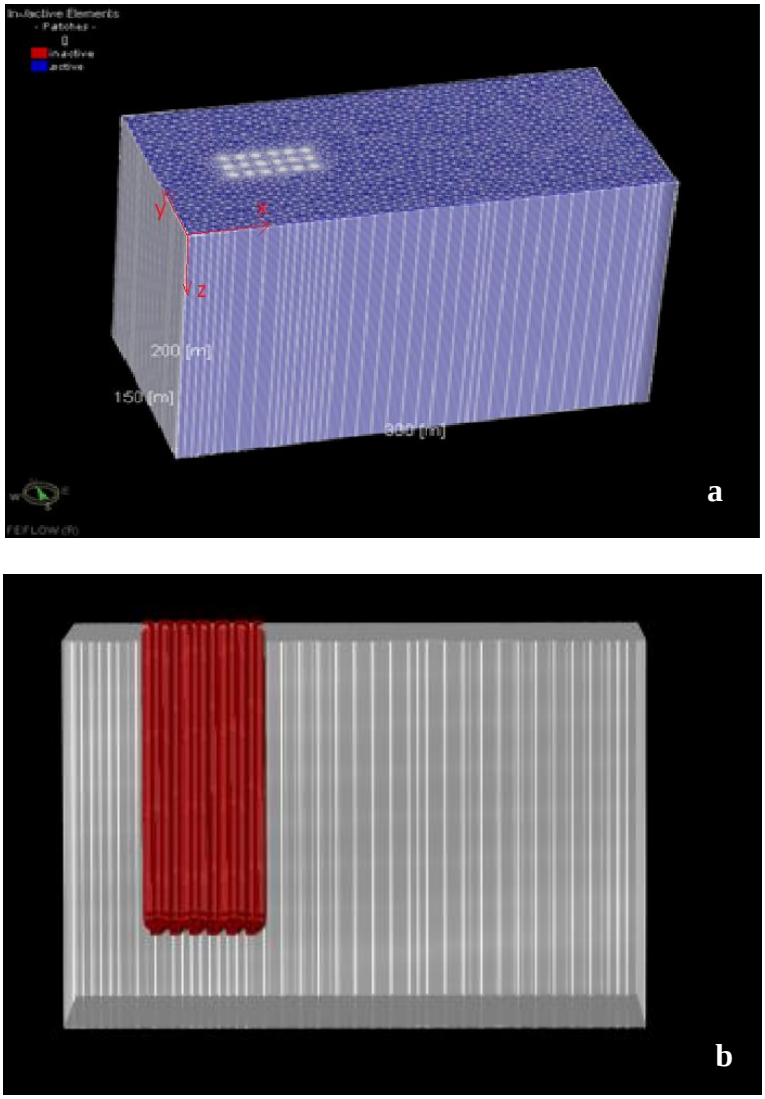

Figure 3.11 a. Resized Model Domain with the Borefield Moved to the Left b. Borehole Heat Exchangers

3.2.6.3 *Meshing*

FEFLOW simulates a BHE as a single node. Therefore, special considerations must be taken while meshing these singular nodes. Diersch (2014) presented a relation for optimal mesh size around a BHE node as follows:

$$\Delta_{BHE} = a r_b, \quad a = \begin{Bmatrix} 4.81 & for & n = 4 \\ 6.13 & for & n = 6 \\ 6.66 & for & n = 8 \end{Bmatrix} \qquad \textbf{(3-23)}$$

Where Δ_{BHE} is the mesh size around the BHE, r_b is the borehole radius and n is the number of surrounding nodes. This relation gives the optimal sizing (H.-J. G. Diersch, 2014). In the current study, triangular meshes (n=6) and boreholes with diameter of 0.15 m (r_b=0.075 m) are used (Table 3.25), therefore:

$$\Delta_{BHE} = 6.13 \times 0.075 \cong 0.46\, m \qquad \textbf{(3-24)}$$

Therefore, in meshing settings all the points (BHEs) were set to be refined and a point target size of 0.46 m were specified. To specify the required number of elements to mesh the rest of the domain a mesh convergence study was conducted that is described in the following section.

Mesh Convergence Study

Mesh convergence studies are conducted to ensure that the mesh chosen does not affect simulation accuracy while optimizing computational time. Since the 18-BHE field

located in Windsor is the most critical case, it was chosen to perform mesh convergence study.

To conduct a mesh convergence study, 5 different meshing with proposed number of elements of 200, 600, 1000, 2000 and 3000 per slice were examined. The top view of the domain with different meshes is shown in Figure 3.12. An observation point named OP1 was selected at 5 m horizontal distance from the rightmost BHE at the middle row (Figure 3.12a). OP1 temperature after one month of operation at depth of 75 m BGS was selected as an indicator of mesh convergence study.

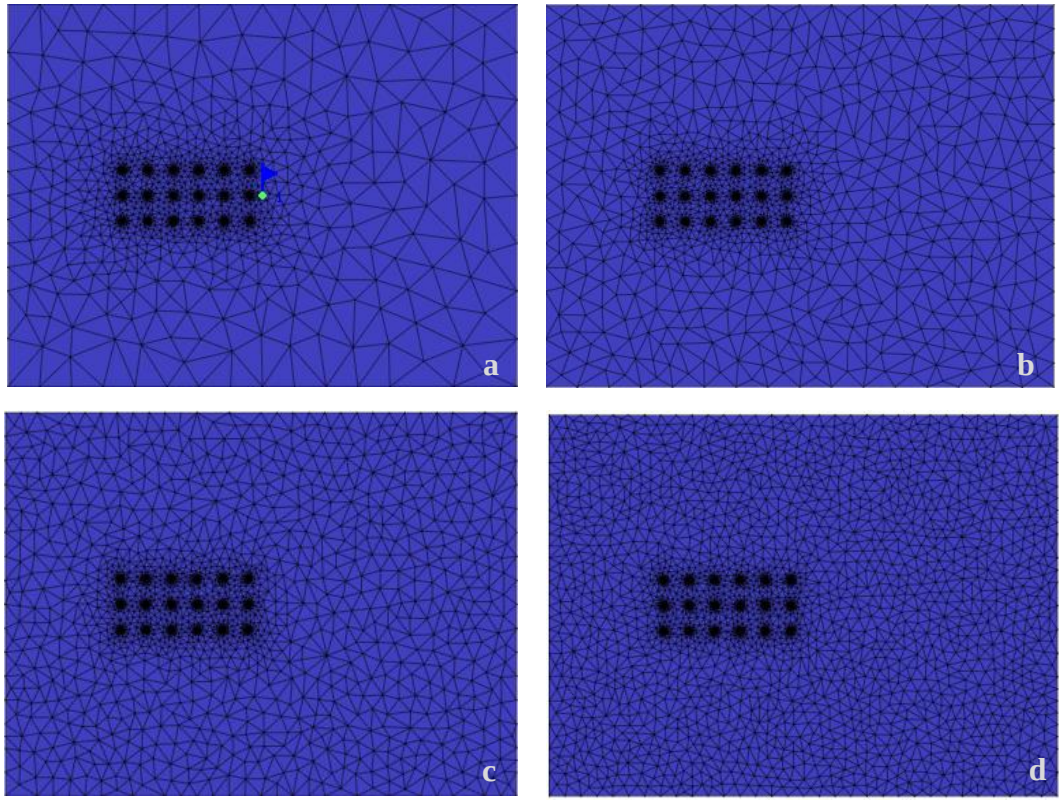

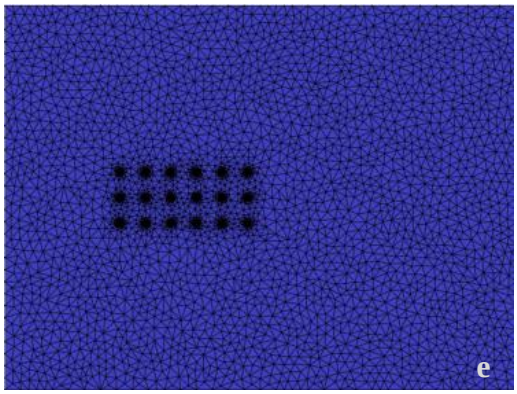

Figure 3.12 Top View of the Domain with Proposed Elements per Slice of a. 200, b. 600, c. 1000, d. 2000 and e. 3000

A groundwater flow with a velocity of 7.3×10^{-7} m/s and initial temperature of 11°C were assigned. One month of operation was simulated with different meshes and OP1 temperature was compared for all the cases (Figure 3.13).

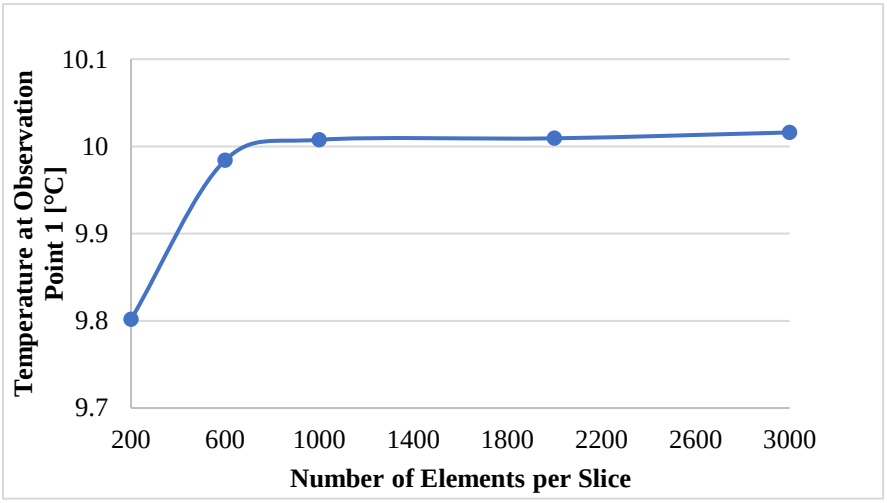

Figure 3.13 Observation Point 1 Temperature after One Month of Operation for Four Sets of Mesh with 200-3000 Elements per Slice

According to above graph, OP1 temperature varies from 9.8 to 10°C as the mesh becomes finer, but the difference between 1000 and 3000 meshes is very minimal. The relative error with respect to the temperature at 3000 elements is summarized in Table 3.26.

Table 3.26 OP1 Temperature and Corresponding Relative Errors for Different Meshes

Number of Elements/Slice	200	600	1000	2000	3000
Total Number of Elements	600,900	670,950	750,900	967,050	1,193,850
Temperature at OP1 [°C]	9.80	9.98	10.01	10.01	10.01
Relative Error [%]	2.14	0.32	0.08	0.07	0

Relative error was calculated as follow:

$$Rel.Error = \frac{|T - T_{3000}|}{T_{3000}} \times 100 \quad \textbf{(3-25)}$$

Where T_{3000} is the OP1 temperature measured in the 3000-element-per-slice mesh in [°C] and T is the OP1 temperature measured in coarser meshes, i.e., 200, 600, 1000 and 2000. According to this table, the mesh convergence is achieved after 1000 elements per slice.

However, meshing with 1000 elements per slice resulted in some oscillations in domain boundaries leading to model divergence. Therefore, a meshing with 2000 elements per slice was used resulting in a smooth solution. Mesh properties for the resized model (Figure 3.11) are summarized in Table 3.27.

Table 3.27 Mesh Properties

Quantity	*Value*
Proposed Number of Elements per Slice	2000
Nodes per Element	6
Element Type	Triangular Prism
Mesh Elements	1,293,400
Mesh Nodes	662,094

3.2.6.4 *Initial Soil Temperature*

According to maps compiled by Majorowicz et al. (2009) shown in Figure 3.3, at depth of 150 m BGS all three cities have a temperature of 10-12°C. Consequently, an initial soil temperature of 11°C was assumed for all cities.

3.2.6.5 *Boundary Conditions*

The current model is saturated and fully confined. Two sets of boundary conditions for fluid flow and heat transport must be assigned.

Fluid Flow Boundary Conditions

Since the aim of the simulations were to examine the effect of building load on thermal plumes, a hydraulic conductivity representative of a coarse sandy soil was chosen (Chiasson, 1999) and a hydraulic head boundary condition of 0 m and -0.03 m were assigned at western and eastern boundaries respectively, leading to a relatively low groundwater flow (West-East):

$$q = -Ki = -7.3 \times 10^{-5} \times \frac{-0.03}{300} = 7.3 \times 10^{-9}\, m/s \qquad \textbf{(3-26)}$$

Where q is volumetric Darcy flux, K is hydraulic conductivity and i is hydraulic gradient.

A no-flow boundary condition was applied on top, bottom, northern and southern boundaries representing a low-permeability aquitard at the bottom of the domain and the confined aquifer at the top (Banks, 2008).

Heat Transport Boundary Conditions

The air temperature was assigned on the top surface as a temperature BC, as suggested by Banks (2008) and Al-Khoury (2009). The air temperature of each city was taken from climate normals (Table 3.1) and was assigned as a time series. Adiabatic BC (no-heat flux) was assigned at northern and southern boundaries.

Finally, eighteen boreholes were assigned using the borehole heat exchanger BC. Boreholes were located at horizontal and vertical distance of 10 m from each other and were linked using a parallel interconnection. Borehole numbers and locations are summarized in Table 3.28. The linked boreholes are known as a BHE array in FEFLOW (Figure 3.14). The fully transient Al-Khoury et al. method aka numerical BHE solution was used (Section 2.4.2.2).

Table 3.28 Borehole Numbers and Locations

Borehole Number	X (m)	Y (m)
1	45	65
2	55	65
3	65	65
4	75	65
5	85	65
6	95	65
7	95	75
8	85	75
9	75	75
10	65	75
11	55	75
12	45	75
13	45	85
14	55	85
15	65	85
16	75	85
17	85	85
18	95	85

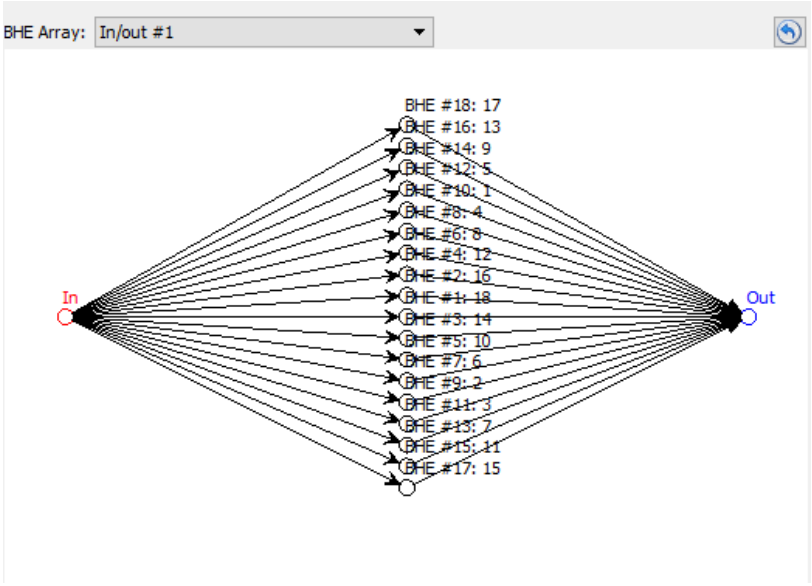

Figure 3.14 FEFLOW BHE Interconnection Editor Showing the BHE Array

The inflow of a BHE array is defined by two parameters, total flow rate of the refrigerant (Q_r) and any of the four parameters that indicate inflow temperature. These parameters are inlet temperature, heat input rate, temperature difference and power (FEFLOW 7.0 Help). In the current case, as well as, most of engineering problems the inlet temperature is not known but the power which should be extracted form the system for space heating/cooling can be calculated (R. Al-Khoury & Bonnier, 2006).

FEFLOW defines power as "the difference in thermal energy per time between inlet and outlet of the BHE" (FEFLOW 7.0 Help), which is the same as the ground load. Therefore, the calculated ground loads (Table 3.20) were assigned as input of the BHE array.

The refrigerant flow rate (Qr) is selected in a way that flow in the pipe becomes turbulent and provides the required heat. Turbulent flow enhances the heat transfer between the fluid and the ground. A flow rate of 4×10^{-4} m^3 s^{-1} is commonly used in the literature for multi-borehole GSHP systems (Rafid Al-Khoury, 2009; Hecht-Méndez et al., 2013). Therefore, a flow rate of 4×10^{-4} m^3 s^{-1} was assumed in the current research. The Reynolds number of the flow inside the tube was calculated to be 5,584 (see Appendix B for details), ensuring turbulent flow. Consequently, a total refrigerant flow rate of 7.2×10^{-3} m^3 s^{-1} (18 BHEs$\times4\times10^{-4}$ m^3 s^{-1}) was assigned to the BHE array.

3.3 Results and Discussion

The model was simulated for ten years of operation for three cases of Toronto, Vancouver and Windsor. The parameters and material properties listed in Table 3.25 were applied. The focus of the following results is on the effect of different building loads induced by different air temperature in various Canadian climatic regions on the development of subsurface thermal plumes.

3.3.1 Surface Temperature Fluctuations

The soil temperature distribution at a point that was not altered by the GSHP system operation was studied. An observation point (OP2) south of the borefield was selected to avoid any temperature changes due to borefield operation and to solely show the soil temperature distribution considering seasonal fluctuations of the surface air temperature. The soil temperature distribution along the model depth for the case of Toronto at the end of January, August and December is illustrated in Figure 3.16. Temperature distribution for the other cities can be found in Appendix C.

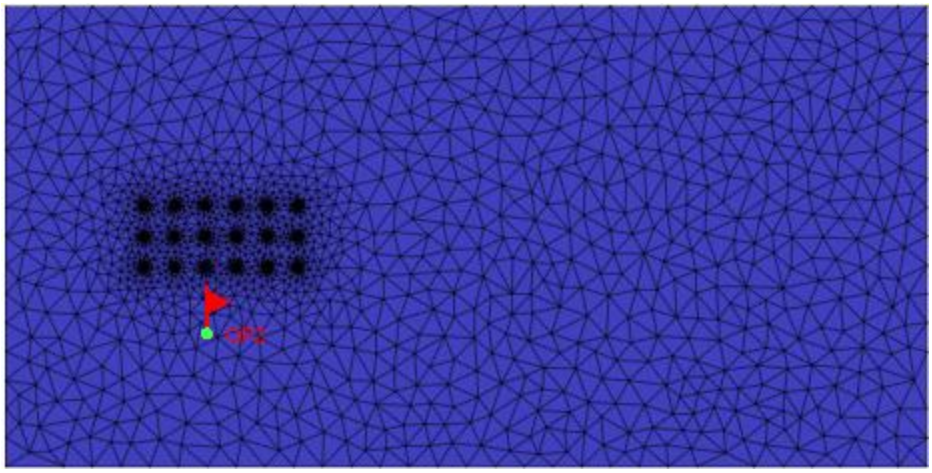

Figure 3.15 Location of OP2 on the Slice View

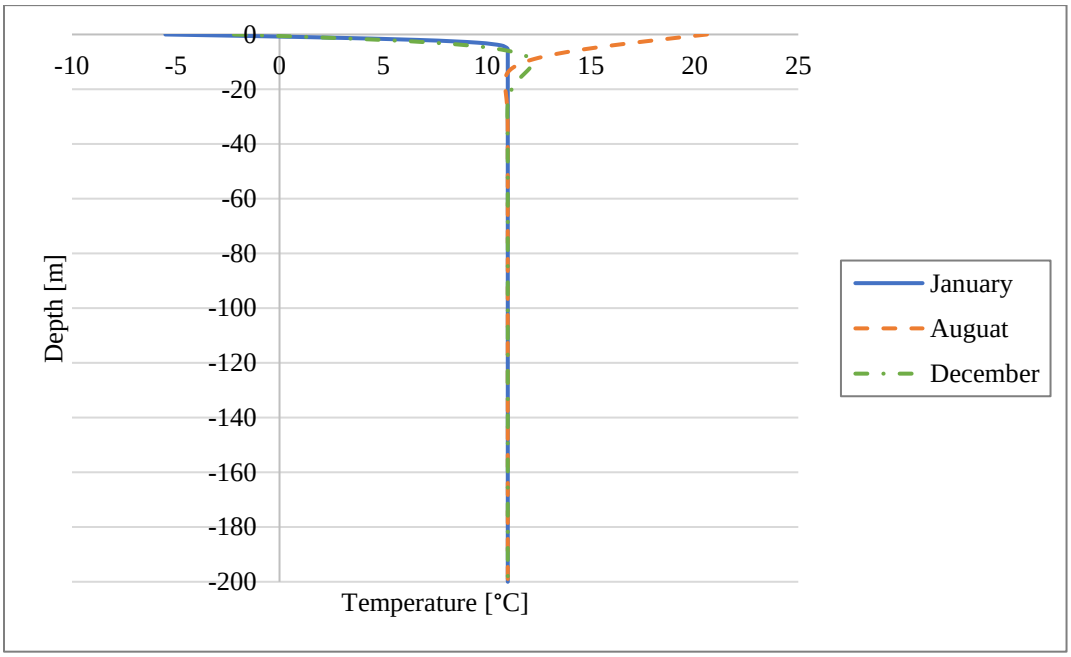

Figure 3.16 Toronto Soil Temperature Profile at OP2 at the End of January, August and December

Figure 3.16 shows that the air surface temperature only affects the upper few meters of the soil temperature, ranging from 8 to 30 m. After this zone, i.e., zone of seasonal fluctuations, soil temperature reached 11°C which was the initial temperature assigned to the whole model.

The soil temperature distribution for Vancouver showed the zone of seasonal fluctuations ranges up to 40 m and 30 m for Windsor (Appendix C).

These results show that zone of seasonal fluctuation varies from one place to another depending on the surface air temperature distribution. But the average zone of fluctuation around the year agrees with Majorowicz et al.'s (2009) estimation of 20 m in Canada.

Figure 3.17 illustrates a 3D view of the model showing the temperature contours at the end of one year of operation for Toronto, Vancouver and Windsor with a cross section along z-axis on the middle row of the borefield. Domain boundaries are shown for the case of Toronto to illustrate the cross section. The zone of seasonal fluctuations can be noted on the upper few meters of the model. Also, the thermal plumes developed around the boreholes can be seen.

For better examination of the temperature contours, a slice view was used rather than a 3D view henceforth. The following section deals with thermal plumes around the borefield to study the effect of building load on the subsurface temperature distribution.

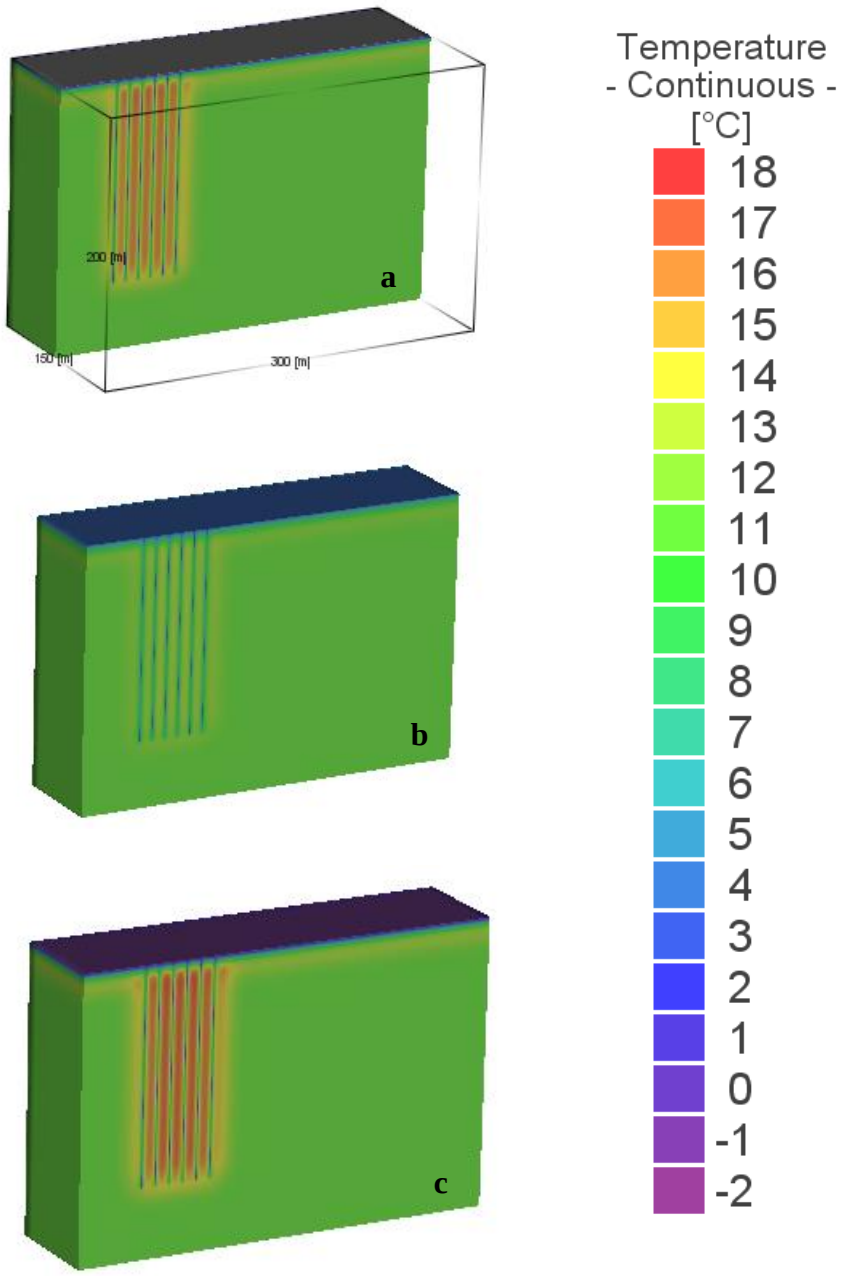

Figure 3.17 A Cross-sectional View of the 3D Model Showing Temperature Contours at the End of December in a. Toronto, b. Vancouver and c. Windsor

3.3.2 Thermal Plumes

The GSHP model was run for 5 months of heating (January to May) followed by three months of cooling (June to August) and 4 months of heating (September to December), for each year. It should be noted that heating mode indicates heating of the building (i.e., heat extraction from the ground), and cooling mode indicates cooling of the building (i.e., heat injection to the ground). Following results show the thermal plumes at the end of each interval in the first year of simulation.

3.3.2.1 *First Year of Operation*

Figure 3.18 shows the temperature distribution around the borefield for the three cities at the end of May of the first year of operation at the depth of 75 m BGS. This depth represents the middle of the borehole depth and therefore is a good representation of borefield temperature distribution.

Toronto and Vancouver show very similar temperature distribution around the borefield which is consistent with their close ground load of 13.2 and 14.0 kW in May, respectively. Windsor showed less temperature disturbance due to lower heating load and consequently less heat extraction during the first five months. The temperature isoline of 10°C which is 1°C lower than the initial ground temperature remained as circles around the boreholes in the case of Windsor, while in the cases of Toronto and Vancouver it moved farther and shaped a rectangular surrounding the whole borefield.

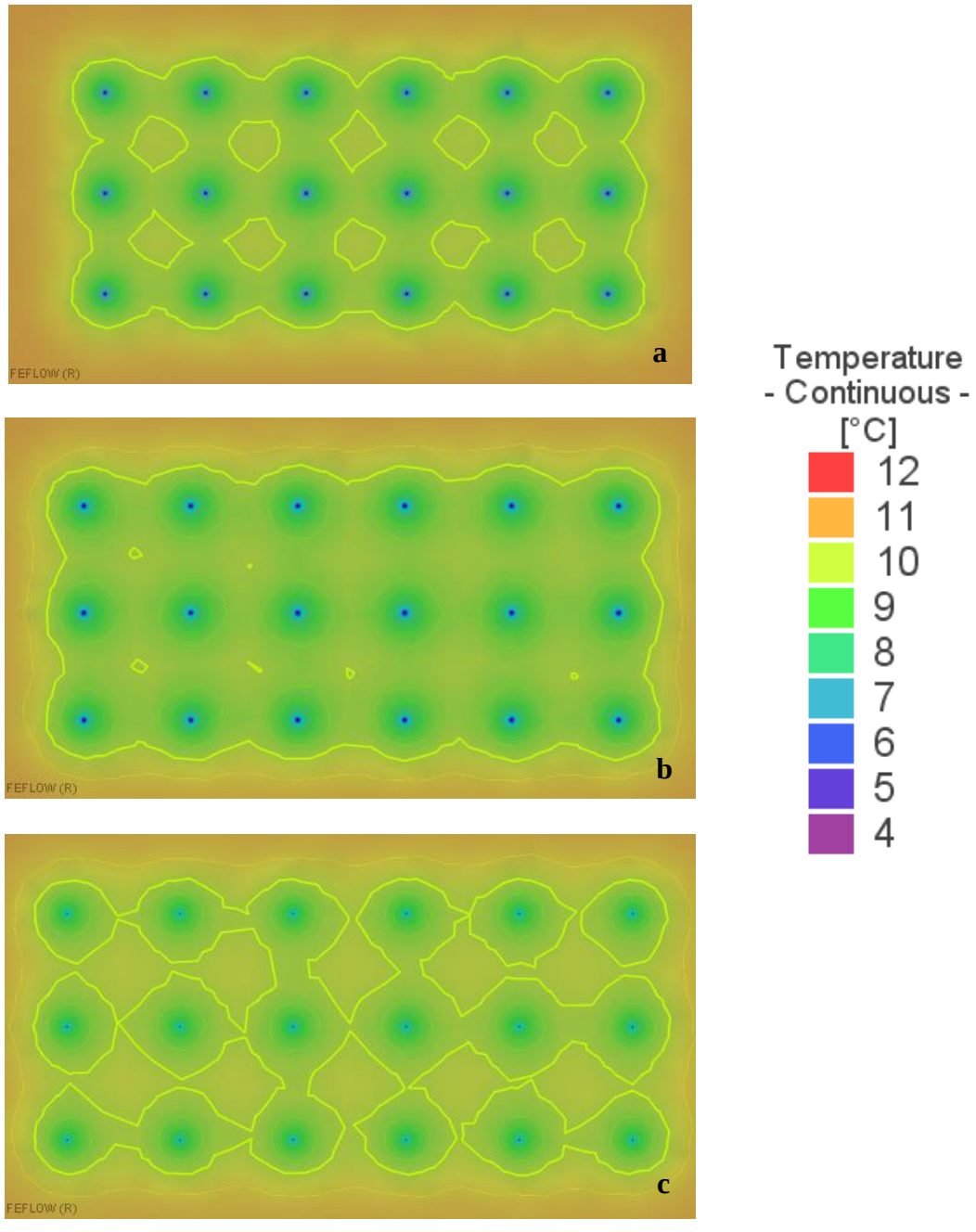

Figure 3.18 Temperature Distribution [°C] around the Borefield at the end of May of the first year at depth of 75 m BGS for a. Toronto, b. Vancouver and C. Windsor

Also, a larger temperature plume around the middle row boreholes developed due to the overlapping effect of the upper and lower BHEs. This can be most clearly seen in the Windsor 10°C isolines.

Temperature distribution around the borefield for the three cities at the end of August of the first year of operation at the depth of 75 m BGS is shown in Figure 3.19. This figure shows that temperature plumes extended the most in the case of Windsor which experiences the hottest summers. Vancouver with temperate climate showed smaller and more focused plumes. For example, the 18°C isolines which are equivalent to 7°C ground temperature disturbance are circle-shaped lines with diameters of approximately 6.7 m, 5 m and 2.8 m in the cases of Windsor, Toronto and Vancouver showing that Windsor has more extensive plumes than Toronto and Vancouver. It should be noted that 18°C isolines are not exact circles and diameters were measured around borehole number 18.

Temperature distribution around the borefield for the three cities at the end of December of the first year of operation at the depth of 75 m BGS is shown in Figure 3.20. After one year of operation, Windsor had highest temperature distribution around the borefield compared to the other cities with a temperature plume of 17-18°C trapped inside the borefield. In the case of Toronto, the confined plume had a temperature of 16-17°C. Vancouver had the lowest temperature and more focused plumes around the boreholes, representative of its moderate climate.

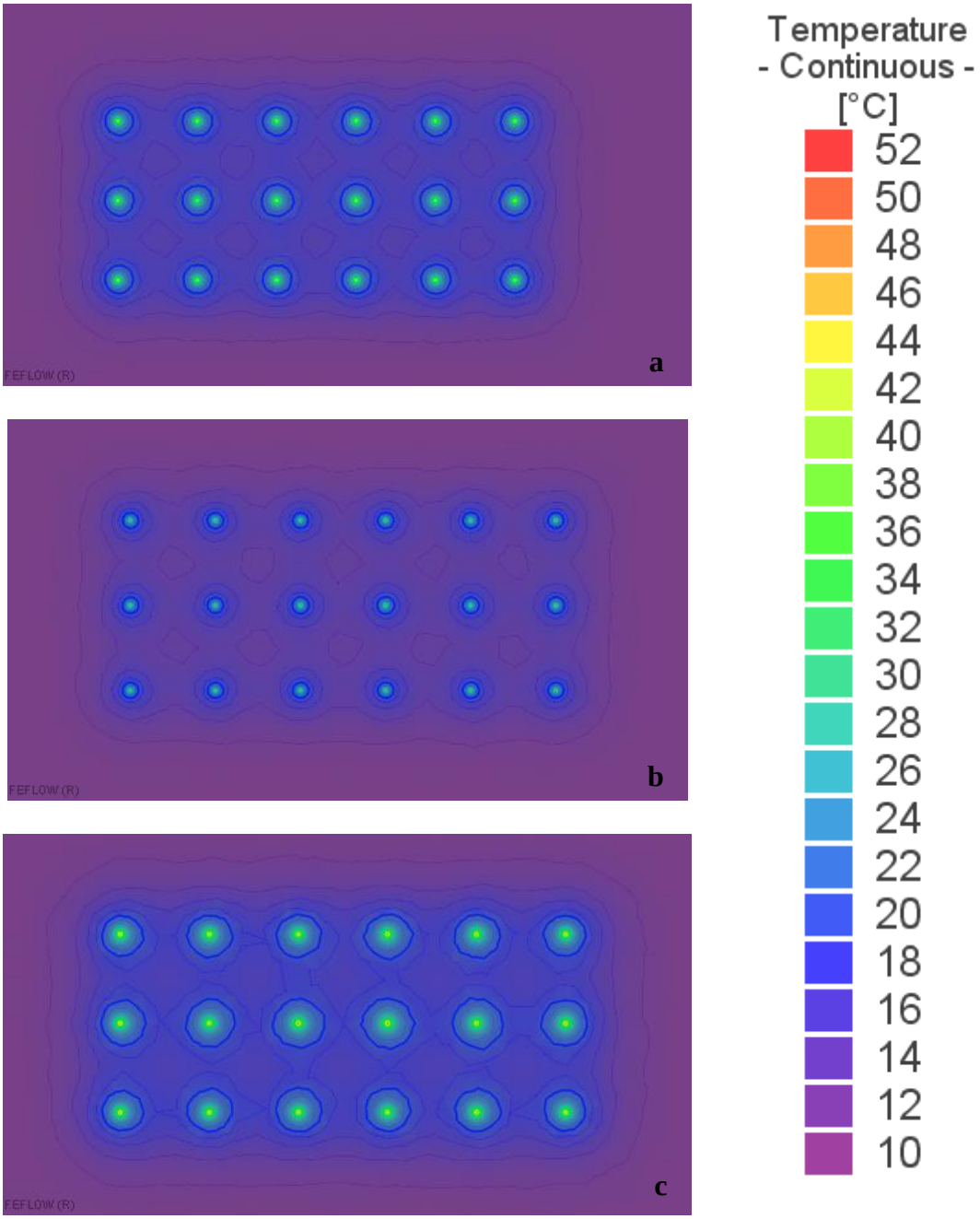

Figure 3.19 Temperature Distribution [°C] around the Borefield at the end of August of the first year at depth of 75 m BGS for a. Toronto, b. Vancouver and C. Windsor

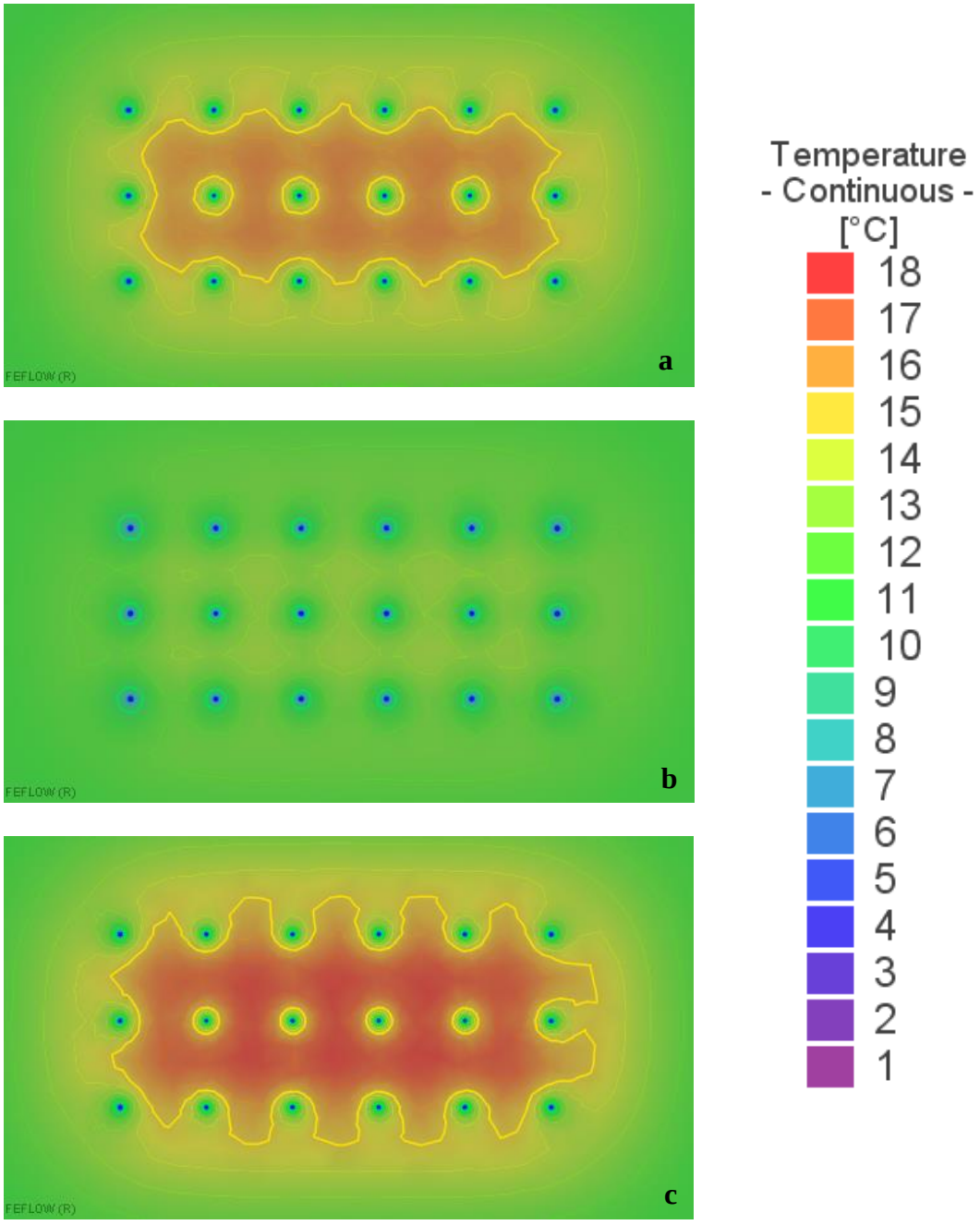

Figure 3.20 Temperature Distribution [°C] around the Borefield at the end of December of the first year at depth of 75 m BGS for a. Toronto, b. Vancouver and C. Windsor

The different temperature disturbance of the cities can be related to their annual load imbalance. From Table 3.20, Toronto, Vancouver and Windsor have load imbalances of -27.38 kW, -12.04 kW and 60.06 kW respectively. An imbalance of -27.37 kW, for instance, implies that the reference building requires 27.37 kW more heating than cooling throughout a year. Vancouver with lowest load imbalance showed less ground temperature disturbance after a year, while Windsor with highest load imbalance showed more extreme temperature disturbance.

3.3.2.2 *10 Years of Operation*

Figure 3.21 illustrates temperature distribution around the borefield for the three cities at the end of May of the tenth year of operation at the depth of 75 m BGS. For Toronto, the first temperature isolines surrounding the boreholes have lower temperature than the initial ground temperature of 11°C which is reasonable due to heat extraction. But between a radial distance of approximately 0.1 m to 47 m from the boreholes temperature is higher than 11°C. This trend contradicts the temperature distribution on the May of fist year where ground temperature was lower than 11°C.

This can be attributed to the heat trapped in the borefield during ten years of operation which has not been counterbalanced by heating mode (heat extraction) or transported by groundwater. It should be noted that current simulations are at a groundwater flow of 7.3×10^{-9} m/s representing a relatively slow flow rate.

In addition, the isoline with 1°C temperature disturbance (12°C isoline) for Toronto is an ellipse with major and minor axes of 133 m and 113 m, respectively. In the case of Windsor, the axes measure 150 m and 124 m due to Windsor's positive load imbalance and consequently more heat being injected into the ground than extracted. Vancouver's 12°C isoline formed smallest ellipse, with major and minor axes 109 m and 83 m, due to its moderate climate and less heat being injected into the ground compared to the other cities.

Comparing the temperatures after the 1st and 10th year (Figure 3.18 and Figure 3.21), it can be seen that the thermal plumes become more extensive year by year due to heat injection during the summer months and a thermal plume with temperature higher than the initial temperature of 11°C was developed inside the borefield for every city.

The temperatures at the end of August of the 10th year reached maximum of nearly 52°C, 37°C and 58°C in Toronto, Vancouver and Windsor, respectively (Figure 3.22). As a comparison, for Toronto and Windsor the 18°C isoline is a rectangular measuring 37 m × 67 m and 42 m × 71 m respectively on the August of 10th year of operation compared to the first year, where this isoline was in the shape of circles with dimeter of just 5 m and 6.7 m confining the boreholes.

In the case of Vancouver, the 18°C isoline is in the shape of circles with diameter of 4 m surrounding each borehole which is almost 1.5 times bigger than the isoline in the

first year. Therefore, all three cities showed that the thermal plumes developed more extensive after ten years of operation.

Figure 3.23 shows the temperature distribution around the borefield for the three cities at the end of December of the tenth year of operation at the depth of 75 m BGS. After ten years of operation the temperature within the borefield reached nearly 22, 15 and 24°C for Toronto, Vancouver, and Windsor, respectively. This signifies an increase of 5, 2, and 6°C over the 10 years of operation.

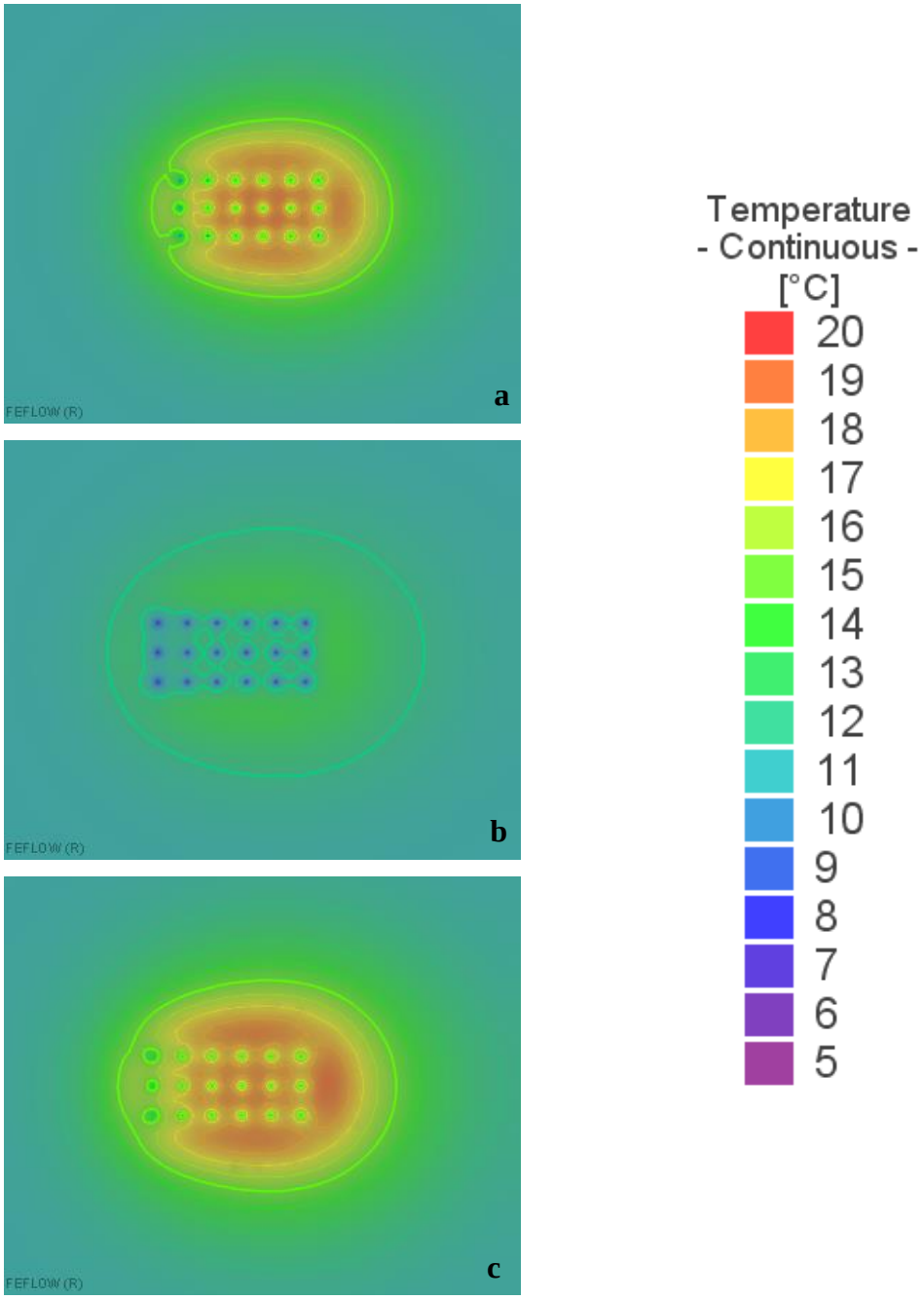

Figure 3.21 Temperature Distribution [°C] around the Borefield at the end of May of the tenth year at depth of 75 m BGS for a. Toronto, b. Vancouver and C. Windsor

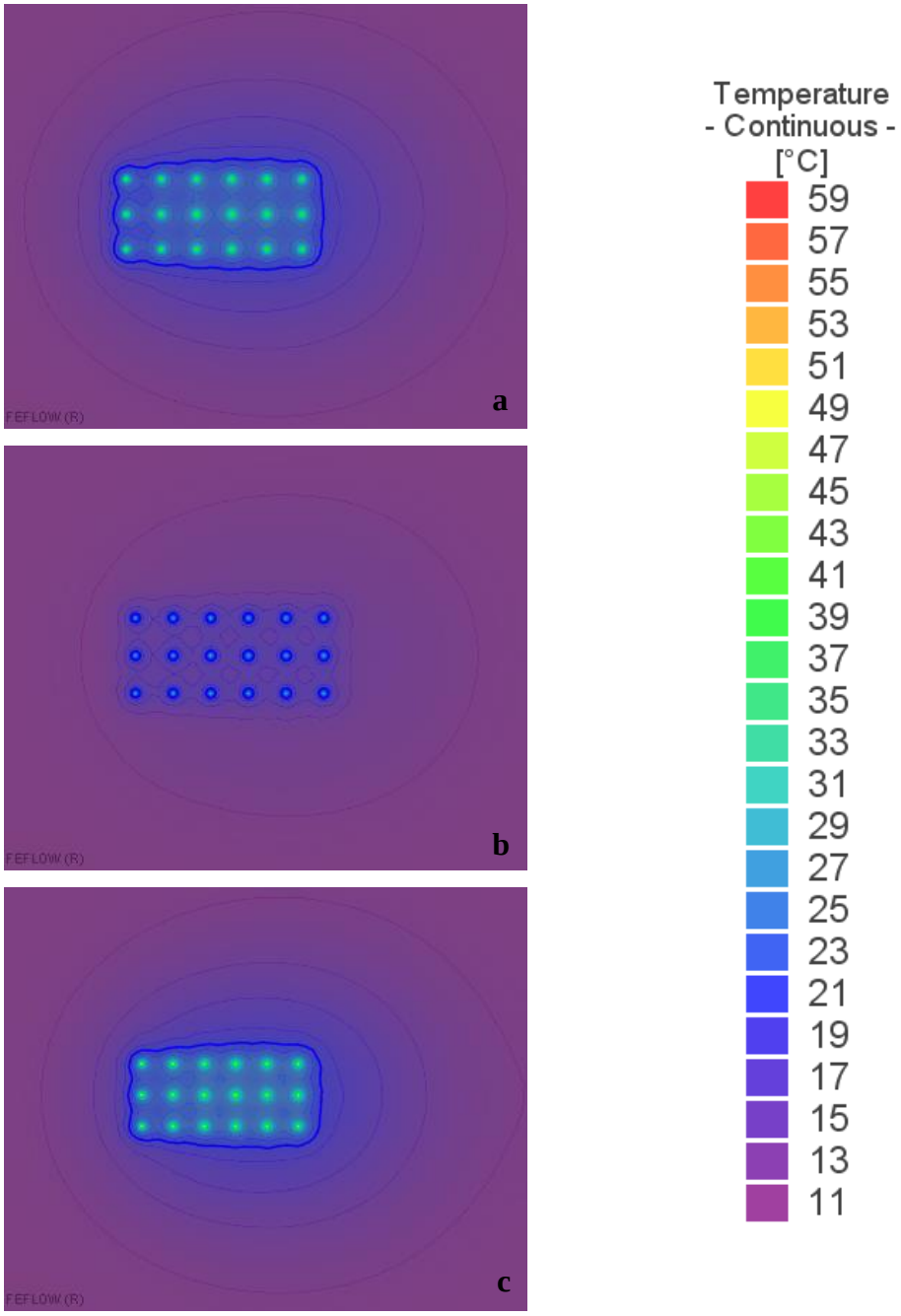

Figure 3.22 Temperature Distribution [°C] around the Borefield at the end of August of the tenth year at depth of 75 m BGS for a. Toronto, b. Vancouver and C. Windsor

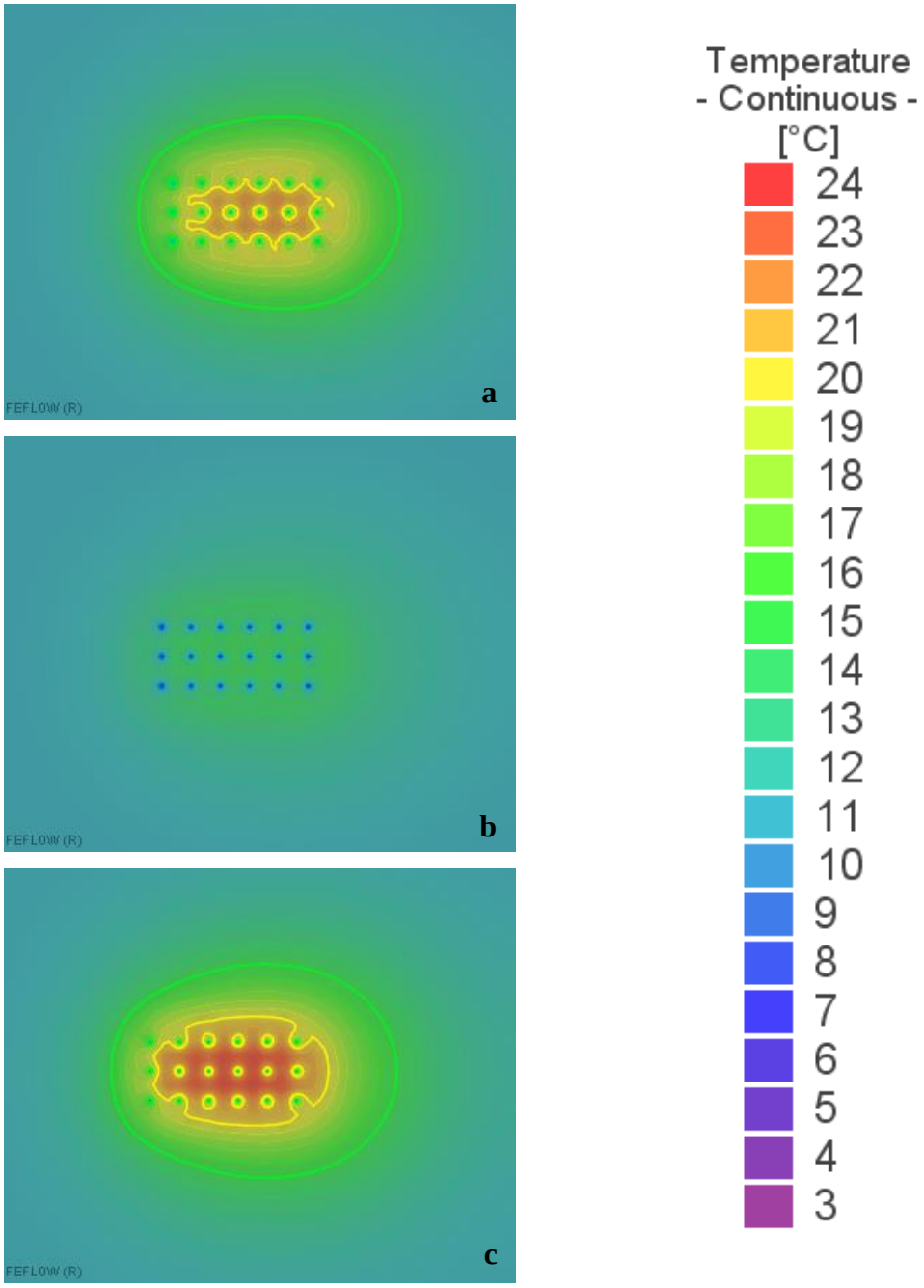

Figure 3.23 Temperature Distribution [°C] around the Borefield at the end of December of the tenth year at depth of 75 m BGS for a. Toronto, b. Vancouver and C. Windsor

3.3.2.3 *Temperature Beneath the Borefield*

The subsurface temperature distribution beneath the boreholes after one year of operation extends a few meters below the borefield (Figure 3.17). To investigate the subsurface temperature beneath the borefield an observation point (OP3) was assigned in the middle of the borefield between boreholes number 9 and 10 where the thermal plumes exist.

Figure 3.24 illustrates temperature changes with depth below the borefield for OP 3 after one year and 10 years of operation for Toronto. According to Figure 3.24a, temperature remained unchanged after 175m BGS for one year of operation. While after 10 years of operation OP3 temperature was 11.64°C at the depth of 200 m BGS. It should be noted that the heat transfer along the z-axis is solely attributed to heat conduction since there is no vertical groundwater flow.

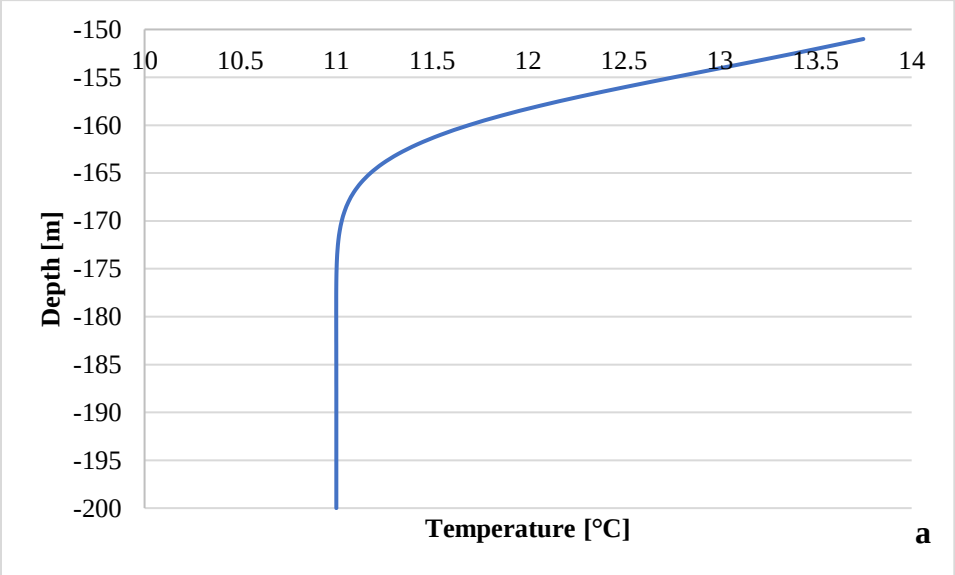

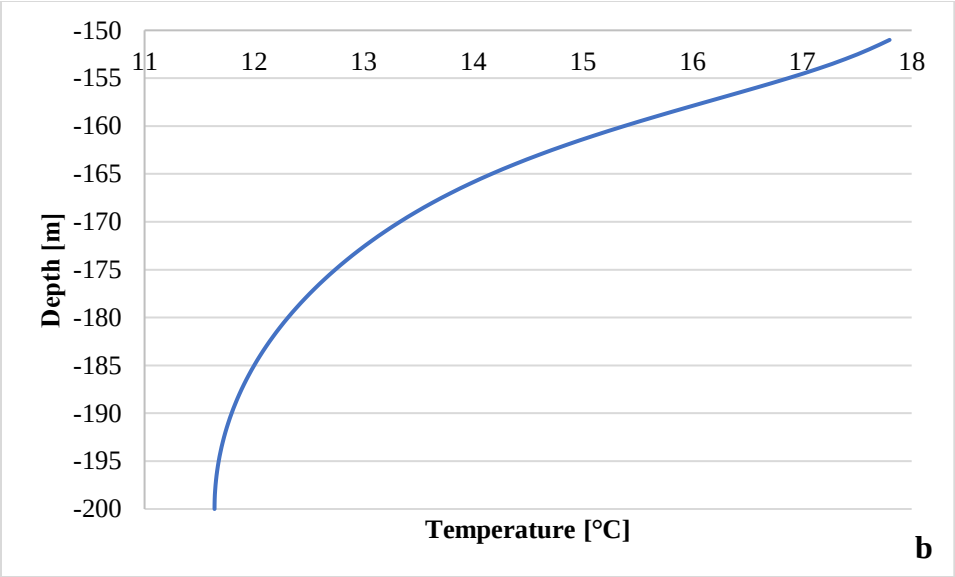

Figure 3.24 Temperature Distribution Beneath the Borefield at OP3 after a. One and b. Ten Years of Operation for Windsor

3.4 Conclusions

In this chapter, a 3D model simulating a borehole-based GSHP system in three cities of Toronto, Vancouver and Windsor was developed in FEFLOW 7.0. The developed thermal plumes in ten years of GSHP operation were compared between the cities to investigate the effect of building thermal load on the thermal plumes.

The borefield temperature contours was presented at the end of May, August and December of the first and tenth year of operation. The results showed that at the end of August, Vancouver with a moderate climate had small and focused plumes, while Windsor with highest heat injection during summer had extensive plumes.

The contours depicted a larger temperature plume around the middle row boreholes due to the overlapping effects from the upper and lower BHEs. After one year of operation, a high temperature plume developed inside the borefield which had a temperature of nearly 18°C for the case of Windsor. Windsor with highest load imbalance had extreme temperature disturbance while Vancouver with lowest load imbalance resulted in smaller plumes confined to the borefield area. Comparison between first and tenth years of operation revealed that plumes grew in both size and temperature disturbance after ten years of operation.

The temperature distribution beneath the borefield was also examined and showed that temperature changes exist up to 25 m below the boreholes after one year of operation. After 10 years of operation temperature changes were observed up to 50 m below the borefield.

Thermal plumes can deteriorate the system performance and affect other subsurface installations including neighbouring GSHP systems. In addition, they can lead to groundwater flow disturbances or potential issues with contaminated sites. In this chapter, thermal plumes induced by a GSHP installation in three different cities were examined. Next chapter is focused on how different parameters may affect location, size and temperature of thermal plumes.

Chapter 4 Sensitivity Analysis

In this chapter, a sensitivity analysis was conducted on the GSHP model developed in Chapter 3. Parameters such as groundwater flow, soil thermal conductivity, volumetric heat capacity, and porosity were examined to determine their effect on development and transport of thermal plumes. Finally, the thermal plumes developed within one year of GSHP system operation in three different geological formations including a heterogeneous soil were compared.

4.1 Effect of Groundwater Flow

Many studies showed the importance of considering groundwater flow in borehole heat exchanger design and performance simulations. According to Wang et al. (2013) groundwater flow improves the heat transfer around boreholes and can reduce design depth of the boreholes and consequently decrease the capital cost of GSHP systems. Gehlin (2002) showed that both loop temperature and soil temperature distribution around the boreholes are dramatically influenced by groundwater flow (Emad Dehkordi et al., 2015).

In this section, effect of groundwater flow on thermal plumes is examined. To do so, three cases of low, medium and high velocity groundwater flow induced by different

hydraulic conductivities were considered. All other properties and boundary conditions remained the same as section 3.2.6.

Clay with an average hydraulic conductivity of 2.2×10^{-10} m/s resulting in a groundwater velocity of 2.2×10^{-14} m/s was selected as the low-velocity case. In Chapter 3, coarse sand with an average hydraulic conductivity of 7.3×10^{-5} m/s was simulated which was considered as the medium-velocity case (resulting in a groundwater velocity of 7.3×10^{-9} m/s).

A groundwater flow with a velocity of 10^{-7} m/s was reported to have a significant influence on BHE loop temperature (Dehkordi & Schincariol, 2014; Lazzari et al., 2010). Therefore, a groundwater flow with a magnitude of 7.3×10^{-7} m/s was selected which was induced by a high hydraulic conductivity of 7.3×10^{-3} m/s, attributed to coarse sandy soil (Chiasson, 1999). Three cases are summarized in Table 4.1.

Table 4.1 Three Cases of Groundwater Flow Sensitivity Analysis

Case	Hydraulic Conductivity [m s^{-1}]	Groundwater Flow Velocity [m s^{-1}]
Low-velocity	2.2×10^{-10}	2.2×10^{-14}
Medium-velocity	7.3×10^{-5}	7.3×10^{-9}
High-velocity	7.3×10^{-3}	7.3×10^{-7}

The sensitivity analysis was conducted in Toronto since it has an average climate as compared to the three cities studied. The 1°C disturbance isoline (10°C in heating mode and 12°C in cooling mode) was used to represent effect of different parameters on thermal plumes. Moreover, the center of energy coordinates was measured as a parameter to quantify the transport of thermal plumes:

$$x_{ce} = \frac{1}{E_t}\int_R x de_t$$

$$y_{ce} = \frac{1}{E_t}\int_R y de_t \qquad \textbf{(4-1)}$$

Where E_t is the total thermal energy in the system, R is the domain, x and y are the horizontal and vertical coordinates, and de_t is an incremental portion of mass in the domain. Above formula was adopted from center of mass definition (Dekker & Abriola, 2000; Krol, 2011).

Temperature contours at the end of May and August of the first year of operation were compared for low, medium and high velocity groundwater flow cases to examine the effect of groundwater flow in heating and cooling modes (Figure 4.1 and Figure 4.2).

From Figure 4.1, low and medium-velocity groundwater flow cases show very similar temperature contours. The 10°C temperature isoline was confined to the borefield measuring a rectangular of 27 m by 57 m in both cases.

For the case of high-velocity groundwater flow, the isoline was transported approximately 63 m from the east boundary of the borefield by groundwater flow. Although a high-velocity groundwater flow resulted in wider plumes, the ground temperature disturbance was much lower than the other cases. Maximum ground temperature disturbance was nearly 3.6°C in high-velocity case and approximately 6.3°C for both low and medium-velocity groundwater flow cases at the end of May (Table 4.2).

Temperature contours after three months of cooling at the depth of 75 m BGS are demonstrated in Figure 4.2. In low and medium-velocity cases the 12°C isoline was a rectangular measuring nearly 35 m by 66 m. In the high-velocity case, the isoline extended approximately 57 m to the east of the borefield. Furthermore, the 10°C isoline induced by 5 months of heating has moved to the east of the borefield.

Center of energy for each case is tabulated in Table 4.2 which shows the effect of groundwater velocity on the thermal plume movement. The x-component of center of energy was moved to the east of the domain as the groundwater flow velocity increased. The vertical component remained unchanged in all scenarios. For low and medium-velocity cases the horizontal shift from the original center of energy at (70m,75m) is very small; nearly 1.5 m in May and 2 m in August. But in the high-velocity case, the horizontal coordinate of the center of energy has moved nearly 13 and 11 m along x-axis in heating and cooling modes with respect to the original center of energy.

Table 4.2 Center of Energy Coordinates for Groundwater Flow Sensitivity Analysis

Case	X_{ce} [m]	Y_{ce} [m]	Max Temperature Disturbance [°C]
Low-velocity, May	71.55	75.01	6.37
Medium-velocity, May	71.62	75.01	6.35
High-velocity, May	83.06	75.00	3.59
Low-velocity, August	72.06	75.01	35.08
Medium-velocity, August	72.16	75.01	34.47
High-velocity, August	81.48	75.01	18.64

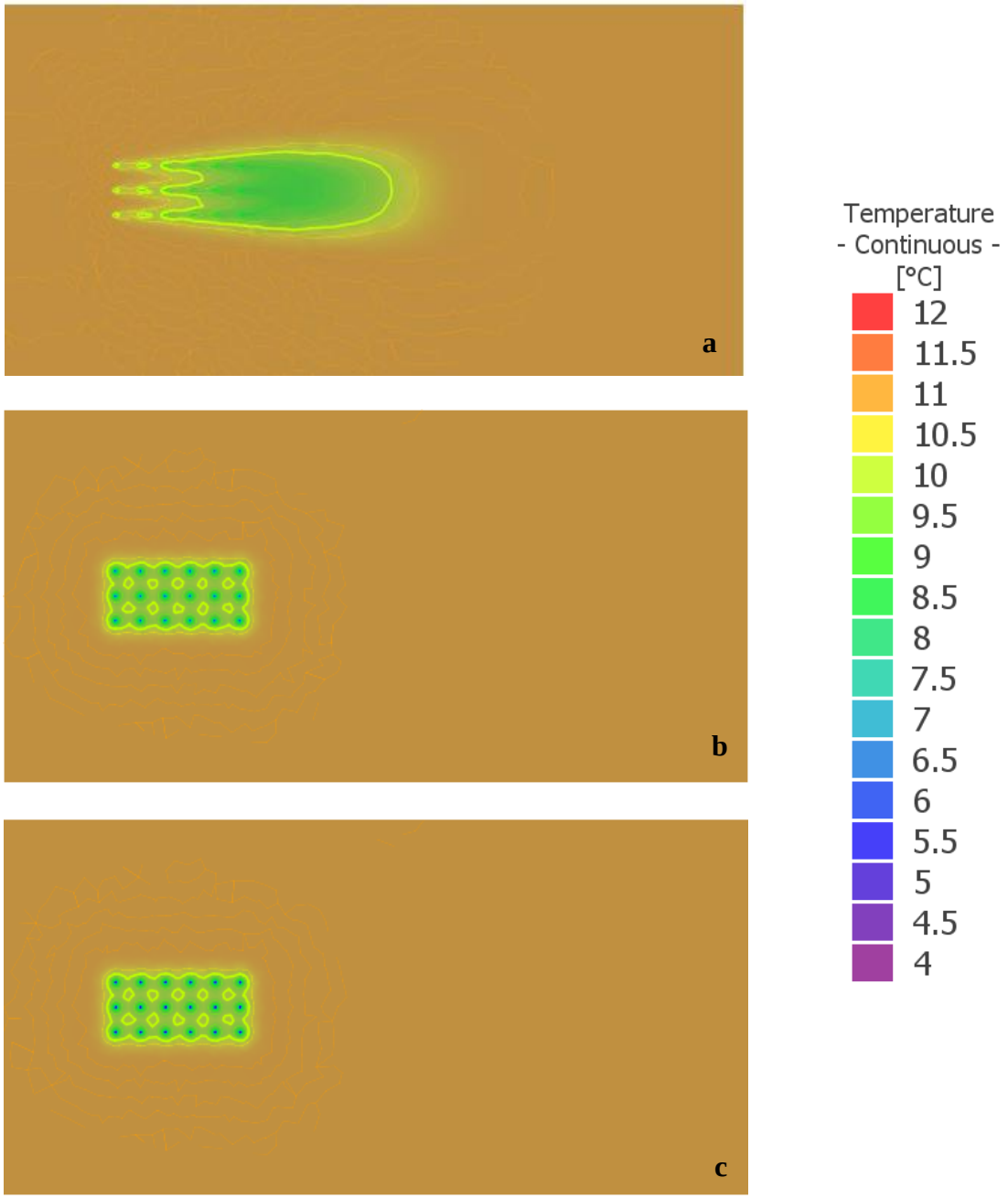

Figure 4.1 Temperature Distribution [°C] at the end of May of the First Year at Depth of 75 m BGS for a. High-velocity, b. Medium-velocity and c. Low-velocity Groundwater Flow

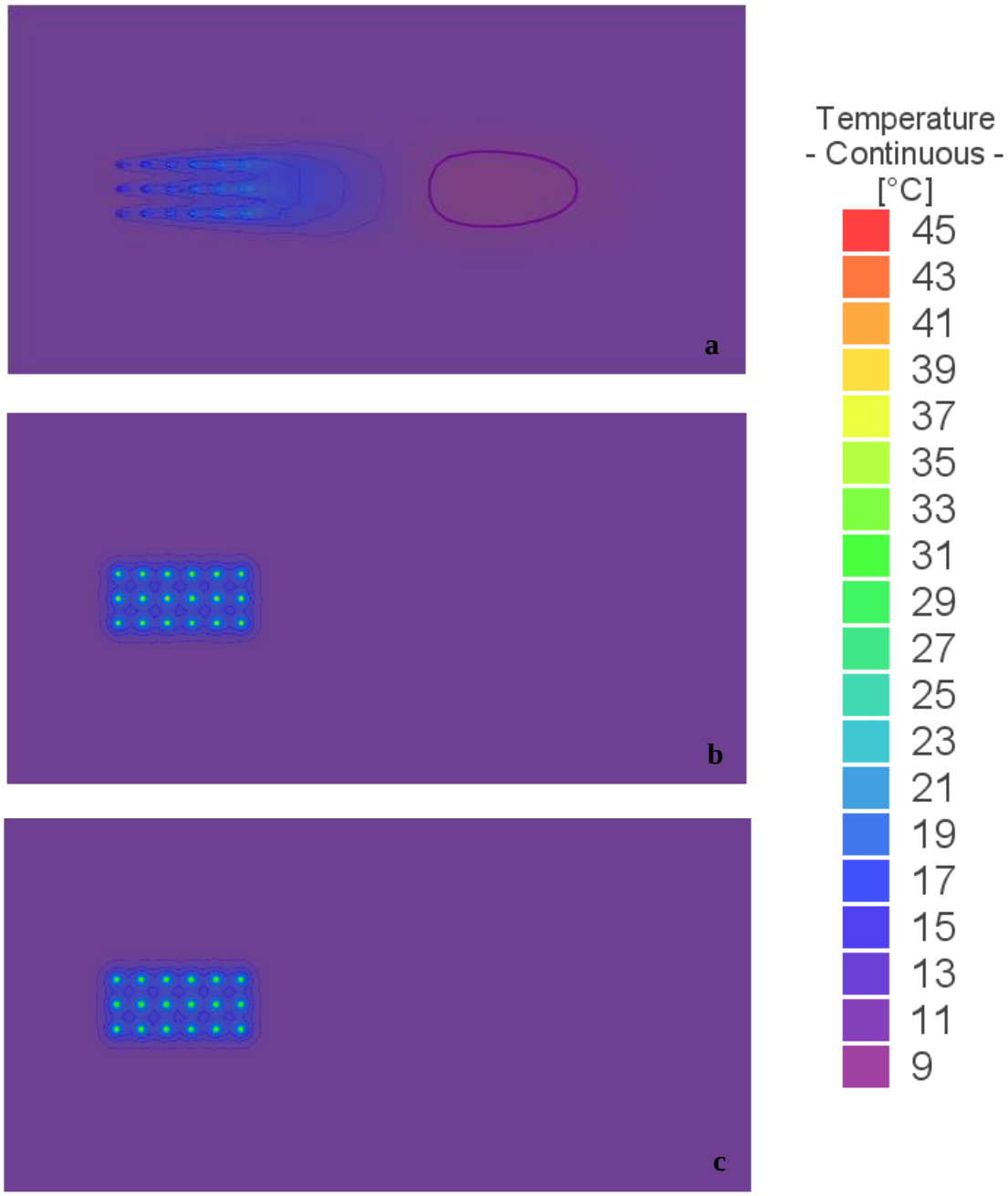

Figure 4.2 Temperature Distribution [°C] at the end of August of the First Year at Depth of 75 m BGS for a. High-velocity, b. Medium-velocity and c. Low-velocity Groundwater Flow

Maximum temperature disturbance listed in Table 4.2 also shows that higher groundwater velocity results in lower temperature disturbance in both heating and cooling modes.

It can be concluded that groundwater flow with velocity in the order of 10^{-9} and 10^{-14} m/s results in the same thermal plumes and center of energy location, while groundwater flow with a velocity of 10^{-7} m/s has a significant influence on borefield temperature contours. Therefore, in the sites with high groundwater flow velocity special consideration should be paid to migration of thermal plumes and how it can affect neighbouring GSHP and other subsurface installations. Lastly, high-velocity groundwater flow moderates the thermal plumes in both heating and cooling modes.

4.2 Effect of Soil Thermal Conductivity

In this section, the sensitivity of the model to soil thermal conductivity is examined. Two thermal conductivities of 0.8 and 0.98 J m^{-1} s^{-1} K^{-1} corresponding to coarse sand and clay were simulated. All other properties and boundary conditions remained the same as section 3.2.6. Figure 4.3 and Figure 4.4 demonstrate temperature contours at the end of May and August at the depth of 75 m BGS, respectively.

The two cases show very similar temperature contours in both heating and cooling modes. At the end of May, the temperature ranges 4.8 to 11°C and 5.4 to 11°C for coarse sand and clay, respectively. This indicates that the higher thermal conductivity results in less ground temperature disturbance and consequently better system performance. Maximum temperature disturbance summarized in Table 4.3 also confirms this

conclusion. The 10°C isoline has the same size in both cases, but in the case of coarse sand, small isolines can be seen inside the borefield showing more ground temperature disturbance.

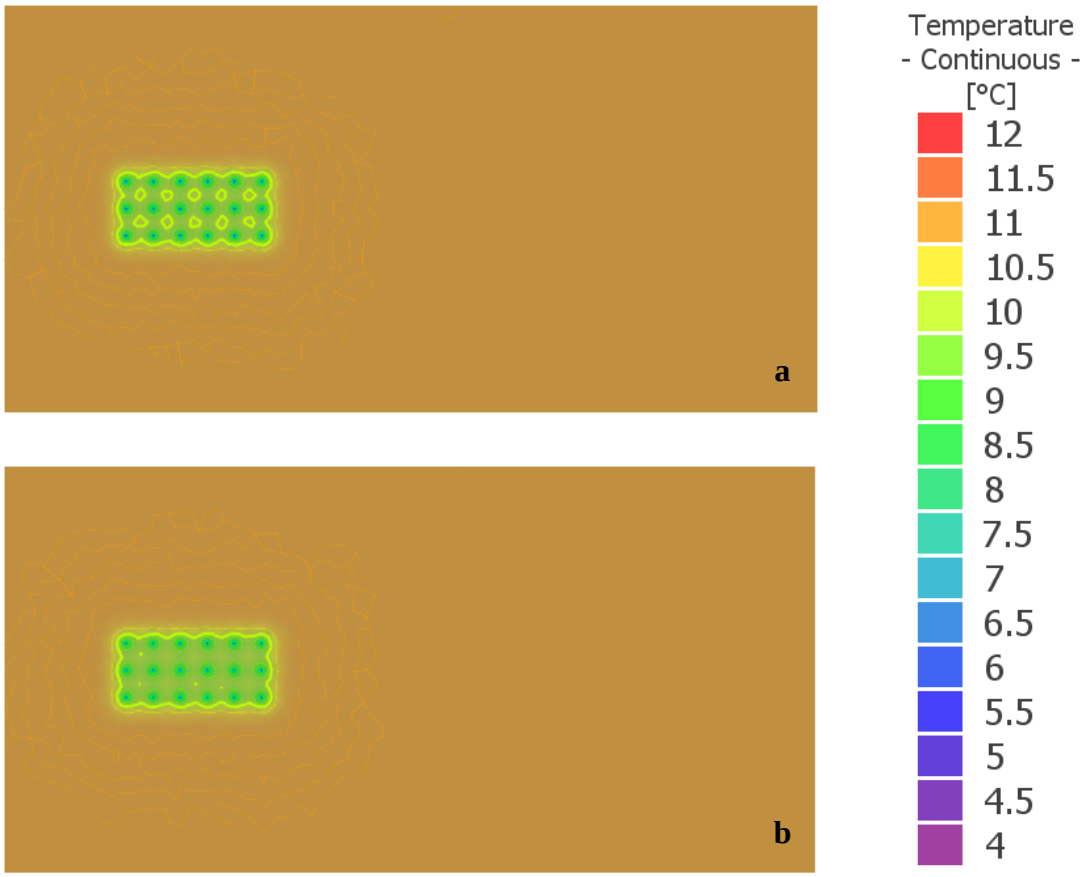

Figure 4.3 Temperature Distribution [°C] at the end of May of the First Year at Depth of 75 m BGS for a. Coarse Sand (0.8 J m^{-1} s^{-1} K^{-1}), b. Clay (0.98 J m^{-1} s^{-1} K^{-1})

Thermal plume horizontal dimension is represented by radial spread (r_{spread}) defined as:

$$r_{spread} = \sqrt{\frac{I_z}{E_t}} \qquad \textbf{(4-2)}$$

$$I_z = \int_R x^2 de_t$$

where I_z is the second moment of energy about the z axis (Dekker & Abriola, 2000; Krol, 2011). Center of energy, radial spread and maximum temperature disturbance for each case is listed in Table 4.3.

Table 4.3 Center of Energy Coordinates for Thermal Conductivity Sensitivity Analysis

Case	X_{ce} [m]	Y_{ce} [m]	R_{spread} [m]	Max Temperature Disturbance [°C]
Coarse Sand, May	71.62	75.01	75.51	6.35
Clay, May	71.80	75.01	75.88	5.71
Coarse Sand, August	72.16	75.01	76.63	34.47
Clay, August	72.43	75.01	77.17	31.26

The center of energy moved slightly (nearly 0.2 m) to the east of the model as the thermal conductivity increased. This can be associated with the fact that higher thermal conductivity of subsurface results in more heat transport between the pipe and subsurface and consequently wider plumes. This is confirmed by the increase of radial spread for the case of clay in both heating and cooling modes. The horizontal shift is negligible compared to those due to groundwater flow (Table 4.2).

From Figure 4.4, the 12°C isoline has the same size in both cases. The temperature ranges 10.9 to 44°C and 10 to 41°C for coarse sand and clay, showing that higher thermal conductivity leads to less ground temperature disturbance.

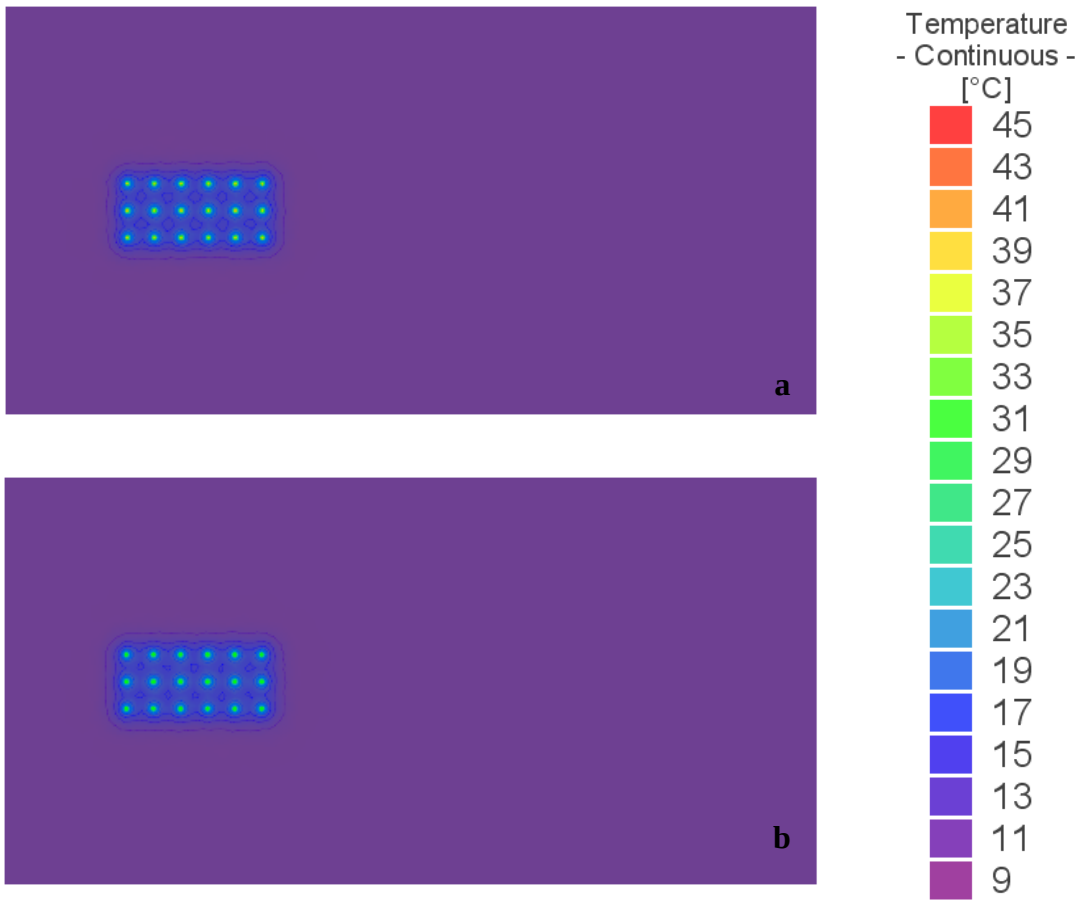

Figure 4.4 Temperature Distribution [°C] at the end of August of the First Year at Depth of 75 m BGS for a. Coarse Sand (0.8 J m^{-1} s^{-1} K^{-1}), b. Clay (0.98 J m^{-1} s^{-1} K^{-1})

To better illustrate the effect of hydraulic and thermal conductivity on center of energy, its coordinate is compared in Figure 4.5. Increase of both parameters result in a shift of the center of energy to the east of the domain.

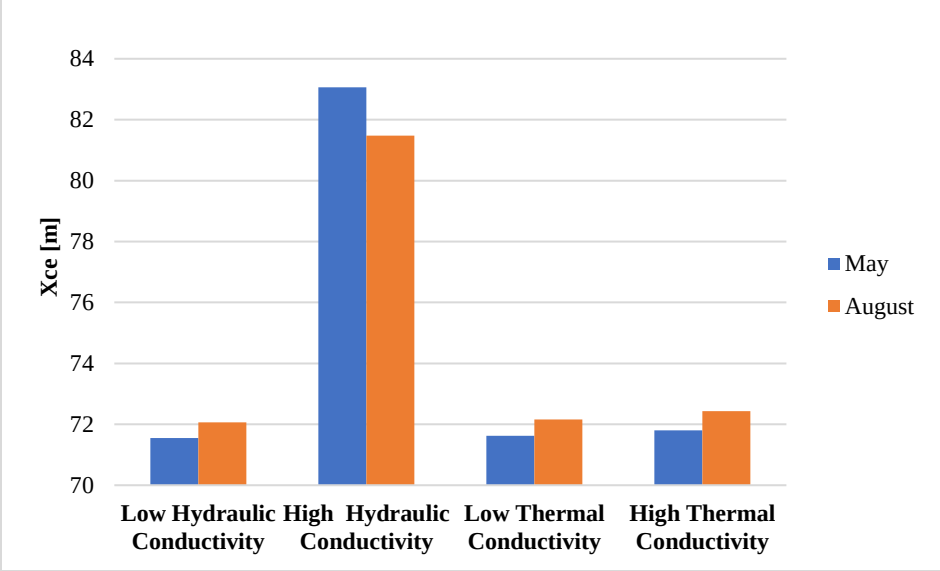

Figure 4.5 Effect of Hydraulic and Thermal Conductivity on Center of Energy Coordination

4.3 Effect of Soil Volumetric Heat Capacity

In this section, the sensitivity of the model to soil volumetric heat capacity is studied. Two cases of 1.4×10^{6} and 3.3×10^{6} J m^{-3} K^{-1} corresponding to coarse sand and clay volumetric heat capacities were considered. All other properties and boundary conditions remained the same as section 3.2.6. Figure 4.6 and Figure 4.7 demonstrate temperature contours at the end of May and August at the depth of 75 m BGS, respectively.

From Figure 4.6 for the case of clay with higher volumetric heat capacity, the 10°C isoline is in the shape of circles with average diameter of 6 m around the boreholes as opposed to a rectangular measuring 27 m by 57 m in the coarse sand case.

At the end of August, the 12°C isoline is a rectangular of 33 m by 63 m in the case of clay which is smaller than coarsy sand isoline of 35 m by 66 m. Therefore, higher volumetric heat capacity resulted in smaller 1°C disturbance isolines in both heating and cooling modes. The radial spread and maximum temperature disturbance of two cases are compared in Table 4.4. Clay with higher volumetric heat capacity resulted in lower temperature disturbance.

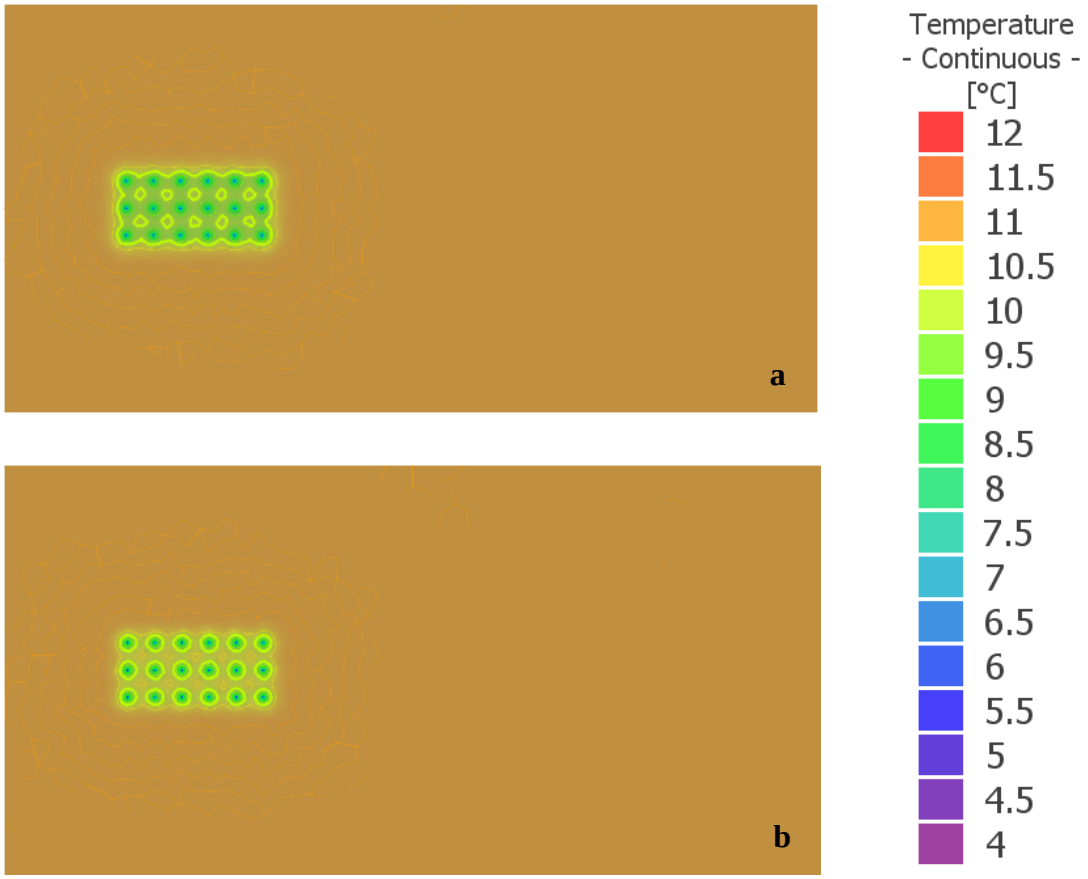

Figure 4.6 Temperature Distribution [°C] at the end of May of the First Year at Depth of 75 m BGS for a. Coarse Sand (1.4×10^{6} J m^{-3} K^{-1}), b. Clay (3.3×10^{6} J m^{-3} K^{-1})

Table 4.4 Center of Energy Coordinates for Volumetric Heat Capacity Sensitivity Analysis

Case	R_{spread} [m]	Max Temperature Disturbance [°C]
Coarse Sand, May	75.51	6.35
Clay, May	75.57	6.07
Coarse Sand, August	76.63	34.47
Clay, August	76.61	32.83

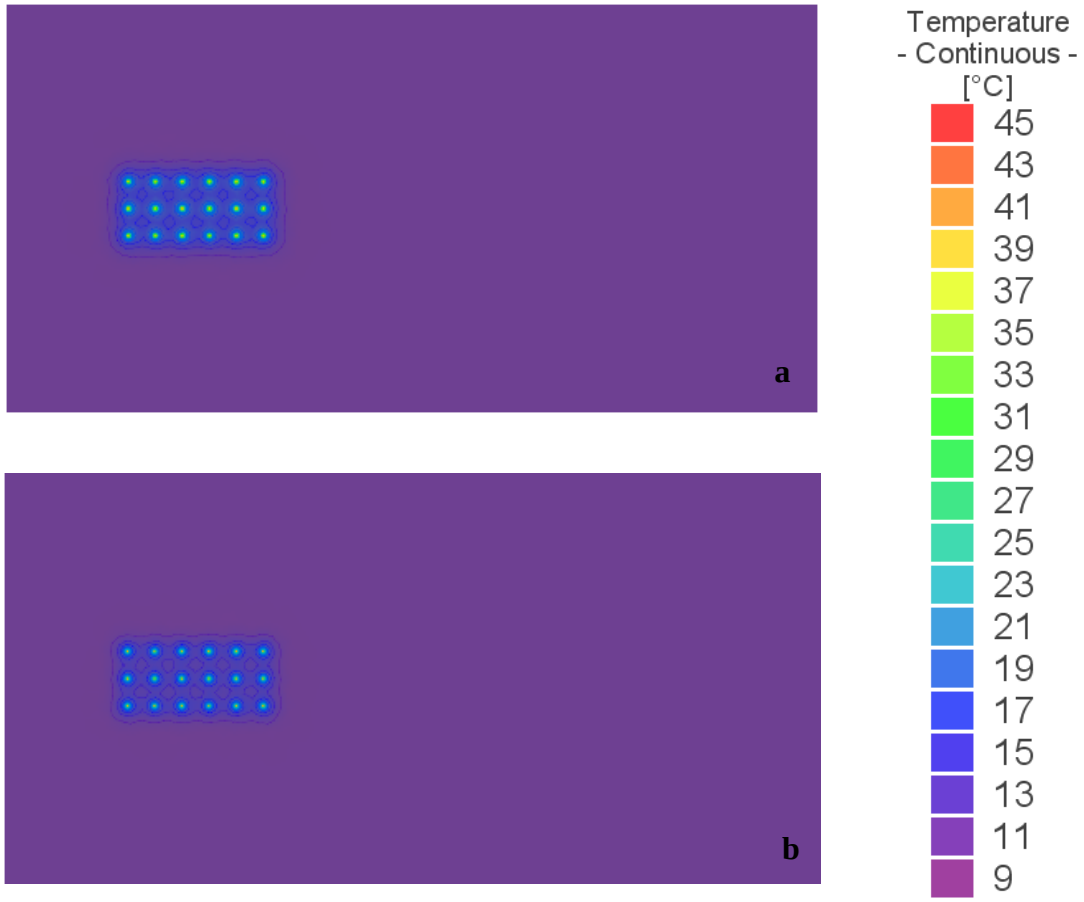

Figure 4.7 Temperature Distribution [°C] at the end of August of the First Year at Depth of 75 m BGS for a. Coarse Sand (1.4×10^{6} J m^{-3} K^{-1}), b. Clay (3.3×10^{6} J m^{-3} K^{-1})

4.4 Effect of Soil Porosity

In this section, the sensitivity of the model to soil porosity is examined. Porosity is an important parameter with respect to thermal conduction and can change. Two cases of coarse sand and clay with porosities of 0.385 and 0.47 were simulated. All other properties and boundary conditions remained the same as section 3.2.6.

At the end of May, the 10°C isoline is in the shape of circles around the boreholes for the case of clay rather than a more extensive rectangular shaped isoline of the coarse sand soil (Figure 4.8). The radial spread is smaller for the clay in both heating and cooling modes with higher temperature disturbance in cooling mode (Table 4.5). Figure 4.9 shows that the temperature isolines are very similar at the end of August. It can be concluded that increase of porosity results in smaller plumes with slightly higher temperature disturbance which is exactly the opposite of thermal conductivity effect.

Table 4.5 Center of Energy Coordinates for Porosity Sensitivity Analysis

Case	R_{spread} [m]	Max Temperature Disturbance [°C]
Coarse Sand, May	75.51	6.35
Clay, May	75.45	6.35
Coarse Sand, August	76.63	34.47
Clay, August	76.53	34.76

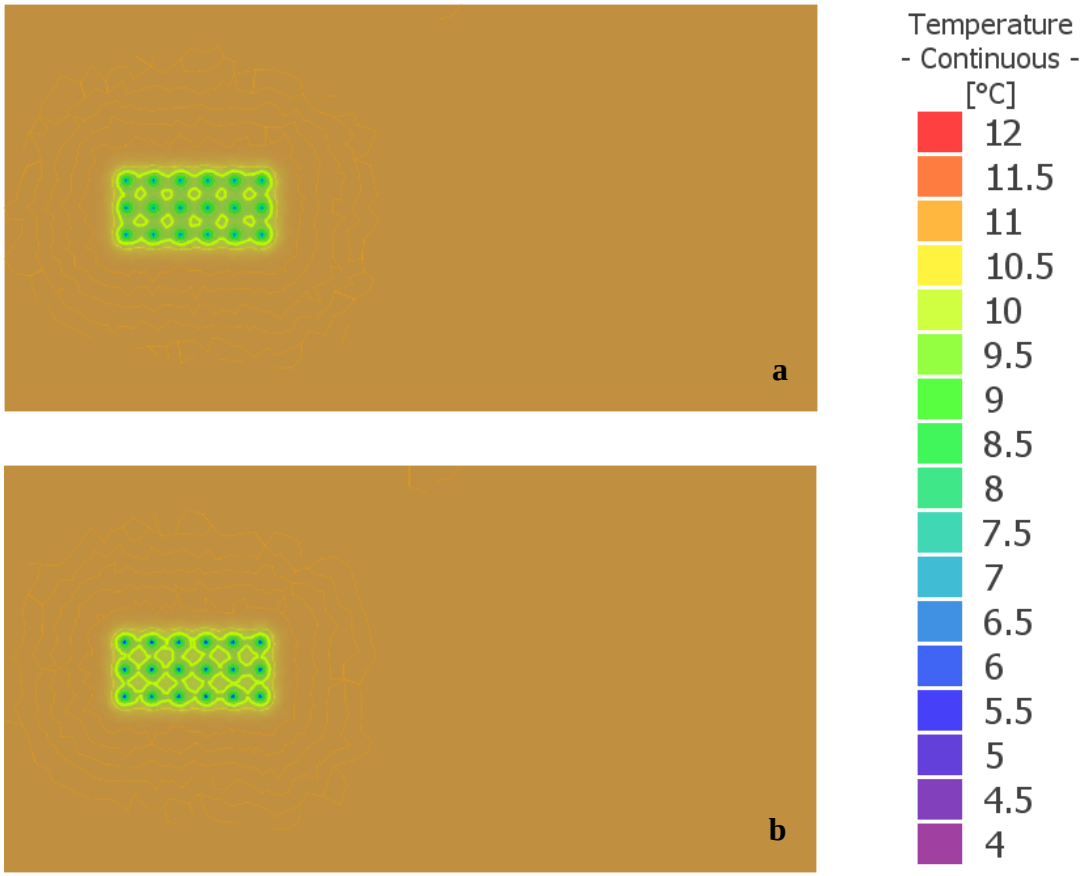

Figure 4.8 Temperature Distribution [°C] at the end of May of the First Year at Depth of 75 m BGS for a. Coarse Sand (0.385), b. Clay (0.47)

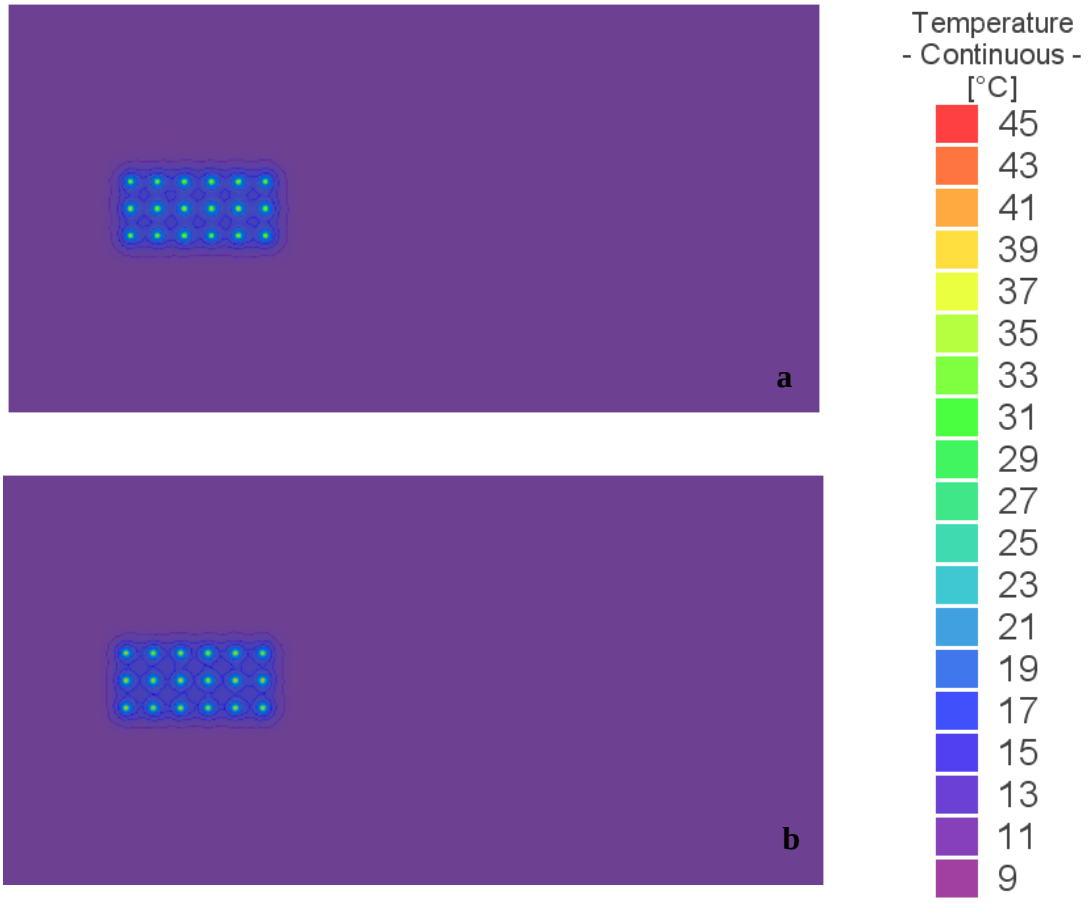

Figure 4.9 Temperature Distribution [°C] at the end of August of the First Year at Depth of 75 m BGS for a. Coarse Sand (0.385), b. Clay (0.47)

4.5 Comparison Between Coarse Sand, Clay, and Layered Soil

Previous sections showed the effects of hydraulic conductivity, thermal conductivity, volumetric heat capacity and porosity on development and transport of thermal plumes in different soils. In this section, a more realistic Toronto lithology was simulated using a layered soil.

Per Agriculture and Agri-Food Canada, the dominant soil of Toronto is Luvisolic whose parent material contains significant amount of clay with underlying shale bedrock. Therefore, a layered soil of clay (0 to 50 m BGS), coarse sand (50 to 100 m BGS) and shale (100 to 200 m BGS) was considered. Typical hydraulic and thermal properties of the selected porous media are listed in Table 4.6 (Chiasson, 1999).

Table 4.6 Porous Media Hydraulic and Thermal Properties (Chiasson, 1999)

Porous Medium	Hydraulic Conductivity [m s^{-1}]	Porosity [-]	Groundwater Flow Velocity [m s^{-1}]	Thermal Conductivity [J m^{-1} s^{-1} K^{-1}]	Volumetric Heat Capacity [J m^{-3} K^{-1}]
Clay	2.2×10^{-10}	0.47	2.2×10^{-14}	0.98	3.3×10^{6}
Coarse Sand	7.3×10^{-5}	0.385	7.3×10^{-9}	0.8	1.4×10^{6}
Shale	1.4×10^{-11}	0.053	1.4×10^{-15}	2.5	3.9×10^{6}
Layered Soil	$1.82\text{x}10^{-5}$	0.24	1.82×10^{-9}	1.7	3.1×10^{6}

The equivalent properties of the layered soil are calculated using (Fetter, 1994):

$$P_{eq} = \frac{\sum P_i m_i}{m} \qquad \textbf{(4-3)}$$

Where P_i is any soil property and m_i is thickness of layer i. The equivalent properties were not used in the model but rather, were calculated to allow comparison between the results of the layered and homogeneous models.

To examine the effect of layered soil, simulations were performed using a domain consisting only of clay, sand, and layered soil. Figure 4.10 illustrates 3D cross-sectional view of the temperature contours at the end of one year of operation for the three cases. To better examine the effect of soil type on thermal plumes, the 1°C disturbance isoline, i.e., 12°C isoline was illustrated.

The simulations revealed that the maximum temperature was approximately 17, 15.7 and 14°C for coarse sand, clay and layered soil, respectively. As it was expected, the case with highest thermal conductivity (layered system) had the lowest temperature disturbance (Table 4.7). In addition, the 12°C isoline in the layered soil extended along the x-axis, due to the higher thermal conductivity. Coarse sand with lowest thermal conductivity showed the highest temperature plume trapped inside the borefield.

The center of energy coordinate at the end of one year of operation was calculated for each case (Table 4.7). It can be seen that the thermal plume of the layered soil was further east (2 m) as compared to the two homogenous cases. This is due to the higher equivalent thermal conductivity. As expected, the y coordinate remained the same in all cases. Regarding the z-coordinate of the centre of energy (depth), it can be seen that it is shallower in the case of layered soil. This can be associated with high shale thermal conductivity which resulted in more heat conduction in the lower 100 m of the domain, resulting in plume with lower temperature disturbance.

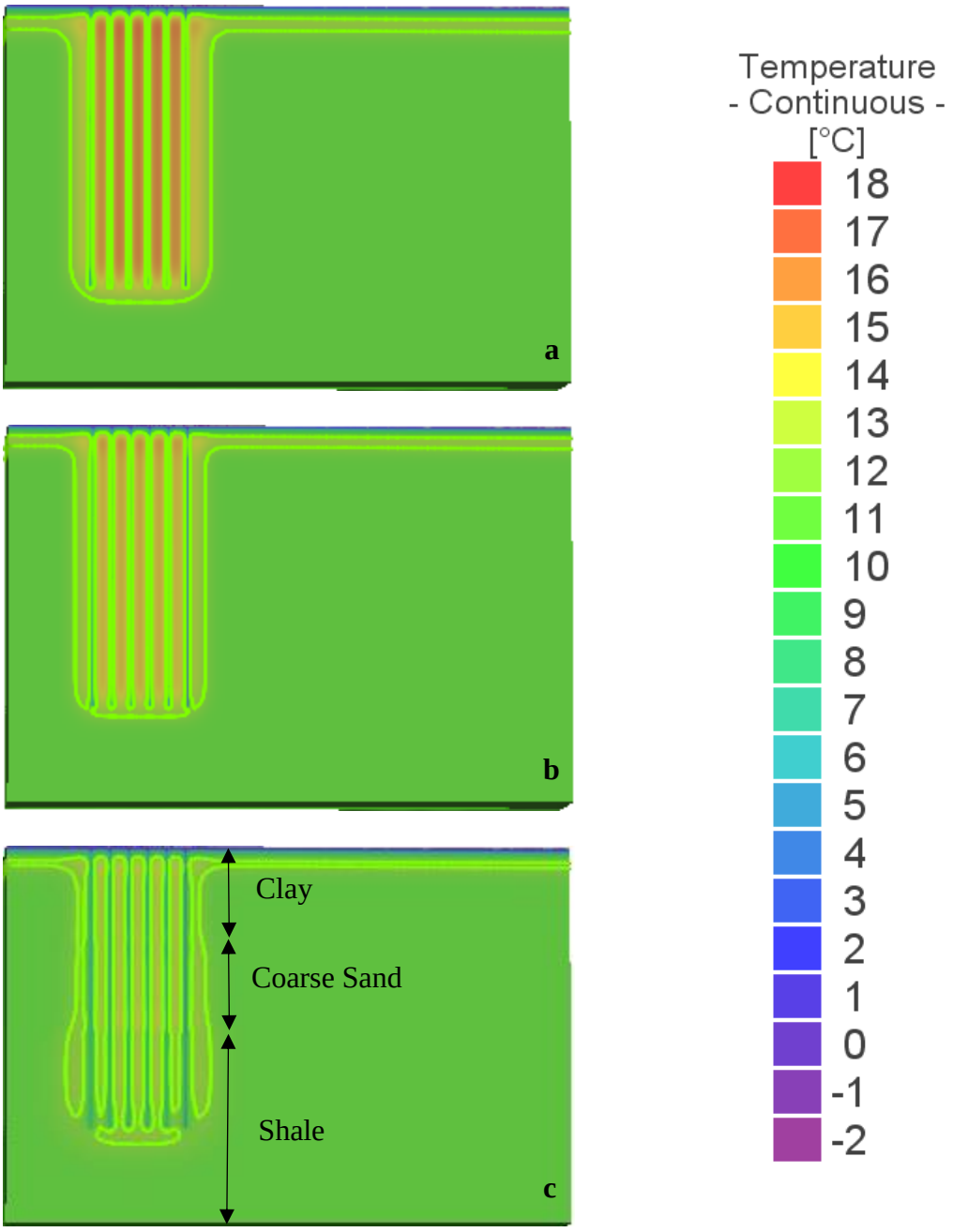

Figure 4.10 The 12°C isoline at the End of December (1 year operation) in Toronto for a. coarse sand, b. clay, c. layered soil

Table 4.7 Center of Energy Coordinates for Different Soil Types

Case	X_{ce} [m]	Y_{ce} [m]	Z_{ce} [m]	Max Temperature Disturbance [°C]
Coarse Sand	78.27	74.97	-65.63	10.94
Clay	78.63	74.99	-63.30	10.74
Layered Soil	80.72	74.99	-59.49	10.41

4.6 Conclusion

In this chapter, sensitivity analysis of different soil parameters on the 3D borehole-based GSHP system model was conducted. Effect of parameters such as hydraulic conductivity, soil thermal conductivity, volumetric heat capacity and porosity on development and transport of thermal plumes were studied.

The temperature contours were presented at the end of May and August of the first year of operation for the city of Toronto. The 1°C disturbance isolines and center of energy were used to examine the size of thermal plumes.

The results showed that hydraulic conductivity was the only parameter that changed the coordination of center of energy significantly due to transport of thermal plumes by groundwater flow. In all other cases, the center of energy remained more or less at the same location. Thermal conduction had the largest impact on the spread of the thermal plume.

High hydraulic conductivity that resulted in a groundwater flow in the order of 10^{-7} m/s led to wider thermal plumes with less ground temperature disturbance in both heating and cooling modes.

Increase in thermal conductivity, volumetric heat capacity and porosity resulted in smaller 1°C disturbance isolines in both heating and cooling modes.

Finally, three different soils of coarse sand, clay and a layered formation that was made up of coarse sand, clay and shale bedrock were compared. The results revealed that the layered soil with highest thermal conductivity led to less temperature disturbance.

Chapter 5 Summary and Conclusions

The use of constant temperature of the ground for space heating and cooling is known as geothermal heating. Geothermal heating has attracted worldwide attention in recent years since it shows promise as an alternative to conventional HVAC systems. It offers low maintenance, high heating/cooling comfort, and a low carbon footprint, compared to conventional systems. Ground source heat pumps are used to extract heat from the ground during cold seasons and inject heat to the ground during hot seasons.

Installation of GSHP systems without an adequate hydrogeological and feasibility study might result in environmental impacts such as thermal plumes that can affect performance of the system and interfere with other subsurface infrastructures. Although significant amount of research has been conducted to examine and optimize the design and performance of GSHP systems, there has been little work done to examine the environmental impacts of GSHP systems.

The objectives of this study were: (1) to develop a 3D model in FEFLOW 7.0 to simulate a GSHP nest in different Canadian climates, (2) to identify the thermally affected zone and study the developed thermal plumes under different building thermal loads, (3) to examine the effect of groundwater flow on development and transport of thermal plumes, and (4) to examine the sensitivity of the model to soil properties such as thermal conductivity, volumetric heat capacity, and porosity.

Chapter 3 of this study dealt with modelling of a vertical closed-loop GSHP system located in different climatic regions of Canada, namely Toronto, Vancouver and Windsor. A 3D model was developed in FEFLOW 7.0 simulating a multi-borehole GSHP system that provided annual heating and cooling of a hypothetical office building to examine the effect of different building thermal loads on development of thermal plumes.

The developed thermal plumes after ten years of GSHP operation were compared between the cities. It was found that Vancouver with a moderate climate had small and focused plumes, while Windsor with highest heat injection during summer had extensive plumes. The results after 10 years of operation, showed that a high temperature plume of 24°C was present inside the Windsor borefield while Vancouver experienced a plume of only 15°C. Moreover, comparison between the first and tenth year of operation illustrated that plumes grew in both size and temperature disturbance with longer operation duration.

Chapter 4 studied the sensitivity of the model to parameters such as hydraulic conductivity, soil thermal conductivity, volumetric heat capacity, and porosity. The results showed that hydraulic conductivity was the only parameter that changed the coordinate of center of energy significantly due to transport of thermal plumes by groundwater flow. In all other cases, the center of energy remained virtually unchanged.

High hydraulic conductivity, that resulted in a groundwater velocity in the order of 10^{-7} m/s, led to wider thermal plumes with less ground temperature disturbance in both

heating and cooling modes. Increase in thermal conductivity, volumetric heat capacity resulted in larger radial spread with lower maximum temperature disturbance. On the contrary, increase in porosity resulted in smaller radial spread with higher maximum temperature disturbance.

Finally, a case with soil heterogeneity was simulated and compared with two homogeneous soils of coarse sand and clay. Results revealed that the layered soil with highest thermal conductivity led to less ground temperature disturbance.

5.1 Recommendations for Future Work

Further studies and research areas are suggested as follows:

- Conduct optimization of the BHE system design using an available design tool such as GLHEPRO for each city to optimize the BHE system.
- Perform additional model validation, using field data from an operating GSHP system in Canada.
- Examine the impact of insulating upper few meters of the borehole to avoid seasonal fluctuations on GHSP performance.
- Simulate two neighbouring GSHP systems to examine the thermal interference between adjacent systems and determine the optimum spacing for Canadian fields.

Bibliography

Agriculture and Agri-Food Canada, Government of Canada, Retrieved from http://sis.agr.gc.ca/cansis/publications/webmaps.html, Last modified 2014-05-13

Al-Khoury, R. (2009). Efficient Finite Element Modeling of Shallow Geothermal Systems. In *2009 Second International Conference on Environmental and Computer Science* (pp. 371–374). IEEE. http://doi.org/10.1109/ICECS.2009.49

Al-Khoury, R., & Bonnier, P. G. (2006). Efficient finite element formulation for geothermal heating systems. Part II: transient. *International Journal for Numerical Methods in Engineering*, *67*(5), 725–745. http://doi.org/10.1002/nme.1662

Al-Khoury, R., Bonnier, P. G., & Brinkgreve, R. B. J. (2005). Efficient finite element formulation for geothermal heating systems. Part I: steady state. *International Journal for Numerical Methods in Engineering*, *63*(7), 988–1013. http://doi.org/10.1002/nme.1313

ASHRAE. (1997). *ASHRAE Fundamentals Handbook*. Atlanta: American Society of Heating, Refrigerating and Air-Conditioning Engineers Inc.

Ball, D. A., Fischer, R. D., & Hodgett, D. (1983). Design methods for ground-source heat pumps. Retrieved from http://www.osti.gov/scitech/biblio/6057439

Banks, D. (2008). *An introduction to thermogeology : ground source heating and cooling / David Banks*. Retrieved from https://books.google.ca/books?hl=en&lr=&id=kKQ1t

9ZfzgC&oi=fnd&pg=PT18&dq=geothermal+heating+and+cooling+HVAC&ots=B8uLzm-l5U&sig=WamqqGa2o1xy1dQ5MPVSNPlT7uY#v=onepage&q&f=false

Bauer, D., Heidemann, W., Mü ller-Steinhagen, H., & Diersch, H. G. (2011). Thermal resistance and capacity models for borehole heat exchangers. *INTERNATIONAL JOURNAL OF ENERGY RESEARCH Int. J. Energy Res*, *35*, 312–320. http://doi.org/10.1002/er.1689

Bhatia, A. (n.d.). Heat Loss Calculations and Principles HVAC HEATING LOSS CALCULATIONS & PRINCIPLES.

Bhatia, A. (2001). Cooling load calculations and principles. *Continuing Education and Development, Inc. New York*, (877).

Blackwell, D. D., Negraru, P. T., & Richards, M. C. (2006). Assessment of the Enhanced Geothermal System Resource Base of the United States. *Natural Resources Research*, *15*(4). http://doi.org/10.1007/s11053-007-9028-7

Camdali, U., Bulut, M., & Sozbir, N. (2015). Numerical modeling of a ground source heat pump: The Bolu case. *Renewable Energy*. http://doi.org/10.1016/j.renene.2015.04.030

Chiasson, A. D. (1999). *Advances in modeling of ground-source heat pump systems*. *Exchange Organizational Behavior Teaching Journal*.

Dehkordi, S. E., & Schincariol, R. A. (2014). Effect of thermal-hydrogeological and borehole heat exchanger properties on performance and impact of vertical closed-

loop geothermal heat pump systems. *Hydrogeology Journal*, *22*(1), 189–203. http://doi.org/10.1007/s10040-013-1060-6

Dehkordi, S. E., Schincariol, R. A., & Reitsma, S. (2015). Thermal performance of a tight borehole heat exchanger. *Renewable Energy*, *83*, 698–704. http://doi.org/10.1016/j.renene.2015.04.051

Dekker, T. J., & Abriola, L. M. (2000). The influence of field-scale heterogeneity on the infiltration and entrapment of dense nonaqueous phase liquids in saturated formations. *Journal of Contaminant Hydrology*, *42*(2–4), 187–218. http://doi.org/10.1016/S0169-7722(99)00092-3

Diao, N., Li, Q., & Fang, Z. (2004). Heat transfer in ground heat exchangers with groundwater advection. *International Journal of Thermal Sciences*. http://doi.org/10.1016/j.ijthermalsci.2004.04.009

Dickson, M.H. and Fanelli, M. (2004). *What Is Geothermal Energy?* Istituto di Geoscienze e Georisorse, CNR, Pisa, Italy. Available via the International Geothermal Association, last accessed August 2017, https://www.geothermal energy.org/what_is_geothermal_energy.html#c313.

Diersch, H.-J. G. (2014). *FEFLOW. FEFLOW: Finite Element Modeling of Flow, Mass and Heat Transport in Porous and Fractured Media* (Vol. 9783642387). http://doi.org/10.1007/978-3-642-38739-5

Diersch, H. J. G., Bauer, D., Heidemann, W., Rühaak, W., & Schätzl, P. (2010). Finite

element formulation for borehole heat exchangers in modeling geothermal heating systems by FEFLOW. *White Papers*, *5*, 5–96.

Emad Dehkordi, S., Schincariol, R. A., & Olofsson, B. (2015). Impact of Groundwater Flow and Energy Load on Multiple Borehole Heat Exchangers. *Groundwater*. http://doi.org/10.1111/gwat.12256

Eskilson, P., & Claesson, J. (1988). SIMULATION MODEL FOR THERMALLY INTERACTING HEAT EXTRACTION BOREHOLES. *Numerical Heat Transfer*, *13*(2), 149–165. http://doi.org/10.1080/10407788808913609

Ferguson, G., & Woodbury, A. D. (2005). Thermal sustainability of groundwater-source cooling in Winnipeg, Manitoba. *Canadian Geotechnical Journal*, *42*(5), 1290–1301. http://doi.org/10.1139/t05-057

Ferguson, G., & Woodbury, A. D. (2006). Observed thermal pollution and post-development simulations of low-temperature geothermal systems in Winnipeg, Canada. *Hydrogeology Journal*. http://doi.org/10.1007/s10040-006-0047-y

Fetter, C. W. (Charles W. (1994). *Applied hydrogeology*. Macmillan. Retrieved from https://books.google.ca/books?id=EIDuAAAAMAAJ&focus=searchwithinvolume&q=Equivalent+Hydraulic+conductivity

Garcia-Gil, A., Vazquez-Sune, E., Schneider, E. G., Sanchez-Navarro, J. A., & Mateo-Lazaro, J. (2014). The thermal consequences of river-level variations in an urban groundwater body highly affected by groundwater heat pumps. *Science of the Total*

Environment. http://doi.org/10.1016/j.scitotenv.2014.03.123

Hecht-Méndez, J., de Paly, M., Beck, M., & Bayer, P. (2013). Optimization of energy extraction for vertical closed-loop geothermal systems considering groundwater flow. *Energy Conversion and Management*, *66*, 1–10. http://doi.org/10.1016/j.enconman.2012.09.019

Hecht-Méndez, J., Molina-Giraldo, N., Blum, P., & Bayer, P. (2010). Evaluating MT3DMS for heat transport simulation of closed geothermal systems. *Ground Water*, *48*(5), 741–56. http://doi.org/10.1111/j.1745-6584.2010.00678.x

Hirsch, C. (1988). *Numerical Computation of Internal and External Flows*.

Huttrer, G. (1997). Geothermal heat pumps: an increasingly successful technology. *Renewable Energy*. Retrieved from http://www.sciencedirect.com/science/article/pii/0960148196001073

Jessop, A. M., Ghomshei~, M. M., & Drury, M. J. (1991). GEOTHERMAL ENERGY IN CANADA*, *206*(5), 369–385. Retrieved from https://journals.scholarsportal.info/pdf/03756505/v20i5-6/369_geic.xml

Jones, F. W., Lam, H.-L., & Majorowicz, J. A. (1985). Temperature distributions at the Paleozoic and Precambrian surfaces and their implications for geothermal energy recovery in Alberta. *Can . J . Earth Sci*, *22*, 1774–1780. Retrieved from https://www.researchgate.net/profile/Jacek_Majorowicz/publication/272943822_The_relationship_of_hydrocarbon_occurrences_to_geothermal_gradients_and_time-

temperature_indices_in_Mesozoic_formations_of_southern_Alberta_Bull_Can_Petrol_Geol_34_226-239/links/54ff183b0cf2eaf210b5466b.pdf

Komor, P. (1997). Space cooling demands from office plug loads. *ASHRAE Journal*. Retrieved from http://search.proquest.com/openview/20b9b040768dae1c8a22e32beac385fe/1?pq-origsite=gscholar&cbl=41118

Krol, M. M. (2011). Impact of Low Temperature Electrical Resistance Heating on Subsurface Flow and Mass Transport. *Simulation*. Retrieved from https://tspace.library.utoronto.ca/bitstream/1807/29777/3/Magdalena_Krol_M_201106_PhD_thesis.pdf

Lazzari, S., Priarone, A., Zanchini, E., Energetica, I., Viale, B., & Pia, O. (2010). Long-Term Performance of Borehole Heat Exchanger Fields with Groundwater Movement. Retrieved from https://www.comsol.no/paper/download/63213/lazzari_paper.pdf

Lee, J. S., Song, K. S., Ahn, J. H., & Kim, Y. (2015). Comparison on the transient cooling performances of hybrid ground-source heat pumps with various flow loop configurations. *Energy*. http://doi.org/10.1016/j.energy.2015.01.076

Li, M., & Lai, A. C. K. (2015). Review of analytical models for heat transfer by vertical ground heat exchangers (GHEs): A perspective of time and space scales. *Applied Energy*. http://doi.org/10.1016/j.apenergy.2015.04.070

Lienhard, J. H. (2010). Heat Transfer. *Journal of Heat Transfer*, *82*(1), 198. http://doi.org/10.1115/1.3246887

Liuzzo-Scorpo, A., Nordell, B., & Gehlin, S. (2015). Influence of regional groundwater flow on ground temperature around heat extraction boreholes. *Geothermics*. http://doi.org/10.1016/j.geothermics.2015.04.002

Lo Russo, S., Gnavi, L., Roccia, E., Taddia, G., & Verda, V. (2014). Groundwater Heat Pump (GWHP) system modeling and Thermal Affected Zone (TAZ) prediction reliability: Influence of temporal variations in flow discharge and injection temperature. *Geothermics*. http://doi.org/10.1016/j.geothermics.2013.10.008

Lo Russo, S., Taddia, G., & Verda, V. (2012). Development of the thermally affected zone (TAZ) around a groundwater heat pump (GWHP) system: A sensitivity analysis. *Geothermics*, *43*, 66–74. http://doi.org/10.1016/j.geothermics.2012.02.001

Majorowicz, J. A., Jones, F. W., Lam, H.-L., Linville, A., & Nguyen, C. D. (1985). TOPOGRAPHY AND THE SUBSURFACE TEMPERATURE REGIME IN THE WESTERN CANADIAN SEDIMENTARY BASIN: IMPLICATIONS FOR LOW-ENTHALPY GEOTHERMAL ENERGY RECOVERY, *14*(23), 175–187. Retrieved from https://journals.scholarsportal.info/pdf/03756505/v14i2-3/175_tatstriflger.xml

Majorowicz, J., Grasby, S. E., & Skinner, W. R. (2009). Estimation of Shallow Geothermal Energy Resource in Canada: Heat Gain and Heat Sink. *Natural Resources Research*, *18*(2), 95–108. http://doi.org/10.1007/s11053-009-9090-4

Nam, Y., Ooka, R., & Hwang, S. (2008). Development of a numerical model to predict heat exchange rates for a ground-source heat pump system. *Energy and Buildings*, *40*(12), 2133–2140. http://doi.org/10.1016/j.enbuild.2008.06.004

Ozudogru, T. Y., Olgun, C. G., & Senol, A. (2014). 3D numerical modeling of vertical geothermal heat exchangers. *Geothermics*, *51*, 312–324. http://doi.org/10.1016/j.geothermics.2014.02.005

Ramamoorthy, M., Jin, H., & Chiasson, A. (2001). Optimal sizing of hybrid ground-source heat pump systems that use a cooling pond as a supplemental heat rejecter--a system simulation approach/Discussion. *ASHRAE*. Retrieved from http://search.proquest.com/openview/a1eb7ad54bbe436595be2ed4f1b5a759/1?pq-origsite=gscholar&cbl=34619

Raymond, J., Frenette, M., Leger, A., Magni, E., & Therrien, R. (2011). Numerical Modeling of Thermally Enhanced Pipe Performance in Verical Ground Heat Exchangers. *ASHRAE Journal*, *117*, 899–907.

Raymond, J., & Therrien, R. (2008). Low-temperature geothermal potential of the flooded Gaspé Mines, Québec, Canada. *Geothermics*. http://doi.org/10.1016/j.geothermics.2007.10.001

Raymond, J., & Therrien, R. (2014). Optimizing the design of a geothermal district heating and cooling system located at a flooded mine in Canada. *Hydrogeology Journal*. http://doi.org/10.1007/s10040-013-1063-3

Raymond, J., Therrien, R., Gosselin, L., & Lefebvre, R. (2011). Numerical analysis of thermal response tests with a groundwater flow and heat transfer model. *Renewable Energy*. http://doi.org/10.1016/j.renene.2010.06.044

Rees, S. J. (2015). An extended two-dimensional borehole heat exchanger model for simulation of short and medium timescale thermal response. *Renewable Energy*. http://doi.org/10.1016/j.renene.2015.05.004

Slenders, H., Dols, P., Verburg, R., & de Vries, A. J. (2010). Sustainable remediation panel: Sustainable synergies for the subsurface: Combining groundwater energy with remediation. *Remediation Journal*. http://doi.org/10.1002/rem.20246

Yang, H., Cui, P., & Fang, Z. (2010). Vertical-borehole ground-coupled heat pumps: A review of models and systems. *Applied Energy*. http://doi.org/10.1016/j.apenergy.2009.04.038

Appendix A

In this appendix, assumptions and sample calculations of building cooling load calculation (section 3.2.2.1) are presented.

- **Conductive Heat Gain Through Roof**

The roof was assumed to be a 2-inch C12, HW concrete with suspended ceiling and mass inside the insulation is selected. According to Table 31 of Chapter 28 of ASHRAE, (1997), this type of roof with R-factor[6] of 25 [hr ft^2 °F Btu^{-1}] has a roof number of 14. Table 30 of Chapter 28 of ASHRAE (1997) lists hourly July CLTD values for different types of roof. Assuming office hours of 8:00 to 17:00, CLTD varies between 20 and 42°F with the maximum CLTD at 17:00 h. Since the current approach uses monthly data rather than hourly, a mean CLTD of 28°F was selected.

As an example, the corrected CLTD and conductive heat gain for June in Toronto is calculated from equations (3-11) and (3-10) to be:

$$CLTD_{Corr.} = 28 + (78 - 68) + (65.48 - 85) = 18.48\ ^\circ\text{F} \quad \textbf{(A-1)}$$

$$\dot{Q}_{roof} = A_{roof} U_{roof} (CLTD)_{Corr.roof} = 5120 \times 0.04 \times 18.48 = 3784.7\ Btu/hr \quad \textbf{(A-2)}$$

[6] $R_{roof} = \frac{1}{U_{roof}} = \frac{1}{0.04} = 25\ \frac{hr.ft^2.^\circ\text{F}}{Btu}$

- **Conductive Heat Gain Through Walls**

Table 33 of Chapter 28 of (ASHRAE, 1997) lists different types of walls. In the current case walls have a U-value of 0.09 [Btu hr^{-1} ft^{-2} °F^{-1}] which corresponds to the R-factor of 11.11 [hr ft^2 °F Btu^{-1}]. From Table 3.2, the principle wall material is 8-inch concrete block and the secondary material is face brick. Therefore, from Table 11 of Chapter 28 of ASHRAE (1997), reference wall has a code number of C8 which according to Table 33B of (ASHRAE, 1997) has a wall type of 16. Table 32 of (ASHRAE, 1997) shows July CLTD for different wall faces. Area of different wall facings of the reference building is given in Table 3.2. Mean CLTD of different walls is listed in Table A.1.

Table A.1 Mean July CLTD for Walls

Wall Face	North	East	South	West
CLTD [°F]	8.9	20.5	11.5	13.3

Example calculations for North facing walls in Toronto's June is as follows:

$$CLTD_{Corr.} = 8.9 + (78 - 68) + (65.48 - 85) = -0.62\ °\text{F}$$

$$\dot{Q}_{walls} = A_{North\ walls} U_{wall} (CLTD)_{Corr._{North\ Walls}} \quad \textbf{(A-3)}$$

$$= 2160 \times 0.09 \times (-0.62) = -120.5\ Btu/hr$$

- **Conductive Heat Gain Through Windows**

Example calculations for Toronto's June is as follows:

$$CLTD_{Corr.} = 8.8 + (78 - 68) + (65.48 - 85) = -0.72\ °\text{F} \quad \textbf{(A-4)}$$

$$\dot{Q}_{windows} = A_{window} \times U_{window} \times (CLTD)_{Corr.window}$$

$$= 2592 \times 0.7 \times (-0.72) \cong -1306.4\ Btu/hr$$

- **Heat Gain Due to Solar Radiation**

Assuming a carpet flooring, from Table 35B of (ASHRAE, 1997) zones are classified as type B. From Table 36 of (ASHRAE, 1997) July *SCL* is obtained as shown in Table A.2. The maximum solar load occurs at 17:00 h, so these *SCL*s are used for further calculations (Table A.2). Also, a *SC* of 0.55 is used for clear glass with light-colored venetian blinds according to an example of (ASHRAE, 1997).

Table A.2 Mean July SCL for Glass

Glass Face	**North**	**East**	**South**	**West**
SCL [Btu/hr.ft^2]	32.9	88.4	58.5	79.0

SCL values apply to 21st day of July. Example calculation for North facing windows is as follows:

$$\dot{Q}_{North\ Windows} = A_{North\ Window} \times SC \times (SCL)_{North} = 720 \times 0.55 \times 32.9 \quad \textbf{(A-5)}$$

$$= 13028.4\ Btu/hr$$

- **Heat Gain Produced by People**

From Table 3 of (ASHRAE, 1997), The sensible and latent heat gains for a seated, very light work office are 245 and 155 Btu/hr per person respectively (ASHRAE, 1997), and, *CLF* for 8 hours of occupancy is obtained form Table 37 of (ASHRAE, 1997) to be 0.83. Therefore,

$$\dot{Q}_{sensible} = 154 \times 245 \times 0.83 = 31315.9\ Btu/hr$$
$$\dot{Q}_{latent} = 154 \times 155 = 23870\ Btu/hr$$
$$\dot{Q}_{people} = \dot{Q}_{sensible} + \dot{Q}_{latent} = 55185.9\ Btu/hr \quad \textbf{(A-6)}$$

- **Heat Gain Due to Convection**

A ventilation rate of 3080 cfm and an infiltration rate of 67 were used, per discussed in section 0. Inside temperature is set to 68°F which from Table 2 of chapter 1 of (ASHRAE, 1997) corresponds to a humidity ratio of 0.014761. Outside air humidity was taken from Table 1.2 of ASHRAE (1997). Example calculations for heat gain due to ventilation and infiltration for the case of Toronto's June is as follows:

$$\dot{Q}_{sensible} = 1.1 \times q_v \times (T_o - T_i) = 1.1 \times 3080 \times (65.48 - 68)$$
$$\cong -8537.8\ Btu/hr$$

$$\dot{Q}_{latent} = 4840 \times q_v \times (HR_o - HR_i)$$
$$= 4840 \times 3080 \times (0.013503 - 0.014761)$$
$$\cong -18753.3\ Btu/hr \quad \textbf{(A-7)}$$

$$\dot{Q}_{Ventilation} = \dot{Q}_{sensible} + \dot{Q}_{latent} = -8537.8 - 18753.3$$
$$\cong -27291\ Btu/hr$$

$$\dot{Q}_{sensible} = 1.1 \times q_v \times (T_o - T_i) = 1.1 \times 67 \times (65.48 - 68) \quad \textbf{(A-8)}$$
$$\cong -185.7\ Btu/hr$$

$$\dot{Q}_{latent} = 4840 \times q_v \times (HR_o - HR_i)$$

$$= 4840 \times 67 \times (0.013503 - 0.014761)$$

$$\cong -407.9 \ Btu/hr$$

$$\dot{Q}_{Infiltration} = \dot{Q}_{sensible} + \dot{Q}_{latent} = -185.7 - 407.9$$

$$\cong -593.7 \, Btu/hr$$

Appendix B

- **Model Resizing**

Initially a domain measuring 200 m×200 m×150 m with the borefield located at the centre of the domain was selected (Figure B.1). Ten-year simulation of the Windsor case showed that the most dissipated plumes are noticed on the end of May and are intensified year by year. Therefore, the temperature isolines on the may of tenth year are considered to examine domain resizing (Figure B.2). The 11.5°C isoline is an ellipse with a minor axis of nearly 148 m. Therefore, the domain width was resized from 200 m to 150 m.

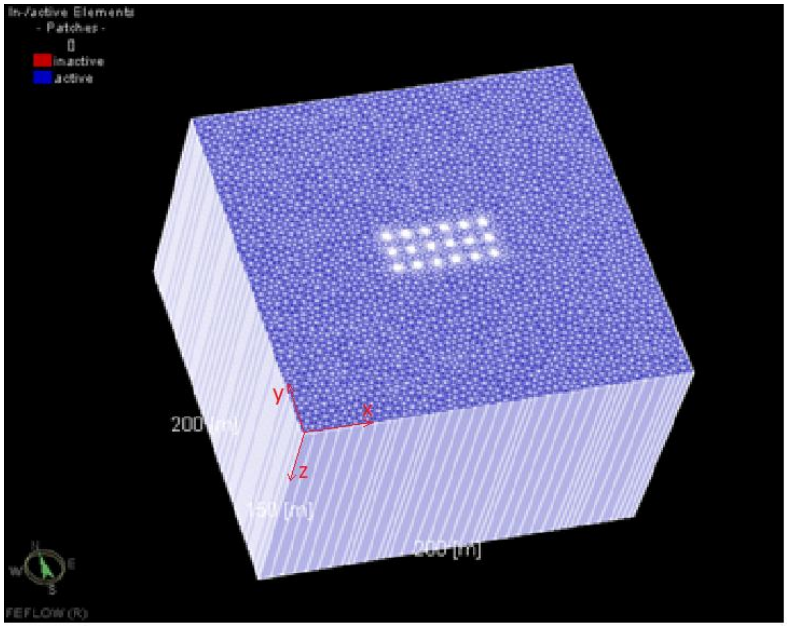

Figure B.1 Initial Model Domain showing the Borefield at the Centre

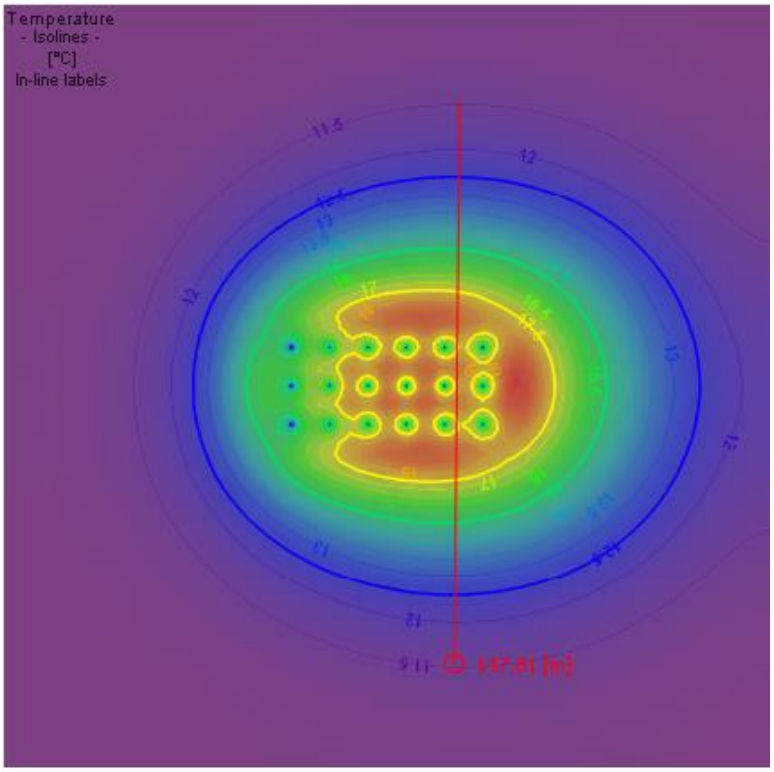

Figure B.2 Temperature isoline at 75 m BGS at the end of May after 10 years of operation (Windsor)

Domain length was increased to 300 m since the horizontal groundwater flow with higher velocity that is assigned in Chapter 4 would change the temperature distribution along the domain length by transferring the thermal plumes. Also, the BHE field was moved from the center of the domain to the left of the domain to allow to catch transfer of thermal plumes by groundwater flow.

Depth of the model was changed from 150 m to 200 m to study the effect of borehole installation on layers beneath the boreholes. The new model domain measures 300 m×150 m×200 m.

- **Reynolds Number Calculation**

Reynolds number in a pipe circulating the refrigerant is defined as (Lienhard, 2010):

$$Re = \frac{\rho_r u_r d}{\mu_r} \quad \textbf{(B-1)}$$

Where ρ_r and μ_r are density and dynamic viscosity of the refrigerant respectively, u_r is the velocity of the refrigerant in the pipe and d is the pipe diameter. Refrigerant velocity is calculated as:

$$u_r = \frac{F_r}{A} \quad \textbf{(B-2)}$$

Where F_r is refrigerant flow rate of 4×10^{-4} m^3 s^{-1}. Combining equations (B-1) and (B-2) and substituting refrigerant properties from Table 3.25 results in:

$$Re = \frac{\rho_r u_r d}{\mu_r} = \frac{4\rho_r F_r}{\pi d \mu_r} = \frac{4 \times 1.052 \times 10^3 \times 0.0004}{\pi \times 0.032 \times 3 \times 10^{-3}} \cong 5{,}584 \quad \textbf{(B-3)}$$

The critical Reynolds number is defined as a Reynolds number below which the flow will always be laminar. The critical Reynolds number in a circular pipe is 2100 (Lienhard, 2010). In the present case with Reynolds number of 5584, flow is turbulent.

Appendix C

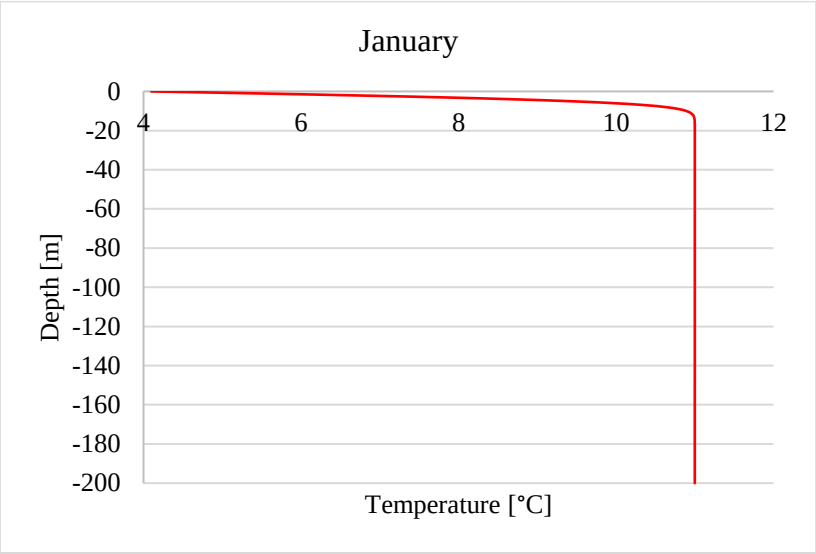
January
0
-20
-40
-60
-80
-100
-120
-140
-160
-180
-200
Depth [m]
4
6
8
10
12
Temperature [°C]

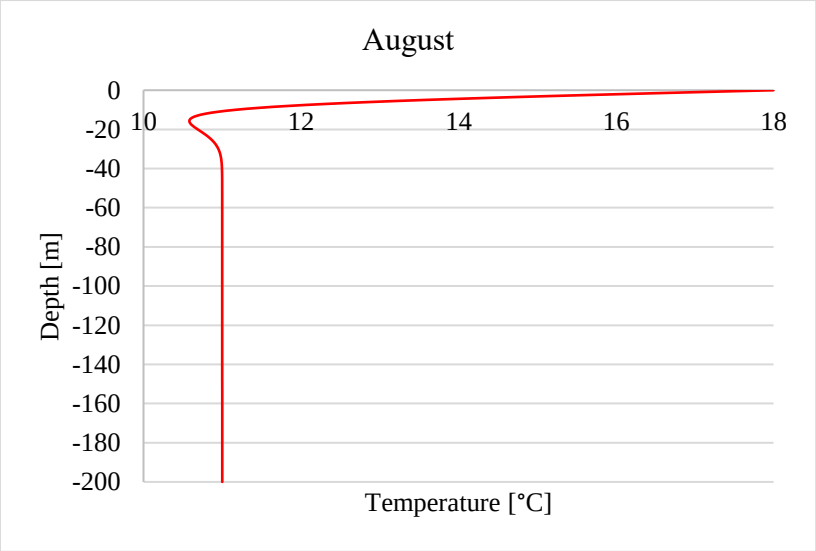
August
0
-20
-40
-60
-80
-100
-120
-140
-160
-180
-200
Depth [m]
10
12
14
16
18
Temperature [°C]

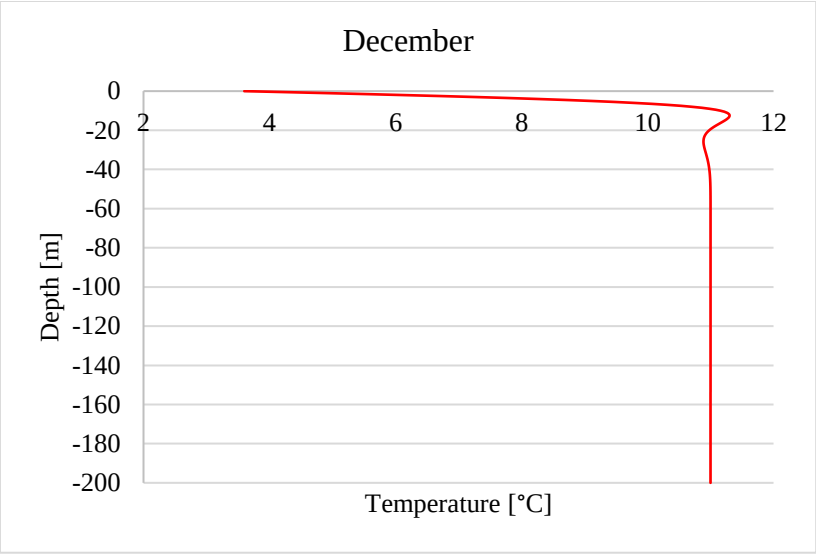

Figure C.1 Vancouver Soil Temperature Profile at OP2 at the End of a. January, b. August and c. December.

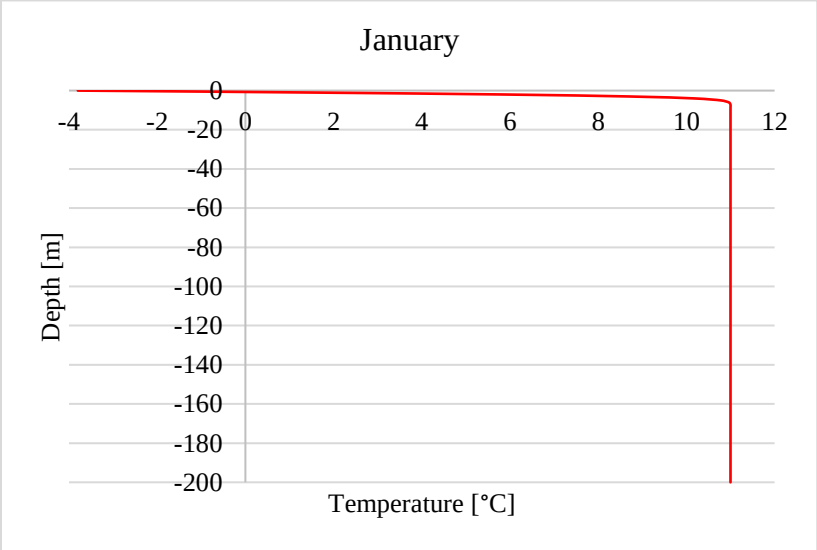

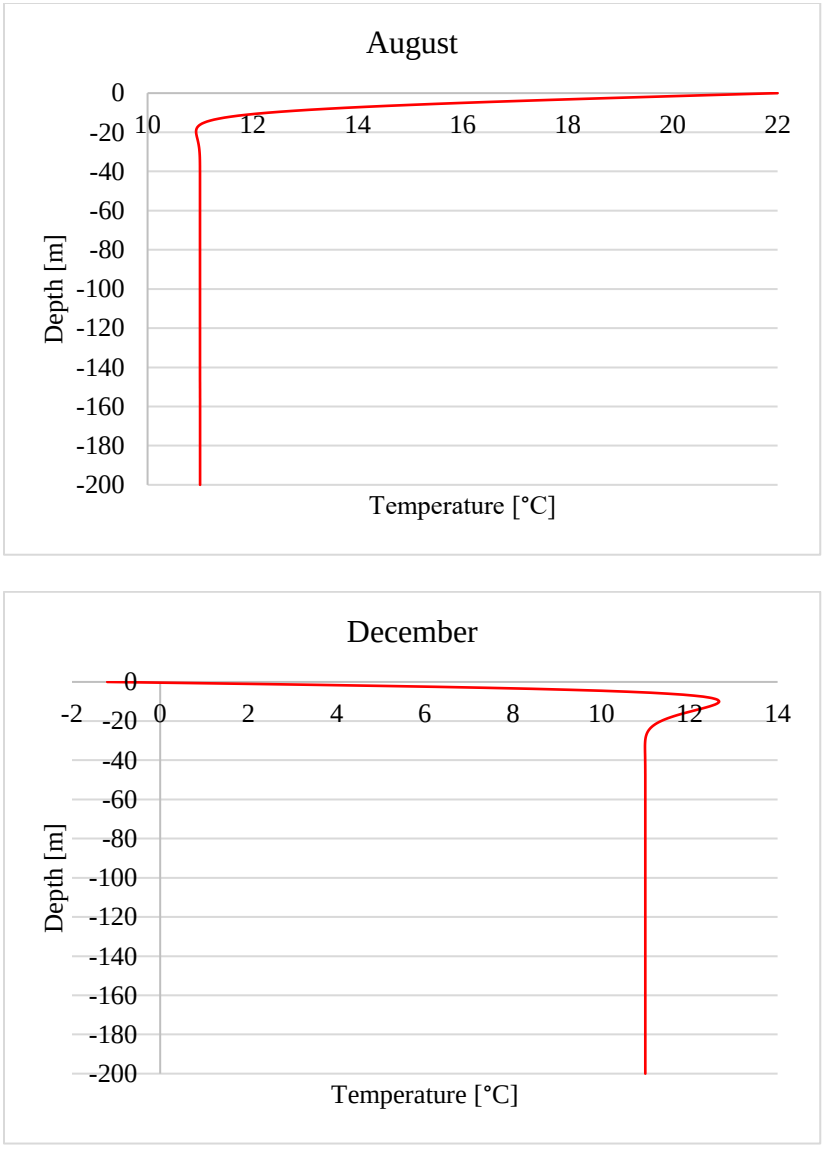

Figure C.2 Windsor Soil Temperature Profile at OP2 at the End of a. January, b. August and c. December